ADVANCED ELECTRONIC MATERIALS Open Access
www.advelectronicmat.de

Check for updates

Printed Memristors: An Overview of Ink, Materials, Deposition Techniques, and Applications

Miguel Franco, Asal Kiazadeh, Rodrigo Martins, Senentxu Lanceros-Méndez,* and Emanuel Carlos**

Industry 4.0 is accelerating the growth of connected devices, resulting in an exponential increase in generated data. The current semiconductor technology is facing challenges in miniaturization and power consumption, demanding for more efficient computation where new materials and devices need to be implemented. One of the most promising candidates for the next technological leap is the memristor. Due to their up-scale manufacturing, the majority of memristors employed conventional deposition techniques (physical and chemical vapor deposition), which can be highly costly. Recently, printed memristors have gained a lot of attention because of their potential for large-scale, fast, and affordable manufacturing. They can also help to reduce material waste, which supports the transition to a more sustainable and environmentally friendly economy. This review provides a perspective on the potential of printed electronics in the fabrication of memristive devices, presenting an overview of the main printing techniques, most suitable for memristors development. Additionally, it focuses on the materials used for the switching layer by comparing its performance. Ultimately, the application of printed memristors is highlighted by showing the tremendous evolution in this field, as well as the main challenges and opportunities that printed memristors are expected to face in the following years.

1. Introduction

As the world is implementing the Internet of Things (IoT) and Industry 4.0 concepts, the amount of generated data is increasing in an exponential trend. To deal with this massive growth of data, the performance of integrated circuit (IC) chips are subjected to higher requirements.[1] Over the past few decades, mainstream computers based on complementary metal oxide semiconductor (CMOS) have become more efficient and perform better supported by the accomplishment of the Moore's Law, which drives the number of transistors on chips to double every 18 months.[2] However, even the most advanced semiconductor technology is confronted with issues related to miniaturization and power consumption.[3] New materials, devices, and more efficient architectures need to be implemented.

One of the most promising candidates for the next technological leap is the memristor, proposed by Chua in 1971 as the fourth elemental passive circuit component,[4] establishing a direct relation between the magnetic flux (φ) and charge (q). Memristors display short and long-term memory, with excitatory and inhibitory capabilities.[5] These inherent properties have significant potential applications across diverse areas. Particularly, they exhibit promising implications for the next generation of non-volatile resistive memories,[6] showcasing characteristics that can enhance data storage efficiency and reliability.[7] Furthermore, these properties provide a unique opportunity for advancing the development of novel neuromorphic paradigms. In the context of neuromorphic computing, memristors offer the prospect of constructing

M. Franco, S. Lanceros-Méndez
Center of Physics
University of Minho and Laboratory of Physics for Materials and Emergent Technologies
LapMET, Campus de Gualtar, Braga 4710-057, Portugal
E-mail: senentxu.lanceros@bcmaterials.net

A. Kiazadeh, R. Martins, E. Carlos
CENIMAT|i3N
Department of Materials Science
School of Science and Technology
NOVA University Lisbon and CEMOP/UNINOVA
Caparica 2829-516, Portugal
E-mail: a.kiazadeh@fct.unl.pt; e.carlos@fct.unl.pt

S. Lanceros-Méndez
BCMaterials
Basque Center for Materials, Applications and Nanostructures
UPV/EHU Science Park, Leioa 48940, Spain

S. Lanceros-Méndez
IKERBASQUE
Basque Foundation for Science
Bilbao 48009, Spain

The ORCID identification number(s) for the author(s) of this article can be found under https://doi.org/10.1002/aelm.202400212

© 2024 The Author(s). Advanced Electronic Materials published by Wiley-VCH GmbH. This is an open access article under the terms of the Creative Commons Attribution License, which permits use, distribution and reproduction in any medium, provided the original work is properly cited.

DOI: 10.1002/aelm.202400212

circuits that mimic the parallel computation capabilities of the human brain.[8] This potential breakthrough could lead to significant advancements in artificial intelligence, allowing for more efficient and low-power processing compared to traditional digital microprocessors.

From the past decade, the advent of paradigms such as digitalization, the IoT,[9] and Industry 4.0 has revolutionized the requirements for sensors and smart devices, emphasizing the need for high power efficiency while keeping the manufacturing costs low. Additive manufacturing technologies have experienced increasing adoption to engineer smart devices with customized properties for electronic applications.[10]

The integration of IoT into every aspect of our lives such as healthcare, transportation, construction, leisure, and sports has accelerated the transformation of everyday objects into smart objects. Semiconductors, sensors, and related electronics are needed for this transformation, but they are difficult to recycle or to provide a second life to the constituent materials. While the addition of intelligence into daily-use devices is appealing and assists in the digitization of the physical world, it also inadvertently reduces their lifespan and significantly contributes to the global electronic waste problem.[11] Global production of e-waste is massive as a result of the effects of digital transformation and consumer behavior.[12] For instance, in 2018, ≈53.6 Mt of e-waste was generated, with an increasing rate of 2 Mt per year. To highlight the extent of the issue, it is estimated that 20–25% of e-waste is legally recycled, with the remaining 75–80 percent being dumped into the environment or sent illegally to developing nations.[13]

Printed electronics, an additive manufacturing category, allows high volume production of thin and flexible electronic devices at low cost.[14] The technology allows the massification of various IoT that offer advanced functionality in an embedded and highly distributed fashion.[14a,15] More importantly, it allows minimization of energy consumption during manufacturing, reduced use of hazardous substances, improvement of recyclability, and decrease the material waste generated, contributing to a more sustainable, greener economy.

Printed electronics (PE) have become an established competitive technology particularly in display technology. As representative examples, a 31-inch flexible inkjet printed OLED TV has been presented at CES 2020, TCL-CSOT (Guangdong Juhua Printed Display Technology Ltd. Co, TCL CSOT & TCL Corporate Research).[16] In 2023, TCL-CSOT stated that OLED displays will be produced by the inkjet printing process in the second half of 2024.[17] The latest market report published by Visiongain[18] suggests that printed electronics have a global market cap of US$10.88 billion in 2023 and is projected to grow at a compound annual growth rate of 15.5% during the next 10 years. As shown in **Figure 1**, over the past two decades, significant progress has been achieved in printed electronics, namely by the advent of aerosol jet printing (AJP) and Electrohydrodynamic printing (EHD) in the late 1990s and early 2000s and the maturation of inkjet printing. This progress in printing technology allowed the opportunity for the deposition of patterned thin films. The first printed memristor was reported in 2012, 4 years after the advent of the memristor, in Hewlet-Packard's (HP) labs. At present, printed memristors started to be applied in diverse applications from neuromorphic circuits to encryption circuits.[19]

The engineering potential of circuit design greatly expands with the maturation of printed memristors. Printing techniques allow large-area multi-layer systems, making it possible to fully print 3D circuits.[20] Hence memristors can be integrated into sensors as in signal processing block or as a sensing component.[21] In the case of printed memristors, it has great potential in flexible electronics to be applied in skin electronics.[22] And so, over the last years, since the publication of the first printed memristor, it has been explored new materials and manufacturing optimization to achieve robust memristive devices.

This review provides a perspective on the potential of P in the fabrication of memristive devices. It is divided into three main sections: the first section presents an overview of the main printing techniques, most suitable for memristors development. Next, the materials used for the switching layer are presented by comparing their performance. Finally, the application of the printed memristors is highlighted, as well as the main challenges and opportunities that printed memristors are expected to face in the following years.

2. Overview of Printing Technologies Used for Memristors

When it comes to making electronic devices, deciding between printing and traditional lithography is crucial, as each method has its own set of strengths and limitations. Photolithographic processing, a subtractive technique widely used in microelectronics, requires many steps, being suitable for patterning small areas.[32] The substrates are exposed to corrosive etchants, use high-energy radiation, and relatively high temperatures during processing. Therefore chemical, radiation, and temperature sensitive substrates are incompatible with photolithographic processing.[33] On the other hand, printing technologies allow a wide variety of substrates, including naturally derived polymers and large-area deposition. Naturally derived polymers are abundant materials originated from living matter.[34] Several natural polymers, including alginate,[35] cellulose,[36] chitin,[37] collagen,[38] keratin,[39] and silk,[40] have been employed as substrates due to biocompatibility, mechanical properties, biodegradability, and renewability.[41]

Table 1 provides an overview of different printing technologies used for the manufacture of printed devices.

Printing technologies are divided into two main categories: contact and contactless techniques. As the name suggests, a contactless printing method avoids making direct physical contact with the substrate, which can be useful when working with substrates or carrier materials that are sensitive. Generally, non-contact printing techniques are droplet-based such as aerosol jet printing, inkjet printing, and EHD inkjet. These methods can be broadly described as computer-controlled, non-contact pattern reproduction methods that implement droplet deposition of ink on a substrate.[42b] Furthermore, these methods make use of digital printing technologies, which make it easier to edit or refine the design because the desired printing pattern is transferred straight from a computer file or data stream to a printing machine. Conversely, contact-printing techniques like screen printing, reverse offset printing, and gravure printing require direct physical contact with the substrate through pressure, which

© 2024 The Author(s). Advanced Electronic Materials published by Wiley-VCH GmbH

2199160x, 2024, 10, Downloaded from https://advanced.onlinelibrary.wiley.com/doi/10.1002/aelm.202400212 by Universidade Do Minho, Wiley Online Library on [20/04/2026]. See the Terms and Conditions (https://onlinelibrary.wiley.com/terms-and-conditions) on Wiley Online Library for rules of use; OA articles are governed by the applicable Creative Commons License

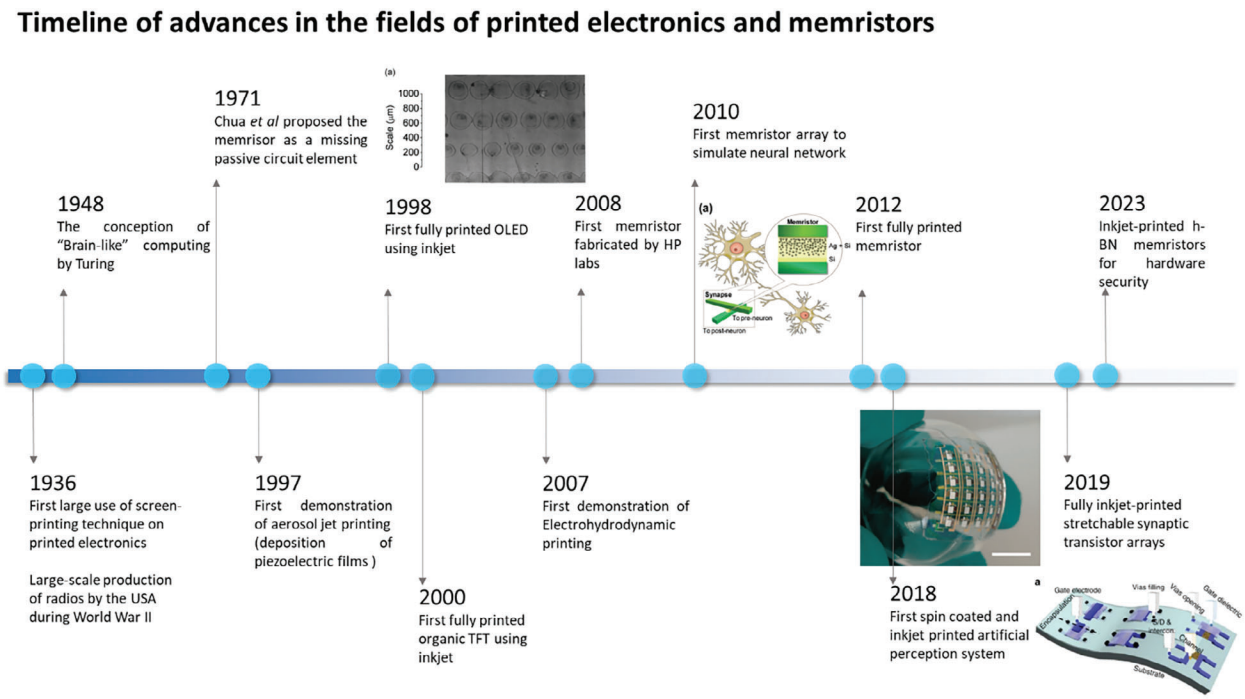


Figure 1. Timeline of significant breakthroughs in PE and computation related to memristors. Back in 1936 the screen-printing technique was adapted from the clothing industry to produce radio components on a large scale for the US military. In 1948, Touring first introduced the concept of "brain-like" computing. The memristor was conceptualized in 1971 by Chua as the fourth elemental passive circuit component.[4] Only in the late 1990s started to have significant breakthroughs in printing technology. The first demonstration of aerosol jet printing occurred in 1997 by printing piezoelectric Pb(Zr, Ti)O_3 thick films on Pt/Cr/SiO_2/Si substrates.[23] In 1998, Hebner et al. printed the first OLED. In this work, inkjet printing was used to deposit patterned luminescent doped polyvinylcarbazol films. Reproduced with permission.[24] Copyright 1998, AIP Publishing. Two years later, the first fully printed thin film transistor (TFT) was reported, based on organic polymers.[25] In 2007, electrohydrodynamic jet printing was demonstrated, achieving 1 µm of resolution.[26] In 2008, it started the advent of the memristor. The first simple physical model and a simulated IV characteristics of a memristor was presented.[27] Two years later the use of Ag-doped amorphous silicon memristor was developed to simulate synaptic plasticity, showing the potential of memristor in artificial synapse. Reproduced with permission.[28] Copyright 2010, American Chemical Society. The first fully printed memristors using metal oxides as the switching layer were published in 2012.[29] In recent years, PE did another leap forward into printed systems. In 2018 an ultra-flexible organic synapse transistor array was fabricated through inkjet printing and integrated into an artificial visual-perception system which can mimic retinal function. Reproduced with permission.[30] Copyright 2018, Wiley-VCH. In the following year, fully inkjet-printed stretchable and low voltage synaptic transistor arrays were developed for neuromorphic computing. Reproduced with permission.[31] Copyright 2019, Springer Nature. Currently fully printed h-BN memristors were developed for data encryption.[19]

limits the range of substrate materials that can be used.[42c] Furthermore, most contact printing methods require a master template, which raises the initial costs associated with stencil production or screen mask. This greatly diminishes the versatility to perform rapid adjustments to the original design. Although the drawback in making rapid design changes, the majority of contact printing techniques allow for low-cost, high-throughput true roll-to-roll (R2R) manufacturing.[47] The ensuing subsection will address various printing techniques and technologies related to PE manufacturing and applied in memristive devices.[42c]

Table 1. Overview of different printing technologies for manufacturing of electronic devices.

	Aerosol Jet	Electrohydrodynamic printing (EHD) inkjet	Inkjet (DoD)	Gravure	Reverse offset	Screen printing
Printing resolution [µm]	10–100	0.04–500	15–100	5–200	1–50	20–100
Layer thickness [µm]	0.1–5	0.01–0.5	0.01–0.5	0.1–8	0.04–2	3–30
Printing speed [m min^{-1}]	0.6–1.2	0.1–3	0.02–5	20–1000	0.06–15	0.6–100
Digital technique	Yes	Yes	Yes	No	No	No
Film roughness	Low	Low	Low	Low	Low	High
Material waste	Minimum	Minimum	Minimum	Yes	Yes	Yes
Substrate interaction	Non-contact	Non-contact	Non-contact	Contact	Contact	Contact
References	[42]	[11a,43]	[11a,42c]	[44]	[42c,45]	[11a,42c,46]

© 2024 The Author(s). Advanced Electronic Materials published by Wiley-VCH GmbH

2199160x, 2024, 10, Downloaded from https://advanced.onlinelibrary.wiley.com/doi/10.1002/aelm.202400212 by Universidade Do Minho, Wiley Online Library on [20/04/2026]. See the Terms and Conditions (https://onlinelibrary.wiley.com/terms-and-conditions) on Wiley Online Library for rules of use; OA articles are governed by the applicable Creative Commons License

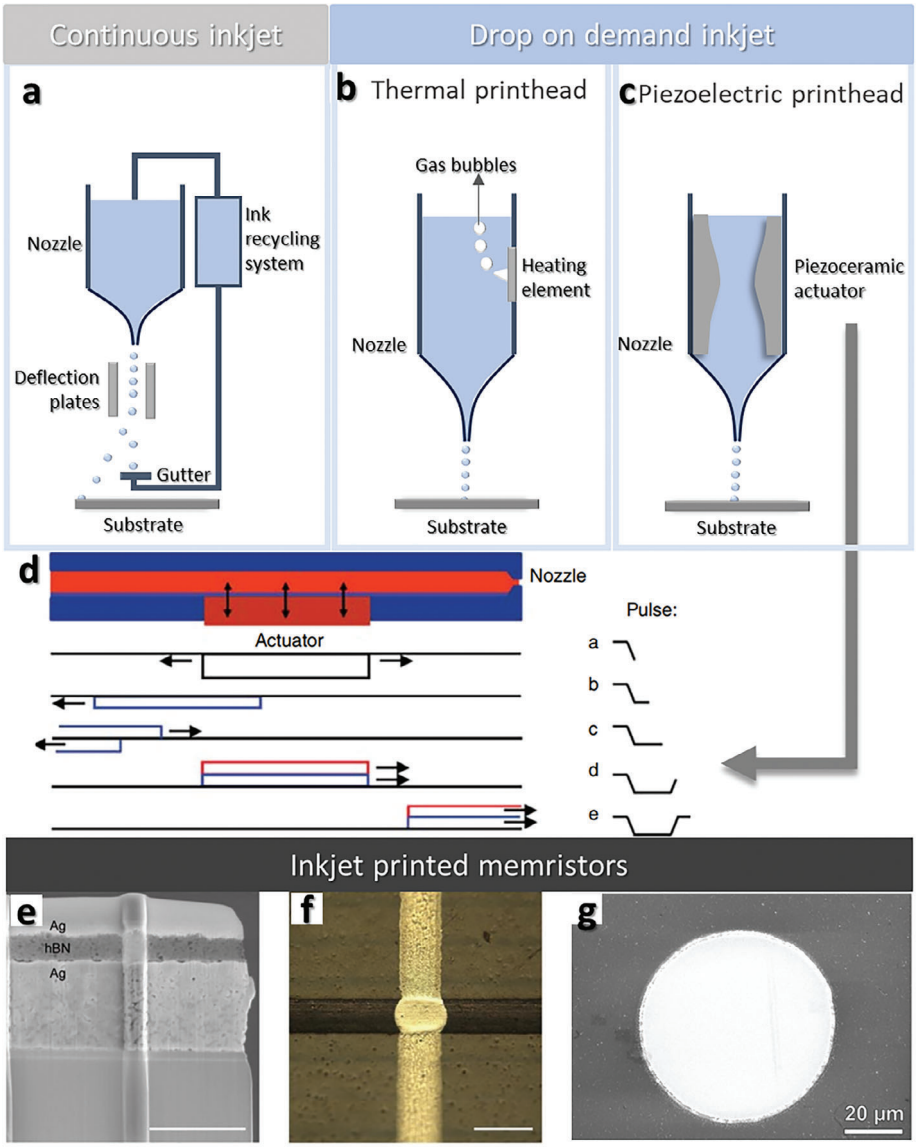


Figure 2. Schematic diagrams depicting a) CIJ printhead, b) thermal DoD printhead, and c) piezoelectric DoD printhead. d) Actuation principle of a piezoelectric DoD inkjet system. Reproduced with permission.[53] Copyright 2015, Wiley-VCH. Microscopic images of the hBN memristors: e) Cross-sectional scanning electron microscopic image and f) optical microscopic image of Ag/hBN/Ag device fabricated by fully-inkjet-printing. Reproduced with permission.[54] Copyright 2023, Wiley-VCH. f) Top-view SEM image of the inkjet-printed Ag/h-BN/Pt memristor. Reproduced with permission.[19] Copyright 2023, Royal Society of Chemistry.

Furthermore, the requirements to print robust memristors will be described by focusing on the most suitable printing techniques for the fabrication of memristors.

2.1. Inkjet Printing

Inkjet printing is a non-contact method based on depositing numerous ink droplets onto a substrate.[42b,48] The droplets, typically have a diameter between 9 and 50 µm,[42b] is manipulated under digital control. An inkjet system comprises a digitally controlled printhead that projects ink droplets. While research inkjet printers usually have one printhead, industrial versions use multiple printheads with hundreds to thousands of integrated micronozzles, largely increasing the throughput.[49]

Inkjet printers are categorized into continuous inkjet (CIJ) and drop-on-demand (DoD) inkjet. The working principle of jet formation in inkjet printing, was initially studied by Savart in 1833 and quantitatively analyzed by Rayleigh in 1879, who demonstrated that the most rapidly growing disturbance in the jet, and thus the distance between the centers of the resulting drops, was about 4.5 times the jet's diameter (known as Rayleigh breakup).[50]

In CIJ (**Figure 2a**), a continuous stream of droplets is ejected by the nozzles. The droplets are steered by a deflection system, which generates an electrostatic field. When the droplets pass

 © 2024 The Author(s). Advanced Electronic Materials published by Wiley-VCH GmbH

2199160x, 2024, 10, Downloaded from https://advanced.onlinelibrary.wiley.com/doi/10.1002/aelm.202400212 by Universidade Do Minho, Wiley Online Library on [20/04/2026]. See the Terms and Conditions (https://onlinelibrary.wiley.com/terms-and-conditions) on Wiley Online Library for rules of use; OA articles are governed by the applicable Creative Commons License

through the deflection plates, they are directed toward the substrate or, if not needed, toward a recycling system.[51] In the field of PE, the continuous mode is not used very often, as the exposure of droplets to environmental conditions and subsequent recycling may contaminate the ink.[48a] In DoD inkjet systems, each printhead has an array of nozzles, and the relative motion of the drop and substrate, the timing of the drop ejection, and the selection of the right nozzle from the array all affect where the drop lands on the substrate. To create the pressure pulse required to eject an ink drop, most modern DoD printers either use the deformation of a piezoelectric ceramic element or the expansion of a tiny vapour bubble created by a small electric heating element on the liquid. Thermal printheads (Figure 2b), which are limited to inks containing volatile solvents, can be more easily and affordably manufactured than piezoelectric printheads, which have the capacity to handle a broader variety of liquids.[52] Piezoelectric DoD machines (Figure 2c) are widely used in research and industry.

A piezoelectric DoD's operating principle is illustrated in Figure 2d and is covered in great detail in ref. [53]. It is possible to alter the drive waveforms to suit printing fluids with various properties. An electric voltage is applied to fire a droplet, and the inverse piezoelectric effect causes the channel cross section to distort. Pressure waves are created inside the channel as a result. Pressure waves travel in the direction of the channel and become reflected when the channel's characteristic acoustic impedance varies.

The piezo element's charging ((a) in Figure 2d) expands the channel cross-section, leading to a negative pressure wave that reflects at the left reservoir. b) This large reservoir serves as an open end, causing the acoustic wave to return as a positive-pressure wave (c). The piezo element's discharging shrinks the channel cross-section back to its initial size, amplifying the positive pressure wave when synchronized with the acoustic wave's travel time (d). The channel structure and driving pulse are engineered to achieve a substantial incoming positive pressure peak at the nozzle (e), propelling the ink through the nozzle. The ink's acceleration in the nozzle's small cross-section (due to mass conservation and incompressibility) culminates in drop formation.[53]

Inkjet is widely used in fully printed memristors achieving device area down to 50 um^2[54] (Figure 2e–g). The main strengths of inkjet printing consist of the flexibility of patterned design, manage to print thin films up to 10 nm of thickness with low roughness, low consumption of inks and minimal waste generated during printing, precise control of the drops and printing large areas using compact set-ups. However, inkjet printing faces some drawbacks: the inks are typically expensive, strict requirements when producing an inkjet ink, nozzles get often clog when using particle-based inks, very sensitive to the interaction between the ink and the substrate (e.g., coffee ring effect) and low throughput when using a single printhead (industrial systems with multiple parallel printhead increase printing speed).

2.2. Electrohydrodynamic Inkjet Printing

EHD inkjet printing started as an advancement of inkjet printing in terms of resolution. Inkjet printing technologies have its lateral resolution limited by the nozzle size. Further decreasing the nozzle size is not a viable approach. At first, a reduced nozzle orifice would have a negative impact on the jetting process because the viscosity and surface tension of the ink make it harder to force droplets out. Moreover, printing with particle-based inks may become unreliable due to clogging, which can be challenging to resolve with inks containing solid content, such as nanoparticles (NPs) or nanowires.[55] By creating an electric field between the nozzle and the substrate, EHD printing solves these problems by drawing ink out rather than pushing it out (**Figure 3a**).

EHD inkjet printing has undergone significant research over the past two decades, mainly due to the advent of solution electrospinning[59] and the possibility of achieving sub micrometre of lateral resolution. Choi and Smith patented this method in 1998, allowing for the printing of coloured inks with a resolution of up to 20 μm.[42b] Rogers et al. used this method for PE in 2007.[26]

Broadly, the components of an EHD printing system are: a camera system for visualizing the ink flow to monitor the jetting behavior and imaging the printed patterns; a nozzle; a substrate stage positioning system; a high voltage supply; and an ink supply system that produces back pressure.[60] When the electric field force is greater than the ink's surface tension force, droplets are produced. After that, ink is supplied to the nozzle's tip to create a hemispherical meniscus.

Depending on the presence of mobile charge carriers in the ink, the ionic components will move to the meniscus surface. The number of charge carriers per unit volume and their drift velocity determine the ink's conductivity.[43c] An electrostatic potential forms between the meniscus and the grounded substrate after a significant amount of charge has accumulated on the ink interface. Since inks are typically not perfect conductors, the resulting electrical stress has a normal and tangential component.[61] The tangential component promotes the meniscus's formation into a cone, known as a Taylor cone,[62] and the normal stress destabilizes the meniscus, causing jetting. When the electrostatic stress rises above this equilibrium, a jet of ink is ejected.[42c]

The speed and form of the produced droplets are influenced by the applied voltage. Drop volumes in the attoliter range can yield very high resolutions.[42c] The "neck-down" ratio, which is the ratio of the inner nozzle diameter to the drop diameter, varies from roughly 10 in conventional systems to 10^3 in highly optimized systems.[63] Furthermore, the two key variables that control the drop size and jetting mode are the applied voltage and the ink flow rate.[56]

At a lower electric field strength, the "dripping" mode takes place, where large-volume droplets are propelled by gravitational pull.[64] For high-resolution printing, the recognizable EHD cone-jet is preferred (Figure 3b). It can be accomplished by creating a constant Taylor cone by strengthening the electric field while decreasing the flow rate.[60] Further increases in voltage cause a complex jetting behavior that eventually results in an atomization or spray mode characterized by numerous, uncontrollable jets.[64] Since most of the substrates in PE are isolators, it builds charges on the substrate causing distortions of the electric field and consequently misallocating drops. Employing an alternating current (AC) electric field allows the use of insulating substrates without any misplacement of drops.[64–65]

© 2024 The Author(s). Advanced Electronic Materials published by Wiley-VCH GmbH

2199160x, 2024, 10, Downloaded from https://advanced.onlinelibrary.wiley.com/doi/10.1002/aelm.202400212 by Universidade Do Minho, Wiley Online Library on [20/04/2026]. See the Terms and Conditions (https://onlinelibrary.wiley.com/terms-and-conditions) on Wiley Online Library for rules of use; OA articles are governed by the applicable Creative Commons License

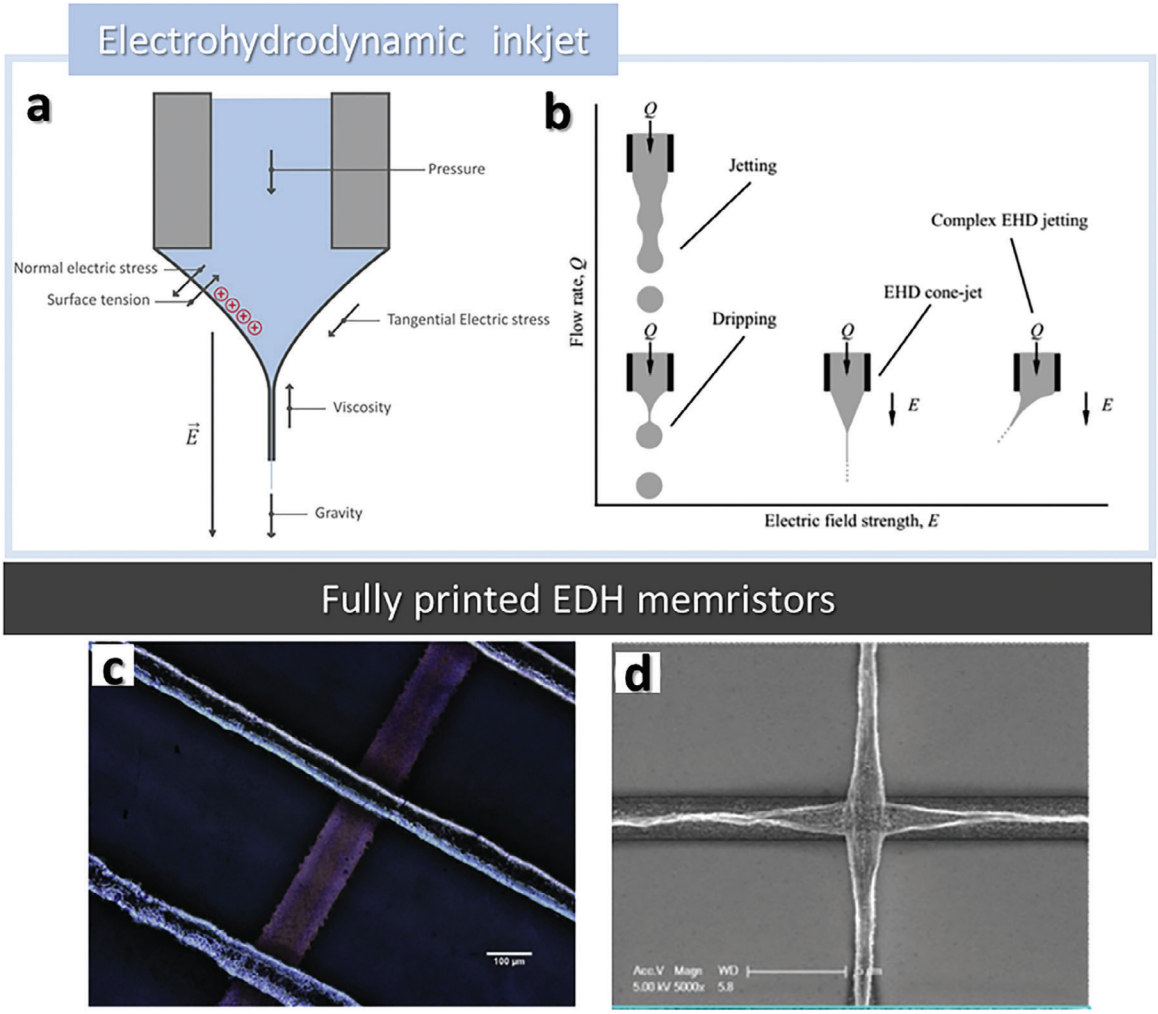


Figure 3. Principles of EHD inkjet. a) Schematic illustration of drop-formation in EHD printing and representation of the forces that act on the ink. Reproduced with permission.[42c] Copyright 2023, Wiley-VCH. b) Different printing modes in EHD printing dependent on the flow rate (Q) and electric field strength (E). Reproduced with permission.[56] Copyright 2007, Cambridge. c) microscopic image of the fabricated memristor crossbar structure, portraying three top silver and one bottom Cu electrodes. The transparency of ZnO active layer is clearly noticeable by the crisp image of the bottom electrode. Reproduced with permission.[57] Copyright 2013, Elsevier Ltd. d) SEM images of two perpendicular Cu nanowires. Reproduced with permission.[58] Copyright 2016, Wiley-VCH.

Figure 3c,d shows examples of fully printed memristors using the EHD printing. The smallest printed memristors crossbars were fabricated using the EHD technique, achieving an area of $6 \times 6\ \mu m^2$ employing an silver (Ag)/nafion/ gold (Au structure[58] and $80 \times 80\ nm^2$ for nanowire EHD (NW-EHD) printing[66] (Figure 3d). Using an inorganic-nanowire-digital alignment technique, the fabrication of 2D arrays of individually conductive, perpendicularly aligned copper (Cu)nanowires with a nanometer-scale Cu_xO layer sandwiched at each cross point was subsequently reported.

Generally, inks with viscosities up to 10 000 cP can be printed, allowing a wide range of inks: from liquids, nano- and microparticles,[26,67] nanowires,[43d,68] to molten metal.[69] When creating the ink for high-resolution printing, the rheological characteristics must be taken into consideration.[70] The nozzle to substrate surface distance should be as small as possible, usually between 0.05 and 1 mm, in order to ensure high accuracy in the drop placement. With EHD, it allows high aspect ratio printing, achieving 40 nm of lateral resolution.[43d] Also, it is one of the most economical manufacturing techniques available. Yet, there are still challenges for EHD, such as multi-nozzle implementation of EHD printing to improve throughout.[71] Practical implementations are still severely limited by the cross-talk between the nozzles. Consequently, a nozzle pitch of at least 2 mm is necessary.[72] Additionally, when using multiple nozzles, the asymmetric electric field created by the cross-talk between the individual jetting streams lowers the quality of the print.[42c]

2.3. Aerosol Jet Printing

The Mesoscale Integrated Conformal Electronics (MICE) project in the late 1990s recognized the need for appropriate direct-write

© 2024 The Author(s). Advanced Electronic Materials published by Wiley-VCH GmbH

2199160x, 2024, 10, Downloaded from https://advanced.onlinelibrary.wiley.com/doi/10.1002/aelm.202400212 by Universidade Do Minho, Wiley Online Library on [20/04/2026]. See the Terms and Conditions (https://onlinelibrary.wiley.com/terms-and-conditions) on Wiley Online Library for rules of use; OA articles are governed by the applicable Creative Commons License

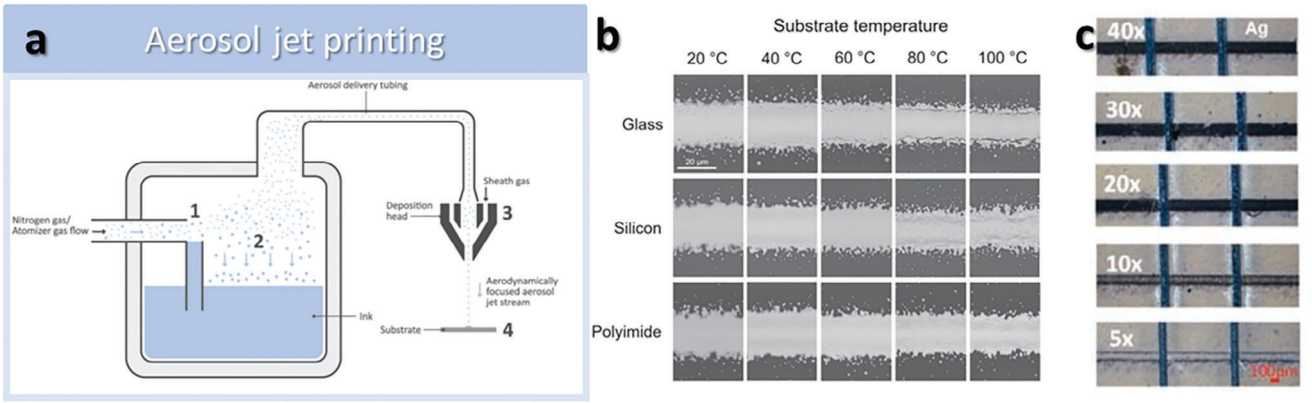


Figure 4. a) Working principle of a compressor nebulizer aerosol jet printer: 1) Atomization of the liquid content; 2) large aerosol are sorted out due to gravity; 3) focusing of aerosol jet due to sheath gas; and 4) deposition on the substrate. Reproduced with permission.[42c] Copyright 2023, Wiley-VCH. b) The influence of substrate temperature on aerosol jet printing of Ag nanoparticle ink for three different substrate materials with the occurrence of overspraying at high temperature. Reproduced with permission.[78] Copyright 2017, IOP Publishing Ltd. c) Printed Ag lines (blue) and MoS_2 lines (black) with 5,10, 20, 30, and 40 printing passes. Reproduced with permission.[79] Copyright 2019, Wiley-VCH.

processes due to the wide range of applications.[73] This resulted in the development of various deposition mechanisms, such as Aerosol Jet and Nanojet systems. AJP emerged in 2001–2002,[74] bringing new capabilities to direct write printing via a directed aerosol stream, allowing for consistent deposition at nozzle-substrate offsets of 1–5 mm.[75]

This method makes it possible to pattern complex surfaces regardless of their shape.[42a] This flexibility facilitates patterning on surfaces inaccessible to physical nozzles, eases control over less precise articulation, and is desirable for assistive manufacturing technologies meant to be used in larger, hybrid manufacturing processes. When compared to alternative direct write technologies, this combination significantly streamlines process integration.

In AJP (**Figure 4a**), the ink is aerosolized and carried via N_2 gas. The droplets that make up the aerosolized ink have a diameter ranging from 2.5 to 5 μm.[76] With this system, it is possible to print feature sizes as small as 10 μm.[71] AJP, as opposed to inkjet printing, allows for a greater range of ink viscosities, from 1 to 2500 cP,[71] facilitating the printing of a wide range of different inks using a single technology. Unlike inkjet or any contact technique, AJP enables printing onto a variety of nanomaterials and surfaces, including patterning biological materials at the nanoscale and placing them onto intricate 3D geometries.[76–77]

In comparison to other droplet-based techniques (inkjet and EHD), there are a few challenges in AJP. One of the difficulties is the nozzle's overspraying, which causes the material to be deposited in spots outside of the printed traces and reduces the lateral resolution[78] (Figure 4b). Another problem with using nanoparticle inks is that the flow of the carrier gas greatly accelerates the evaporation of solvents. The physical and rheological characteristics of the ink are altered by drying, necessitating adjustments to the printing parameters and causing sludge to accumulate at the bottom of the ink container.[42c] There are a few reports that used fully AJP memristors.[79–80] Figure 4c shows an example of fully printed MoS_2 memristors.[79]

2.4. Screen Printing

One of the most popular deposition methods for printing electronics is screen printing, which uses screen masks to deposit materials onto large-area substrates. Because of its ease of use, scalability, environmental friendliness, and high throughput, this technique holds great promise for low-cost mass production of large-area electronics.[81]

During World War II, this method was first used in the PE field to mass-produce radio circuitry.[82] It was particularly good at depositing thick conductive materials with patterns that effectively transferred power with little to no voltage loss. This made it the perfect substitute for physically routing wires, especially for wartime electronics production.[83]

The operation of a screen-printing machine (**Figure 5a**) involves filling the open mesh areas with ink, facilitated by the motion of a squeegee. In the reverse motion, the ink is transferred onto the substrate surface under a specific squeegee force. Shearing stress is created in the ink and its viscosity is reduced as soon as the squeegee makes contact with it. Through a mesh's openings, the ink is carefully transferred and deposited onto a substrate. To specify the geometry of the printed pattern, a mask, or stencil, with patterned features is utilized.[83] In order to create a printing screen, the proper mesh apertures of a regular stencil are blocked off using a photo emulsion layer.[76] Alternative techniques, such as creating openings on a thinned silicon wafer via photolithography, can be used to create higher-resolution masks.[76,84]

To enable high-precision printing of fine line grids even at high printing velocities, advanced screens, and highly effective metallization pastes have been developed.[46,88] The most adopted strategy is the adoption of finer meshes with a decrease in wire thickness and an increase in mesh count (wires per inch), making it possible to print up to 20 μm of lateral resolution[46] (Figure 5b).

The viscosity of the ink is a critical parameter to regulate. It should be low enough to allow for easy flow through the mesh when the shearing stress is applied, but high enough to maintain its form when the shearing stress is removed and prevent

© 2024 The Author(s). Advanced Electronic Materials published by Wiley-VCH GmbH

2199160x, 2024, 10, Downloaded from https://advanced.onlinelibrary.wiley.com/doi/10.1002/aelm.202400212 by Universidade Do Minho, Wiley Online Library on [20/04/2026]. See the Terms and Conditions (https://onlinelibrary.wiley.com/terms-and-conditions) on Wiley Online Library for rules of use; OA articles are governed by the applicable Creative Commons License

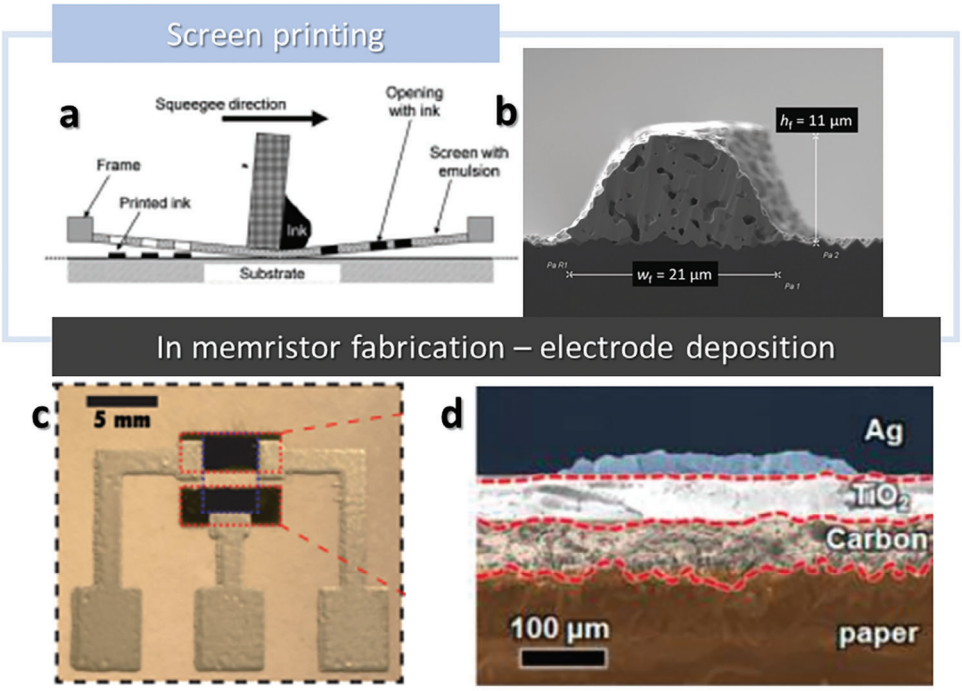


Figure 5. a) Schematic of screen-printing technique. Reproduced with permission.[271] Copyright 2009, Elsevier Ltd. b) SEM images of high-resolution screen printed Ag structure with a nominal contact finger width of 20 µm. Reproduced with permission.[46] Copyright 2022, Elsevier Ltd. c) Schematic of the p6DTP-based three-terminal synaptic device. Reproduced with permission.[86] Copyright 2023, Wiley-VCH. d) Cross-sectional SEM image of the Ag/TiO_2/C paper-based memory. Reproduced with permission.[87] Copyright 2014, American Chemical Society.

lateral flow. Viscosities in the range of 500–5000 cPs are considered ideal for this method.[42c] That means the inks have a high load content and often need a binder to increase the viscosity of the ink. Other parameters such as substrate, printing speed, mesh opening, squeegee angle, and pressure greatly influence the final dimensions of the printed structures. Potts et al. have shown in conductive carbon paste that high printing speeds decrease the viscosity of the ink.[89] As the printing speed is increased, there is a general decrease in the amount of ink deposited, and line resistance tends to increase. The printed dimensions of the line are greatly influenced by screen optimization. Tepner et al. looked into the relationship between the rheological behavior of commercial Ag-pastes used for the front-side metallization of solar cells and the screen-printed geometry of Ag-electrodes.[90] A reduction of the screen opening width causes a diminished cross-sectional area of the printed structure, thus restraining the lateral conductivity. So far, no study has been performed on how the high roughness inhered of the screen-printing process affects uniformity and, consequently, device-to-device variation.

Compared to droplet-based techniques, screen printing enables thicker layers with high throughput and easy scalability due to its compatibility with R2R process. Furthermore, nozzle-based printing techniques' frequent clogging issues are avoided with screen printing. Unlike digital printing technologies which is quick and cost-free to change the design, screen printing requires the fabrication of a patterned screen. Also, due to the contact of the screen with the substrate, the film rugosity is high. Its overall characteristics make screen printing the most used technique for printing passive circuit components like resistors, capacitors, and inductors as well as interconnects circuits.[85,91] In memristor fabrication it is used as the electrode deposition (Figure 5d,e).[87,92]

2.5. Gravure Printing

Gravure printing is a contact technique that is scalable, offers micron-scale resolution, and contrasting with screen-printing technique, generates high-quality, low-roughness patterns.

In gravure printing, the design elements are engraved onto the printing cylinder's surface, made from metals such as Cu with a chromium coating,[44c] while the non-image areas stay at the initial level.[11a] Within a partially filled ink fountain, the engraved printing cylinder revolves (**Figure 6a**). The entire surface of the cylinder collects ink from the fountain, where any excess is removed with a doctor blade from the non-image areas, leaving the ink in the engraved cells. The ink is then transferred directly from the cells to the substrate in a printing nip while under pressure. The ink transfer can be improved by using an electrostatic assistance system (ESA), which produces an electric field across the nip.[11a] The ink is lifted from the cells and onto the substrate with the help of the electric field. Lastly, hot air is used to evaporate the solvent, drying the printed layer.

Since gravure printing provides roll-to-roll deposition of functional materials with a lateral resolution of up to 5 µm[93] and

© 2024 The Author(s). Advanced Electronic Materials published by Wiley-VCH GmbH

2199160x, 2024, 10, Downloaded from https://advanced.onlinelibrary.wiley.com/doi/10.1002/aelm.202400212 by Universidade Do Minho, Wiley Online Library on [20/04/2026]. See the Terms and Conditions (https://onlinelibrary.wiley.com/terms-and-conditions) on Wiley Online Library for rules of use; OA articles are governed by the applicable Creative Commons License

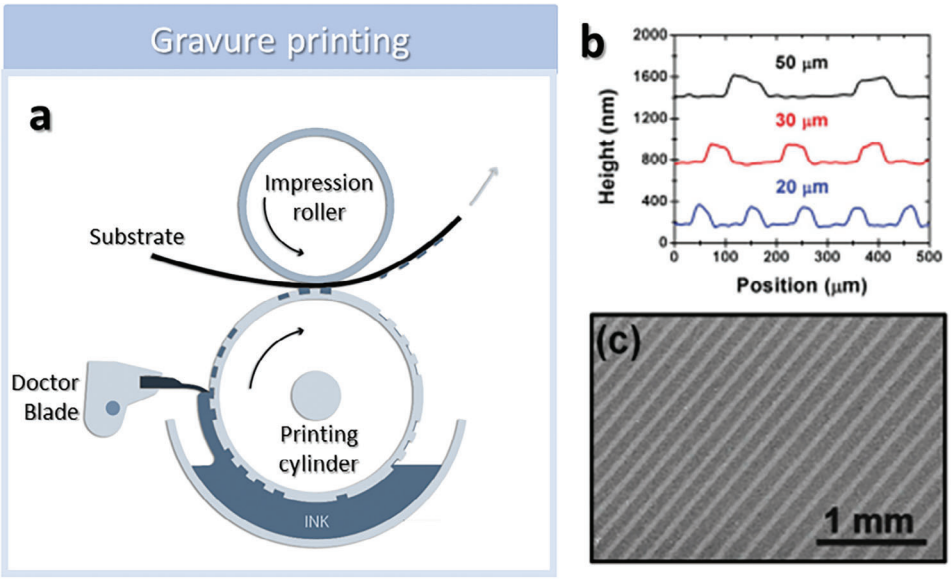


Figure 6. a) Schematic of gravure printing. b) Line height profiles measured by optical profilometry. c) Large area scanning electron micrograph of printed lines. Reproduced with permission.[93] Copyright 2014, Wiley-VCH.

high speed of up to 1 km min^{-1},[11a] it is a promising option for PE (Figure 6b,c), great for mass production of thick films. However, gravure printing is not recommended for design optimization by the fact the production of a printing cylinder, usually laser engraved, which is costly and time consuming.[11a] Gravure printing was employed to fully print an organic electrochemical memristor.[94]

2.6. Reverse Offset

Reverse offset printing (ROP) is a high-precision R2R-compatible printing technique.[95] The idea was first presented in 1980 and has since undergone significant development.[96]

The steps in the ROP process can be outlined as follows, as shown in **Figure** 7a. The coating step is the first step. A coater

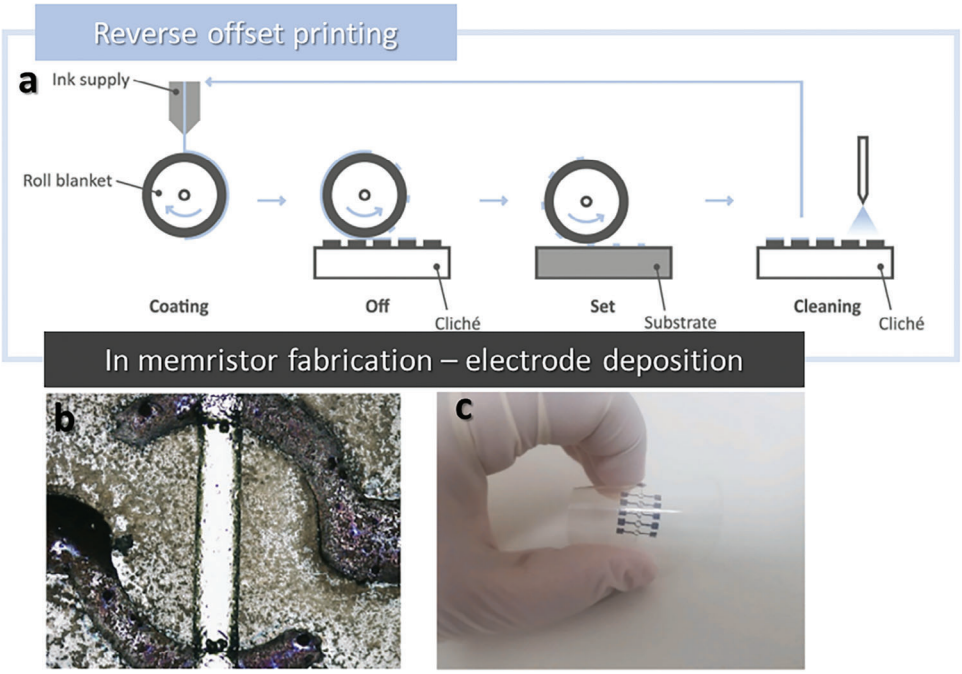


Figure 7. a) Schematic principle of roll-to-sheet reverse offset printing. Reproduced with permission.[42c,98] Copyright 2023, Wiley-VCH. b) microscopic image of the Ag top and bottom electrodes sandwiching the EHD deposited composite SrTiO3/PVA thin film and c) image of the actual all printed flexible resistive switching device. Reproduced with permission.[99] Copyright 2020, Elsevier Ltd.

 © 2024 The Author(s). Advanced Electronic Materials published by Wiley-VCH GmbH

2199160x, 2024, 10, Downloaded from https://advanced.onlinelibrary.wiley.com/doi/10.1002/aelm.202400212 by Universidade Do Minho, Wiley Online Library on [20/04/2026]. See the Terms and Conditions (https://onlinelibrary.wiley.com/terms-and-conditions) on Wiley Online Library for rules of use; OA articles are governed by the applicable Creative Commons License

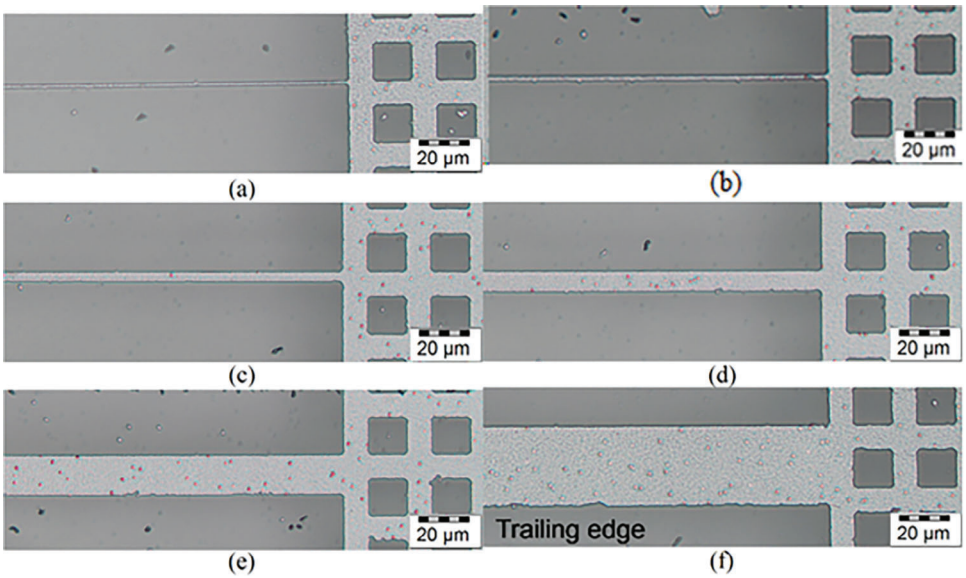


Figure 8. Light microscopy images of printed lines of the sample RO1. The width of the lines is a) 1, b) 2, c) 4, d) 8, e) 16, and f) 32. Printing direction is from up to down such that the trailing edge is the lower edge of the line. Reproduced with permission.[95a] Copyright 2018, IOP Publishing Ltd.

applies an ink with a viscosity ranging from roughly 20 000 to 1 000 000 cP to a polydimethylsiloxane (PDMS) sheet, also known as a blanket. After that, the ink is left to rest for a period of time that can range from a few seconds to thirty seconds, which allows it to become semi-dried.[97] Step two is called the "Off-Step". To remove extraneous ink portions from the PDMS, the semi-dried ink layer is in contact with a relief called a cliché. Rectangular cross-sectional shapes are preserved in the pattern on the PDMS as a result of the complete transfer of ink sections that come into contact with the cliché surface without leaving any deposits behind. This phenomenon happens because the ink has sufficiently hardened to withstand deformation brought on by the Laplace pressure after pattern generation, squeeze flow, and in-plane cohesive failure during the transfer. For the ink surface to retain the proper tackiness against the cliché and the target substrate, it must stay slightly wet (semi-dried).[97] If the layer is completely dried, the ROP process becomes unfeasible as the surface loses its tackiness. Furthermore, the coating process determines the final pattern's thickness, so it stays constant throughout the procedure. This produces a consistent pattern thickness across all pattern shapes, a characteristic that cannot be achieved with other printing techniques.[97]

Lastly, the remaining ink on the PDMS, which corresponds to the cliché's engraved area, is transferred to the substrate by contact. To be used again in a later procedure, the leftover ink on the cliché needs to be cleaned with the respective solvent.[97] Similar to screen printing ROP is used in electrode deposition in memristors (Figure 7b,c).[99–100]

During the past decades, scientific efforts have been dedicated to improving the ROP process. The overall quality of this technique was enhanced by the precision of the placement,[101] managing the transfer of ink,[102] the surface energies,[103] and the materials that were utilized.[45a] Even so, processing speed has increased while associated processing costs have decreased, ROP is still a slower and an expensive technique compared to screen-printing. The creation of clichés is one area where cost savings are possible. It is typically produced using photolithography or nanoimprint lithography, making the manufacturing of the cliché cost-intensive.[45b] A R2R-imitating reverse offset printing method that can achieve 1 µm of lateral resolution was developed by Sneck et al. and tested at a laboratory scale[95a] (**Figure 8**).

2.7. Overview on printed techniques used for memristor fabrication

One of the many promising features of memristors is their small area. Additionally, reduced device area of the memristor implies smaller parasitic capacitance, and consequently decreasing the switching time[104] and improving its electrical characteristics.[105] Therefore, high-resolution additive techniques are very promising for memristor fabrication. Nevertheless, another aspect needs to be taken into consideration when selecting the most appropriate printing technique. Printing thin films with low film roughness are key aspects of avoiding pinholes and improving yields.[106]

Printing technologies are unsuitable for high-density circuits with nanometer-scale feature sizes, which are common in today's most advanced digital integrated circuits.[42c] The state-of-the-art lithography methods will always be a further step ahead in minimum feature size than the state-of-the-art printed electronic equipment of today (**Figure 9**).

Despite PE not being well-suited for high performance circuits such as analog to digital converters, signal processing and transmission applications, numerous opportunities exist for the advancement of PE.[85] The possibility of large area deposition with high throughput on any substrate, shows great potential on sensors,[107] signal amplifiers[108] and filters,[109] and on display technology[110]

© 2024 The Author(s). Advanced Electronic Materials published by Wiley-VCH GmbH

2199160x, 2024, 10, Downloaded from https://advanced.onlinelibrary.wiley.com/doi/10.1002/aelm.202400212 by Universidade Do Minho, Wiley Online Library on [20/04/2026]. See the Terms and Conditions (https://onlinelibrary.wiley.com/terms-and-conditions) on Wiley Online Library for rules of use; OA articles are governed by the applicable Creative Commons License

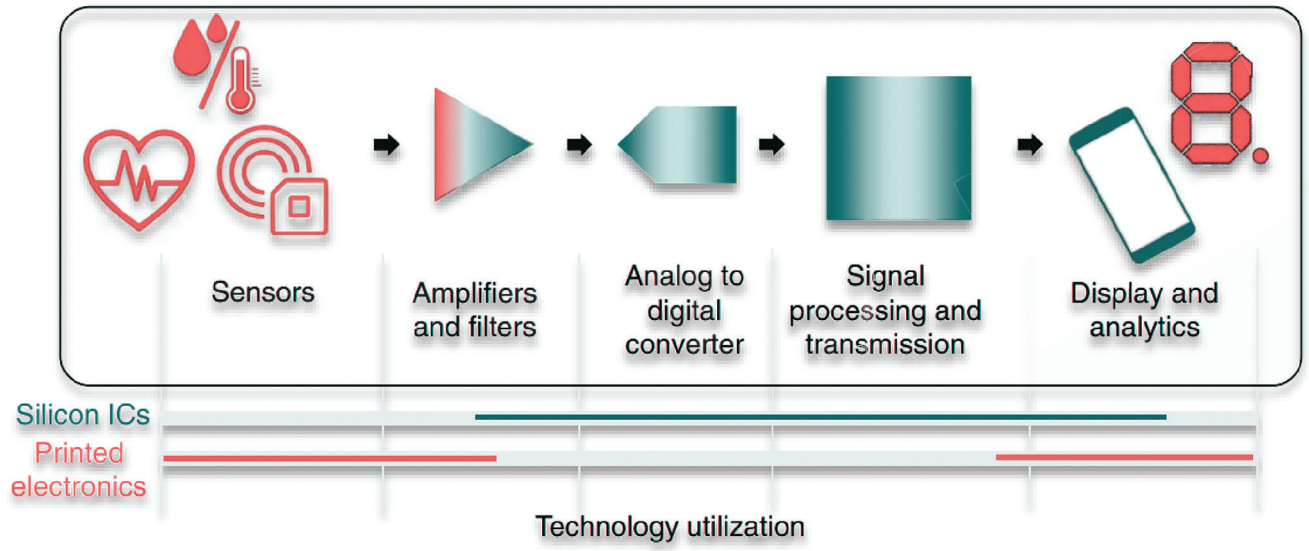


Figure 9. Performance comparison and utilization of PE and silicon ICs in FHE systems. System-level implementation of FHE showing the utilization of both PE and silicon ICs. The color bars under the system blocks show where silicon ICs (blue) and PE (orange) are utilized. Reproduced with permission.[85] Copyright 2020, Wiley-VCH.

The core challenges of printing techniques are related with ink development/optimization, substrate compatibility and multistack layering[111] limiting the performance, yields and minimum feature size. Printing large-area, pinhole-free, defect-free layers has already been accomplished. On multilayer devices, the minimum feature size is not only limited by the printing resolution but also by the alignment accuracy of the equipment. As an example, in EHD, which is a high-resolution printing technique, features down to 40 nm are possible to print.[43d] Commercial EHD systems like eNanojet printed by Enjet Inc,[112] are made to print fine lines as thin as 1 µm in width. However, at a motion repeatability of ±1 µm, the positioning system's mechanical accuracy is only ±15 µm, strongly decreasing the resolution on multilayer devices, being vastly limited by these two parameters. Most of the current printed systems have a mechanical accuracy of ≈10 µm. Scrona, a Swiss start-up commercialized an EHD system with a 1 µm of position accuracy and 50 nm of position repeatability.[113] Hence, printed electronic equipment still needs to improve on mechanical accuracy to achieve printing nano-scale devices. It is useful to remind that increasing accuracy will contribute to a cost increase of the equipment.

Since the publication of the first printed memristor in 2012 using metal oxides as a switching layer,[29] there was a steady increase in the number of publications over the years. Overall, until April of 2024, 57 articles were published in printed memristors where at least the RS layer was printed (**Figure 10**a)

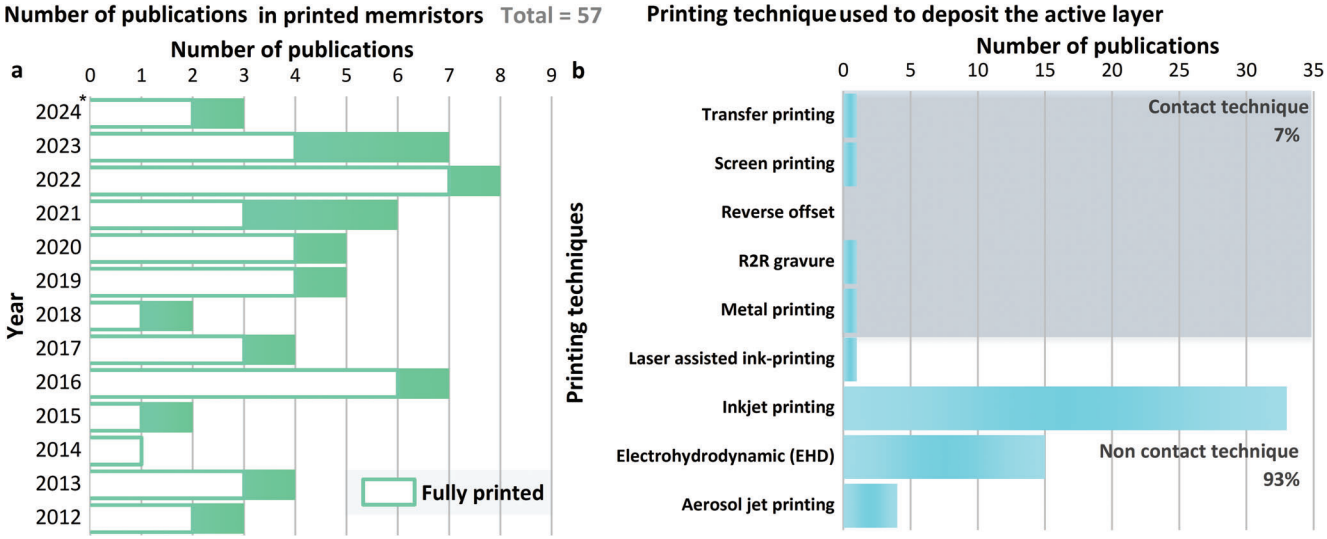


Figure 10. a) Number of publications in printed memristor until April 2024 and (b) the printed techniques used to deposit the active layers, making the distinction between contact and non-contact printing techniques.

© 2024 The Author(s). Advanced Electronic Materials published by Wiley-VCH GmbH

2199160x, 2024, 10, Downloaded from https://advanced.onlinelibrary.wiley.com/doi/10.1002/aelm.202400212 by Universidade Do Minho, Wiley Online Library on [20/04/2026]. See the Terms and Conditions (https://onlinelibrary.wiley.com/terms-and-conditions) on Wiley Online Library for rules of use; OA articles are governed by the applicable Creative Commons License

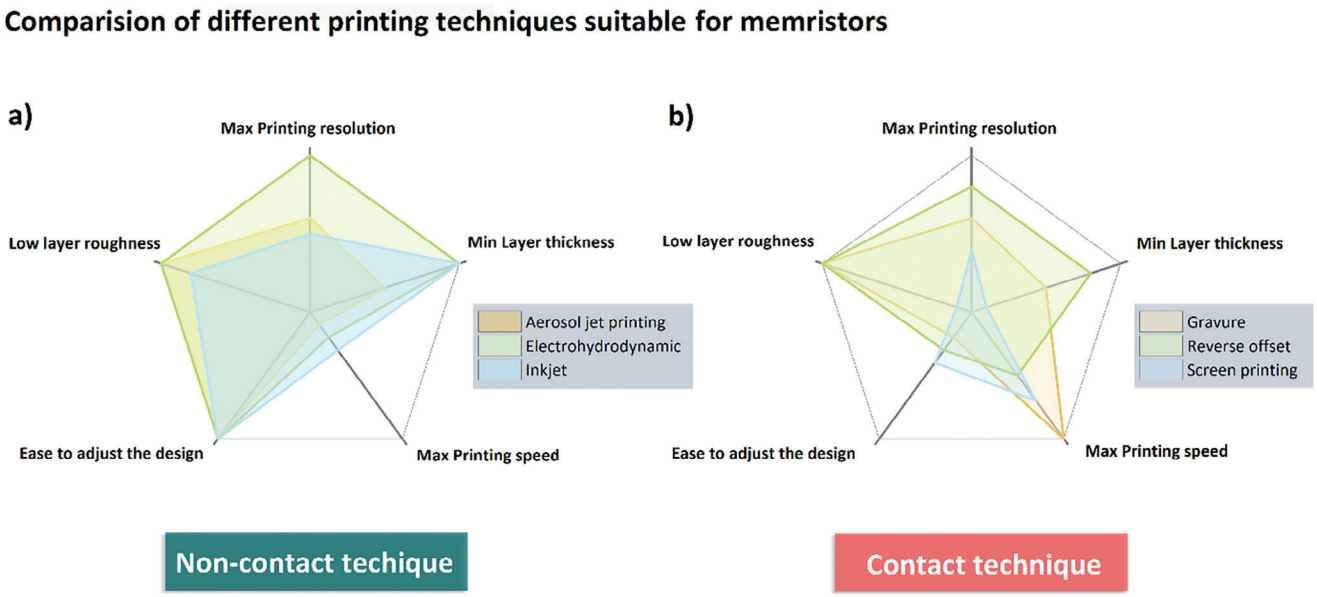


Figure 11. Comparison of different printing techniques for memristor fabrication divided by a) non-contact and b) contact printing techniques.

Despite the potential of PE, most of the solution-processed memristors use spin coating as the main deposition technique for the switching layer.[114] Despite spin coating being a well-known technique that generates smooth thin films, the layers are not patterned, requiring extra steps (e.g., lithography) to pattern the devices.[114a] When creating circuits that require individualized memristors it adds cost and complexity.

93% of the published works used non-contact printing techniques to deposit the switching layer (Figure 10b). Twenty-nine of the 57 works used inkjet printing, followed by EHD with 19 works. As discussed earlier, these two techniques show the highest potential to fabricate memristors. Since memristors have multiple layers, it is essential to consider that the resolution is limited by the motor accuracy of the system, and it is identical between the two techniques. Reverse offset is the contact technique that started to generate more interest in memristor fabrication. Still, just three works used ROP to pattern the bottom electrode.

Taking account to those limitations on printing systems, **Figure 11** and **Table 2** compares the potential of contact and non-contact printing techniques for the fabrication of memristors. Non-contact printing techniques show great potential on memristor fabrication and research. The capability of high-resolution printing combined with printing sub 100 nm layers and the ease of tunning the design without any cost makes AJP, EHD, and inkjet printing the most suitable techniques for memristor research. On the other hand, contact techniques, especially screen printing, do not allow to print films with thickness below 1 µm and the film rugosity is very high (≥100 nm best case scenario). Another drawback is that changing the design requires new screens/cylinders/cliché which takes time, and it is costly when optimizing the design. Nonetheless, reverse offset printing is a contact technique that can show potential for scalable memristor fabrication.

In this aspect, printed memristors are in the early stages of research and optimization. Droplet-based non-contact techniques are the most suitable for memristive applications due to their ease of changing the design and tuning the RS thickness with low rugosity, a key aspect for the performance of the memristor. Still, there is a need to miniaturize the devices to improve switching speeds. Nonetheless, by using smaller nozzles, the risk of clogging greatly increases, and the research of particle-free inks, such as precursor-based inks, should be prioritized.

Contact-based techniques have not been adopted for the fabrication of memristor. As indicated above, one big limitation for initial research is the cost of changing the design by requiring new screens, cylinder, or cliché. Screen printing is only recommended to deposit the top electrode due to the high rugosity inherent to its technique. Both gravure printing and ROP can provide uniform devices due to low roughness and high film uniformity. Moreover, ROP allows to print thin films with a thickness under 50 nm.[45a] Still, no printed crossbar structures have been published using contact-based techniques.

3. Ink Requirements

An additional crucial element in PE, is the tailoring of the functional ink designed to be applied with a specific printing process. Functional inks used in PE must be capable of forming a homogeneous layer and be compatible with the other inks that are sequentially implemented.[11a]

Functional inks have typically at least two main constituents: the active material, which is dispersed (typically referred to as filler),[115] or dissolved in a medium. In most of the inks, the fillers are dispersed in a liquid solvent. The purpose of the solvent is to control the final viscosity of the ink and dissolve or disperse the solid components presents in the formulation. To ensure good drying behavior, a solvent for PE, except for AJP which requires volatile solvents, is recommended to have a boiling temperature between 80 and 160 °C[42b] Over the past years, it has been shown that the solvent can significantly affect the

 © 2024 The Author(s). Advanced Electronic Materials published by Wiley-VCH GmbH

2199160x, 2024, 10, Downloaded from https://advanced.onlinelibrary.wiley.com/doi/10.1002/aelm.202400212 by Universidade Do Minho, Wiley Online Library on [20/04/2026]. See the Terms and Conditions (https://onlinelibrary.wiley.com/terms-and-conditions) on Wiley Online Library for rules of use; OA articles are governed by the applicable Creative Commons License

Table 2. Overview of the potential of several printing techniques for the fabrication of memristors. The advantages, challenges, and recommendations are divided into contact and non-contact techniques.

	Advantages	Challenges	Recommendation	Printing technique	Minimum line width [μm]	Lowest memristive device area [μm^2]
Non Contact printing	Easy to optimize the design	Lower printing speed compared to R2R	Aim to scale down the devices into its resolution limit	Inkjet Printing	15	20 × 20
	Easy to tailor the RS thickness	Crosstalk between nozzles if multi nozzle setup (EHD printing)		EHD Printing	0.04	6 × 6 (EHD) 0.08 × 0.08 (NW-EHD)
	Scalability to industry (inkjet)	Coffee ring effect if the conditions are not optimized	Development of particle free inks (e.g., Precursor based inks)			
	Low film roughness if the conditions are optimized	Strict ink rheology (inkjet)		Aerosol Printing	10	70 × 70
		Nozzle clogging, serious issue when aiming for sub micrometre resolution				
Contact printing	High printing speed (gravure)	High film roughness (screen printing)	Screen printing is mostly suitable for top electrode deposition due to surface roughness	Screen Printing	10	–
	Versatility in ink rheology	Difficulty of printing films lower than 100 nm (screen printing, gravure)	Gravure and ROP can give uniform devices due to low roughness and high film uniformity both techniques need to be explored for printed memristors	Gravure Printing	50	–
	R2R compatible	Changing the design can be costly (gravure, ROP)		Reverse Offset printing	20	–

final nanocomposites' structure.[116] On multilayer structures, solvents must be chosen in a way to avoid interaction with the previous layer. Hence, orthogonal solvents must be selected to ensure that the material deposited in a previous layer is not dissolved by solvent from the subsequent layer.[85] Nonorthogonal solvents cause the preceding layer to swell leading to a rougher surface, thus decreasing the device's performance[85] or, as an extreme case, it provokes pinholes and decreases device yields.[117]

When formulating an ink, there are some considerations to take into:[85] reducing the coffee-ring effect (in case of inkjet printing), enhancing surface wetting while reducing ink spreading, long-term ink stability, improving particle dispersion, improving adhesion to the substrate, and compatibility with the targeted printing technique which the ink will be used.[118] Most of the cases require the addition of additives.[11a,42b,119] Inks based on NPs are prone to sedimentation, agglomeration, and aggregation, which causes them to deteriorate over time. Polymer binders are added to reduce intermolecular interactions between NPs, improving their stability and extending their shelf life. A variety of additives can also be added to an ink in tiny amounts (usually less than 4%),[42b] to improve performance and stability.[42b] The most often used additives in the formulation of inks are dispersing agents (surfactants), rheology modifiers, defoamers, plasticizers, and biocides.[42b,120] Due to the use of toxic and environmentally damaging solvents, the PE field faces scalability issues.[121] These solvents pose health, safety, and environmental risks, especially in open environments where workers are exposed to fumes from the solvents. To scale into industry and large R2R machines, alternative "green" solvents should be adopted.[122] In the fabrication of the RS of the memristors one adopted approach is using water-based formulations with the additions of dispersants to improve ink stability and lower its surface tension.[19,99,123] Additionally, nontoxic formulations based on 2-propanol (IPA)[124] or a mixture of IPA and 2-butanol were developed.[54,79]

For a specific printing process, it is required to tune the properties of the ink, including particle size, solid content, surface tension, and viscosity to achieve a high-quality printed film. **Table 3** summarizes the different ink characteristics required for the most common printing methods.

Non-contact droplet-based printing techniques allow the deposition of low-viscosity inks. The advantage of developing low-viscosity inks is the ease to design binder-free stable inks, thus enabling the print of high-purity materials without deteriorating the functional properties.[85,125] On the other hand, the ink rheological requirements can be stricter. On the extreme side, in inkjet printing technique, the inks must meet certain physical requirements to ensure stable drop formation.[42b] The Reynolds (Re), Weber (We), and Ohnesorge (Oh) values are dimensionless numbers to describe those requirements. The dimensionless Z parameter ($Z = \frac{1}{Oh}$), proposed by Fromm[126] evaluates the printability of an ink for inkjet printing. Reis and Derby state that the workable interval for inkjet printing is $1 < Z < 10$.[127] Nonetheless, another interval of $4 < Z < 14$ has been reported by Jang et al.[128] The upper limit marks the beginning of satellite drop formation, while the lower limit shows the lowest Z value below which the drops cannot be effectively ejected from the nozzles. In addition to the primary drop, tiny droplets known as satellite drops are also created in the nozzle during the thread breakup process.[129] Another important aspect to consider on

© 2024 The Author(s). Advanced Electronic Materials published by Wiley-VCH GmbH

2199160x, 2024, 10, Downloaded from https://advanced.onlinelibrary.wiley.com/doi/10.1002/aelm.202400212 by Universidade Do Minho, Wiley Online Library on [20/04/2026]. See the Terms and Conditions (https://onlinelibrary.wiley.com/terms-and-conditions) on Wiley Online Library for rules of use; OA articles are governed by the applicable Creative Commons License

Table 3. Overview of ink characteristics for the most common printing methods.[42b,c,85]

	Aerosol Jet	EHD inkjet	Inkjet (DoD)	Gravure	Reverse offset	Screen printing
Viscosity [cP]	1–2500	1–10 000	5–50	10–1000	20 000–100 000	100–1 000 000
Surface tension [mN m^{-1}]	10–20	20–50	25–50	41–44	30–37	30–50
Maximum particle size [nm]	1/10th of nozzle diameter	1/10th of nozzle diameter	1/10th of nozzle diameter	15 000	10 000	1/10th of mesh opening
Maximum preferred particle size [nm]	50	50	50	3000	3000	100
Maximum solid loading [wt%]	55	20	20	30	90	90

droplet-based printing techniques is the maximum particle size to avoid clogging the nozzles. Furthermore, the maximum particle size must be no more than $1/10^{th}$ of the nozzle diameter.[11a] Therefore, the inks tailored for those techniques need to have solvents that ensure the functional particles keep dispersed with low levels of agglomeration. In some cases, it needs to add additives to improve stabilization of the filler as well as centrifugation and filtering steps to remove big particles from the ink.[114a]

With respect to contact techniques such as screen-printing and reverse offset, they require thick pastes with solid content up to 90% wt. In this case, additives (binders) such as resins or polymers are used to increase viscosity. The tradeoff is the degradation of the functional properties of the printed films, which can be minimized with a suitable filler/binder.[115,130]

During device fabrication, the interaction between the substrate and the ink has a significant impact on the printing quality.[11a] The quality of printing is affected by the interactions between the ink and substrate, including drop impact, spreading, wetting, solvent evaporation rate, penetration, and solvent evaporation and particle merging on the substrate after printing.[11a,131]

The wetting characteristics can be evaluated by the contact angle technique. The surface tension of the liquid, the surface energy of the substrate, and the surrounding circumstances all affect the contact angle.[11a,131–132] An increased ink spreading is caused by a small value, which indicates that the substrate's surface energy exceeds the ink's surface tension. Conversely, a high value indicates that the substrate's surface energy is less than the ink's surface tension, which results in less ink spreading across the substrate at all. Higher contact angles allow for thicker patterns and a reduction in line width, which enable higher resolutions. However, when the contact angle is too high, the particles cannot fuse and a film is not formed.

To increase the substrates' surface wettability, surface treatments like oxygen plasma or ultraviolet/ozone treatment are frequently used. When the formed hydrophilic groups C—O, C═O, and COO react with water, they can produce hydroxyl groups, which reduces the contact angle and increases the substrate's wettability.[133] Moreover, combined surface treatment with optimized substrate temperatures during printing, leads to the formation of homogeneous layers.[134]

The postprinting procedure has a direct impact on the performance of the memristor. Overall, 80% of the reported memristive devices fabricated using printing techniques employed low thermal annealing post-treatment ($T < 200$ °C) as observed in **Figure 12**, thus making it compatible with R2R printing techniques.

In the case of thin films with metallic constituents (e.g., metal oxide, metal-based 2D materials), to assure reproducibility and stability of the devices, the elimination of the metal–hydroxyl bonds must occur at low processing temperatures.

One approach is the development of binder-free inks in conjunction with low boiling point solvents to remove the need for a postprinting treatment. Fend et al. used a solvent exchange process to formulate a stable binder-free MoS_2 ink dispersed in a mixture of IPA and 2-butanol.[79] The formulated ink was tailored for AJP without requiring any post-deposition processing step while assuring a uniform RS layer. Alternative methods to conventional thermal annealing consist of UV photoactivation processes (lamp or laser), both compatible with R2R manufacturing.[114a] The use of UV irradiation induces photochemical cleavage of alkoxy groups and activates metal and oxygen atoms to enable metal-oxygen-metal (M–O–M) network formation of the as-deposited films at low temperature. By adopting this method in conjunction with a 150 °C annealing, Carlos et al. achieved electrical characteristics similar to high-temperature annealed films with high yield.[135] In the case of metallic electrodes, Li et al. employed a local laser sintering process after fabricating the memristive crossbar. An 830 nm laser with a power of 100 mW was utilized, making the Ag lines conductive by driving off the Ag ink's binder.[80a] These innovative routes allow the realization of low-temperature thin films with high quality, while

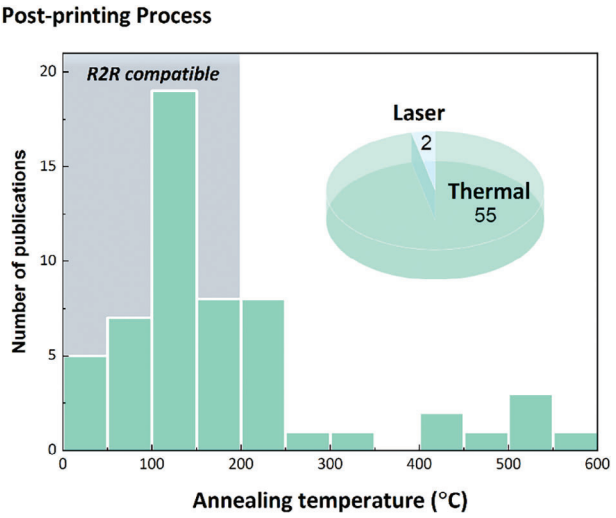


Figure 12. Post-printing processes applied in printed memristor, highlighting the annealing temperature of the reported printed memristors.

© 2024 The Author(s). Advanced Electronic Materials published by Wiley-VCH GmbH

2199160x, 2024, 10, Downloaded from https://advanced.onlinelibrary.wiley.com/doi/10.1002/aelm.202400212 by Universidade Do Minho, Wiley Online Library on [20/04/2026]. See the Terms and Conditions (https://onlinelibrary.wiley.com/terms-and-conditions) on Wiley Online Library for rules of use; OA articles are governed by the applicable Creative Commons License

being compatible with large-area manufacturing and flexible electronics (Figure 12).

4. Memristors

When exposed to specific electrical fields, some materials exhibit the property known as resistive switching (RS), which is the ability to cyclically change their electrical resistivity between different stable levels.[136] As a result, various logic states can be represented by these resistive states. Despite the fact that RS has been recognized for more than 50 years, proposed by Chua as the fourth fundamental circuit component in 1971,[4] research in RS devices did not become widespread until 2008 with the development of the first simple physical model and a simulated IV characteristics of a memristor.[27]

The majority of research on RS materials and devices found stable RS between two resistive states: high-resistive state (HRS) and low-resistive state (LRS).[136] Certain active materials possess the capacity to transition between multiple stable resistive states.[137] Applications involving multilevel information processing can make use of these devices. However, the intrinsic variability of the device parameters (currents, switching voltages) in each state makes it more difficult to reliably distinguish each conductive state in multilevel devices. This difficulty increases when studying large groups of samples statistically.[136]

A memristor cell is a two-terminal device with two electrodes (M) sandwiching the memristive active layer (I) in a metal-insulator-metal (MIM) configuration. The memristive layer can be made of a variety of materials and typically exhibits some ionic or electronic conductivity such as oxides,[104,114a,137a–c,138] sulfides (chalcogenides included),[139] amorphous Si,[140] perovskites,[141] organic compounds,[142] organometallic molecules,[143] 2D materials,[114b,144] or quantum dots (QD).[145] Because of being a two-terminal device, The memristors can be vertically stacked in 3D structures and readily integrated in the crossbar array with a small area of $4F^2$, where F is the minimum feature size.[1a]

Memristors can be divided into volatile and nonvolatile. In volatile memristors, the current would decay back to HRS after the removal of the external excitation (**Figure 13a**). The decay time follows a decay exponential fitting, being characterized by the relaxation time, τ, ranging from milliseconds to nanoseconds.[1a] The distinctive features of volatile memristors, in conjunction with their short and long-term memory performance, prove to be valuable for specific in-memory computing applications aimed at classifying consecutive temporal events. This depends on both the SET switching time and the relaxation time.[146] Other possible applications of volatile memristors are true random number generators where relaxation time a lower than milliseconds and a SET time around microseconds are needed. Another application involves artificial neurons, where a train of spikes reaches a certain threshold, triggering the neuron to switch (fire). In this context, relaxation times in the microsecond range are required.[146] The relaxation behavior becomes a key aspect in neuromorphic applications.[6] For integrate-and-fire neurons, the device resistance should relax back to the resting state to be able to fire continuously during the application of a pulse train.

The volatile phenomena can be explained by the ion migration resulting in the formation and spontaneous rupture of conductive paths,[146–147] thermal effects by joule heating,[148] or electronic effects[149] which could be modulated by external characteristics such as voltage amplitude, pulse width, and ambient temperature.[1a]

As for nonvolatile memristors, the current resistance state holds after the removal of electrical stimulus. Non-volatile RS can show three distinctive modes of operation in order to provoke HRS-to-LRS (set) and LRS-to-HRS (reset) transitions when inducing electrical stress. Bipolar RS is the most common operation reported in non-volatile memories. It is categorized by the SET and RESET occurring at opposite voltage polarities (Figure 13b). To prevent cell damage, current compliance (cc) is frequently utilized for the SET operation. Unipolar RS is characterized by both SET and RESET occurring at the same voltage polarity (Figure 13c). During set transition, the LRS current must be limited by cc. During reset transition, the cc at LRS

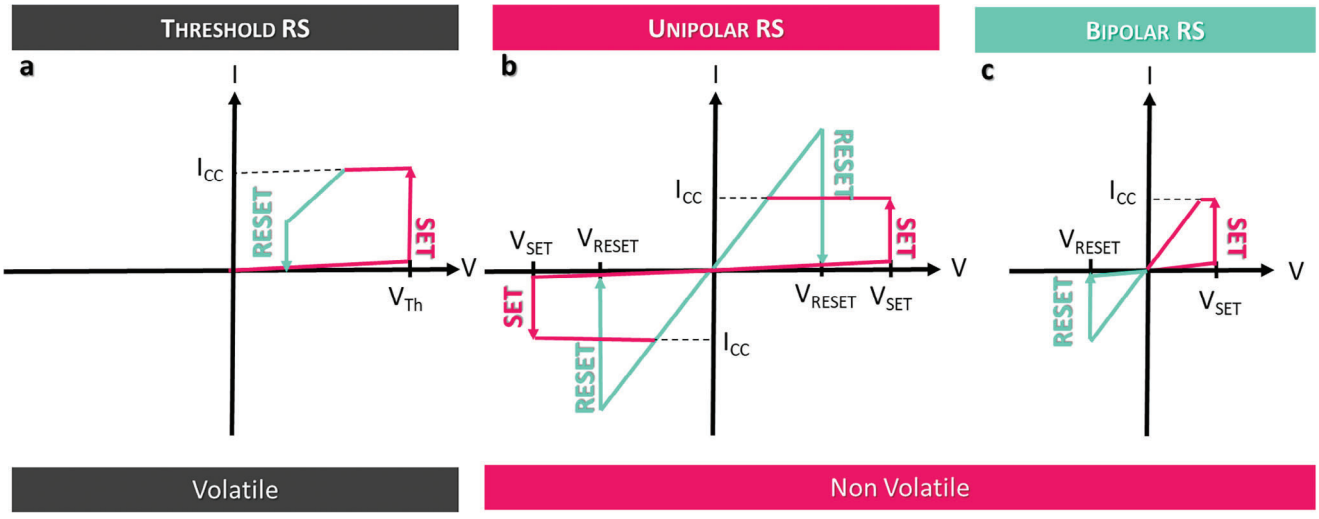


Figure 13. Schematic of different modes of RS: a) volatile threshold RS, b) non-volatile bipolar RS, and c) non-volatile unipolar RS.

© 2024 The Author(s). Advanced Electronic Materials published by Wiley-VCH GmbH

2199160x, 2024, 10, Downloaded from https://advanced.onlinelibrary.wiley.com/doi/10.1002/aelm.202400212 by Universidade Do Minho, Wiley Online Library on [20/04/2026]. See the Terms and Conditions (https://onlinelibrary.wiley.com/terms-and-conditions) on Wiley Online Library for rules of use; OA articles are governed by the applicable Creative Commons License

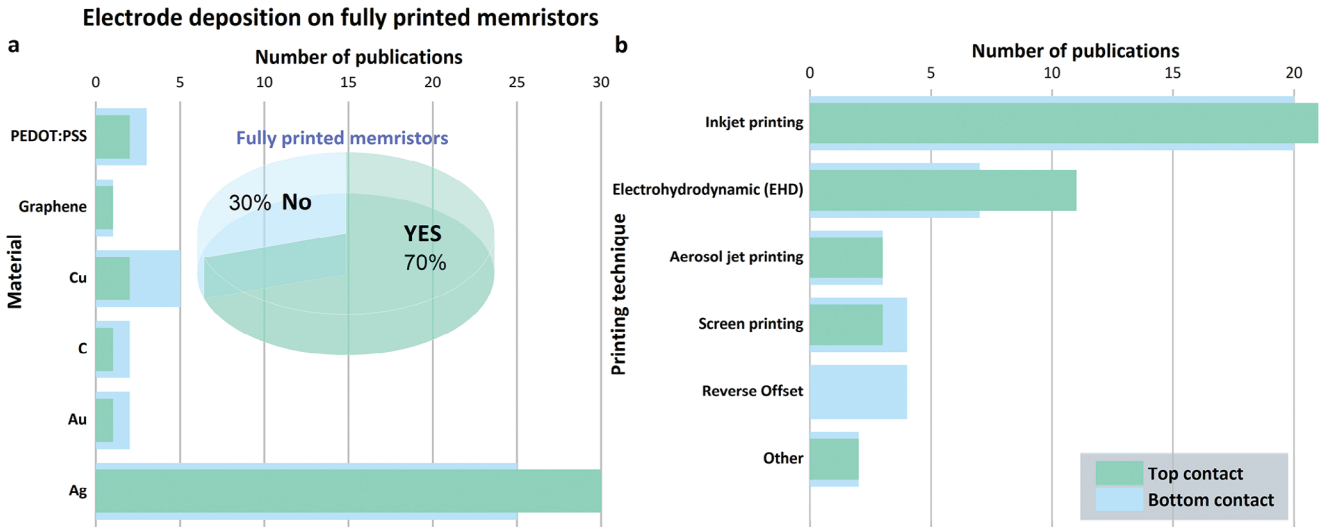


Figure 14. Electrodes used on fully printed memristors: a) by material and b) by printing technique The green bars correspond as the top electrode whereas the blue bars correspond the bottom electrode.

must be removed for the current can exceed the cc value which leads to change back into the HRS. If the unipolar RS can be performed with both voltage polarities it is referred to as apolar RS.[150] In all cases, the read operation is performed at a much smaller voltage magnitude to avoid a change in the current state.

Nonvolatile memristors can be broadly classified into three groups according to the effects of atomic configuration, magnetic, and electrostatic forces.[151] In magnetic tunnel junctions (MTJ),[152] where the tunneling probability is dependent on the direction of the magnetization, magnetic effects result from the tunnel magnetoresistance, giving rise to the Stoner-Wohlfarth magnetic RAM. Combining the spin-transfer torque (STT) phenomenon yields STT-MRAM.[153] The mechanisms for electric/electronic effects RS are either electrostatic trapping/detrapping (nanometallic cell) or ferroelectric polarization affecting the resistance of a 2-terminal device, such as a ferroelectric tunneling junction (FTJ).[154] Magnetic and electrical properties are combined in multiferroic tunnel junction (MFTJ) cells.[155] Most of the fabricated memristors have their mechanism based on electrostatic trapping/detrapping. Thus, Dittman et al. subcategorized this class of memristive devices in the following way according to atomic configuration:[151] Nanoelectromechanical (NEM) memories can be regarded as electrostatically driven nanoscale relays.[156] Organic molecules exhibit a wide range of effects, where the RS is caused by redox reactions.[143] Phase-change memories have their RS triggered by changes of different crystalline phases of chalcogenides materials.[157] Mott transition memories are caused by a local structural phase transition between two crystalline phases in narrow band gap Mott insulators.[158] At last, the Redox-based memristive effects fall into three main categories: electrochemical metallization mechanism (ECM), valence change mechanism (VCM), and thermochemical mechanisms (TCM). These mechanisms depend on resistance changes brought about by ion motion across nanometer dimensions.[151] Most of the printed memristors have their RS based on VCM and ECM.[151,159]

On ECM, based on the electrochemical redox of active metal elements in solid electrolytes inside a memristor, the concept

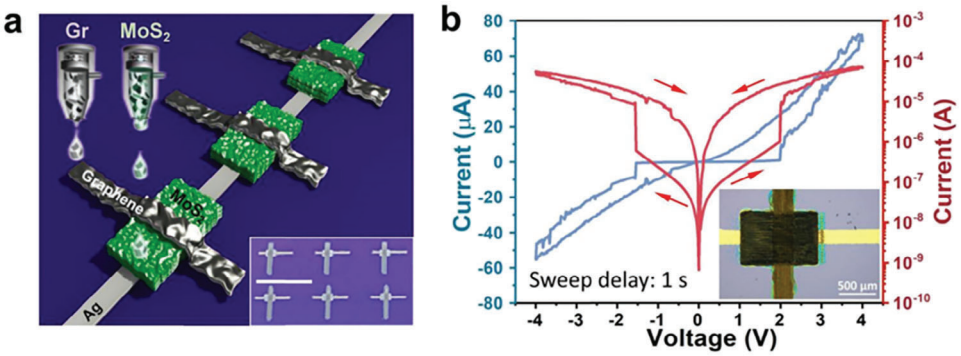


Figure 15. Electrical properties of fully printed Ag/MoS2/Gr memristors. a) Schematic of fully printed Ag/MoS2/Gr memristors. Inset: Optical picture of 6 printed devices on silicon, scale bar: 5 mm. b) Representative *I–V* curve of the Ag/MoS2/G device; inset: optical image at high magnification of the Ag/ MoS2/G memristor. Reproduced with permission.[123a] Copyright 2024, Royal Society of Chemistry.

© 2024 The Author(s). Advanced Electronic Materials published by Wiley-VCH GmbH

2199160x, 2024, 10, Downloaded from https://advanced.onlinelibrary.wiley.com/doi/10.1002/aelm.202400212 by Universidade Do Minho, Wiley Online Library on [20/04/2026]. See the Terms and Conditions (https://onlinelibrary.wiley.com/terms-and-conditions) on Wiley Online Library for rules of use; OA articles are governed by the applicable Creative Commons License

of electrochemical metallization is proposed. The design of an ECM cell needs to employ an electrochemically active electrode such as Ag, Cu, Ni, and an inert electrode (Pt, Pd, Au, TiN as examples).[159a] The breakage or formation of metallic conductive filaments (CFs), which bridge the two electrodes throughout the insulating layer, controls the transition of the memristor between the high resistance state (HRS) and low resistance state (LRS).[160]

In VCM, the RS is caused by the migration and redistribution of oxygen vacancy defects, which modifies the electrostatic barrier at the Schottky interface.[159b] This RS mechanism mainly occurs in metal oxides by the migration of ions of the metal oxide layer.[151] A high-work function metal, such as Pt or TiN, has been utilized as a bottom electrode to establish a Schottky interface with the RS layer.[151,159b] The top electrode must be electrochemically active, employing a metal with high oxygen affinity (e.g., Ta, Ti, Hf).[151,159b] As a result, it allows redox reactions/ion exchange and forms an ohmic contact with the oxide, promoting the formation of oxygen vacancy defects.[161] Oxygen anions in the RS layer with low migration barrier can migrate in the direction opposite to or along the electric field at external voltage biases.[162] A redox reaction is subsequently caused by a change in the stoichiometry, which is manifested as a valence change in the cation sublattice and an alteration in the electronic conductivity.[135]

In the following subsections, different materials used to print memristors will be presented, including both electrodes and RS layer. Moreover, the functional characteristics of the different class of RS materials will be compared.

4.1. Electrodes for Fully Printed Memristors

Memristor cells typically consist of two asymmetric electrodes: an ohmic counter electrode, which is typically made of an inert conductive material, and an electronically active electrode (AE), which is typically a metal with a high work function where the switching usually takes place.[151] Unipolar switching[163] or complementary switching[164] is frequently the result of using symmetric electrodes. It can occur bipolar switching if there are defects on one of the electrodes that lead to an asymmetric barrier.[165] To accomplish fully printed bipolar memristors it requests a range of different conductive inks to make possible the design of an asymmetric barrier.

Seventy percent of the published papers (40 of the 57) are on fully printed memristors (**Figure 14**). Ag is by a large margin the most commonly employed material for electrodes. As for RS material, 29 used metal oxide, a more mature class of materials in memristor fabrication, followed by 2D and organic compounds, with 6 published works each. In relation to the materials used as electrodes, 25 used Ag in both electrodes, and 30 used Ag as the top electrode. Other materials such as Au, Cu, carbon, graphene, and PEDOT:PSS were used in at least one of the electrodes in an asymmetric configuration.

A large majority of the published works (32 of 57) used commercial inks while 7 works do not specify the inks used in electrode fabrication. Similar to the deposition of the RS layer, droplet-based printing techniques were largely used to print the electrodes. The conducting inks can be grouped into four main classes: metal, carbon-based, conjugated polymers, and conductive metal oxide inks.[11a,166]

4.1.1. Metal inks

There are two types of metal ink formulations: particle-free and nanoparticle-dispersion. While metallic salts are dissolved in a solvent to form a precursor solution that transforms into elemental metal after post-processing, metallic NPs are synthesized, dispersed, and stabilized in a solvent for the former.[42b] The main advantages of particle-free inks is the lower layer rugosity when compared to nanoparticle inks,[167] a crucial aspect when choosing the ink for the bottom layer. Further, the probability of clogging the nozzles is low due to the fact that the precursor is dissolved rather than suspended.[168]

Due to their excellent electrical conductivity, the majority of functional inks used in PE are based on Ag., with a resistivity up to 5.6×10^{-06} Ω cm[169] and low sintering temperature. It is a reactive electrode, hence can be applied as an active electrode. Commercial Ag inks are widely available, from Ag nano dispersions optimized for droplet base techniques to Ag pastes optimized for ROP and screen printing. Several different commercial Ag NP-based inks were used in printed memristive crossbars with a solid content from 20 to 45 wt%. Xu et al. printed 6 µm width Ag lines by EHD with a line resistivity of 40 Ω.cm.[66] ROP gives high-resolution patterning with good uniformity. Rehman et al. used commercial Ag pastes to pattern 100 µm width bottom electrodes by ROP with good layer uniformity and a resistivity of 0.02 Ω.cm.[99–100,123b]

Copper is a cost-effective alternative for Ag inks with low sintering temperature (<100 °C). However, during storage, printing, and sintering, Cu NPs oxidize when exposed to ambient oxygen, making them challenging to address. Xu et al. demonstrated fabrication of 80 nm diameter Cu-NWs using a homebuilt EHD-based printing system for memristive crossbars. After a 500 °C annealing step to remove the binders followed by a 300 °C in H_2 atmosphere, the printed Cu-NWs showed metallic properties with an electrical conductivity of 8.15 S μm^{-1}.[58]

As inert metal alternatives, Au and platinum (Pt) are widely used as one of the electrodes on memristor.[151,170] The main issue of Pt is that it requires high sintering temperatures (>300 °C)[168,171] and it is an expensive metal (40 times more than Ag). Au is a suitable alternative for an inert electrode due to the possibility of developing sintering-free nanorod Au ink.[172] As a drawback, Au has a high surface energy that makes Au NPs prone to agglomeration.[42b] Further, it is one of the most expensive metals, costing 80 times more than Ag. Xu et al. printed 6 µm width Au lines as bottom electrode by EHD with a line resistivity of 130 Ω.cm, three times more resistive than the printed silver top electrode.[66]

4.1.2. Carbon-Based Inks

Carbon is an abundant material with a scalable and sustainable production capability, in contrast to metals, which may be scarce and cause environmental problems during extraction and

© 2024 The Author(s). Advanced Electronic Materials published by Wiley-VCH GmbH

2199160x, 2024, 10, Downloaded from https://advanced.onlinelibrary.wiley.com/doi/10.1002/aelm.202400212 by Universidade Do Minho, Wiley Online Library on [20/04/2026]. See the Terms and Conditions (https://onlinelibrary.wiley.com/terms-and-conditions) on Wiley Online Library for rules of use; OA articles are governed by the applicable Creative Commons License

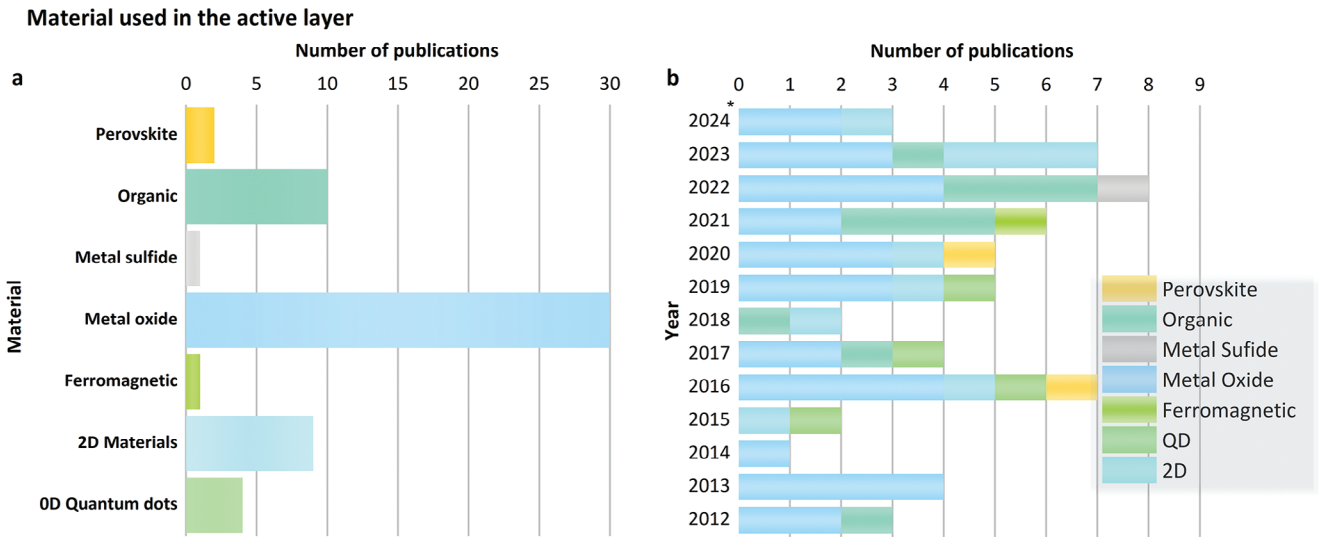


Figure 16. Material used in the RS layers and their use over the years until April 2024.

refining.[130] Carbon black pastes for screen printing techniques are also commercially available. Lien et al. used screen-printing technique to deposit a carbon bottom electrode.[87]

Carbon can form multiple allotropes with distinctive mechanical and electrical properties due to its four unpaired electrons in sp^2 valence orbitals.[173] Among the most significant carbon allotropes are graphene (G) and carbon nanotubes (CNTs).[42b]

CNTs are a one-dimensional carbon allotrope with a small diameter (≈10 nm) and with a length on the order of micrometers. CNTs have very high mechanical strength, and high conductivity with high optical transmittance (T), achieving a sheet resistance of 150 Ω sq^{-1} at 90% *T*.[174] Nevertheless, CNTs are difficult to disperse in solvents due to the strong van der Waals force.[175] One solution to achieve high-concentration stable dispersions on polar solvents is the use of COOH functionalized CNT.

Graphene is a 2D carbon allotrope, with good electrical, mechanical, and thermal properties,[176] that has become a suitable material for the development of flexible conductive patterns.[177] Graphene has a higher conductivity than CNT, achieving sheet resistance down to 0.77 Ω sq^{-1}.[178] However, its aspect ratio can easily clog the nozzles when deposing using drop-based techniques. Peng et al. developed a water-based graphene ink, where the graphene was produced by liquid-phase exfoliation of graphite.[123a] The ink has a graphene concentration of 2 mg mL^{-1}, dispersed in a mixture of propylene glycol and water in a ratio of 1:10, with Triton X-100 and Xanthan gum as dispersants. The graphene ink was applied as the top contact of a fully inkjet-printed G/MoS_2/Ag memristor by adopting a crosspoint structure (**Figure 15**a). The graphene was printed with 60 printing passes, achieving a layer thickness of 200 nm. The printed memristors show bipolar RS with a memory window between 10^3 and 10^5 (Figure 15b).

4.1.3. Conjugated Polymers

Conjugated polymers are assembled by alternating single and double bonds of carbon (aliphatic or aromatic) along the backbone chain.[42b] With the electrons delocalized in 2p orbitals, this results in high electrical conductivity.[42b] PEDOT:PSS is the most extensively used conjugated polymer in the field of PE as it exhibits the highest conductivity among organic materials (4600 S/cm).[179] Another main advantage is that it can be easily dispersed in a large range of solvents, including water. Additionally, fluorine and amine-based additives have been added to PEDOT:PSS to fine-tune its work function.[180] Delfag et al. used a commercial PEDOT:PSS ink to inkjet print PEDOT:PSS lines with 200 µm width, without requiring any sintering process to be applied in memristive crossbars.[123f,181]

4.1.4. Conductive metal oxide inks

Conductive metal oxide is commonly synthesized by doping to change the cation or the anion lattice. Antimony tin oxide

Table 4. Printed memristors using QD in the RS layer. *Fully printed devices; T_{max}: maximum processing temperature, A_{cell}: cell area (in bold: crossbar arrows); BE: bottom electrode; TE: top electrode; t_{switch}: switching time R_{on}/o_{ff}: resistance on/off ratio; n.d., not defined.

Year	RS Printing technique	T_{max} [°C]	A_{Cell} [µm²]	BE	RS	TE	V_{SET} [V]	V_{RESET} [V]	Endurance	Retention [s]	t_{Swith} [µs]	R_{On}/R_{off}
2015*[200]	EHD	120	200 × 200	Ag	GQD/PVP	Ag	1.8	−1.8	500	2.5×10^6	n.d.	14
2016*[201]	EHD	100	250 × 250	Ag	GQD/PVP	Ag	0.65	−0.69	100	9.36×10^4	n.d.	7
2017[202]	EHD	130	n.d.	ITO	GQD/PVP	Ag	4	−4	100	n.d.	n.d.	13
2019*[123c]	Inkjet	60	300 × 300	Ag	FG/PVA	Ag	2.5	−2.5	n.d.	n.d.	n.d.	10^5

© 2024 The Author(s). Advanced Electronic Materials published by Wiley-VCH GmbH

2199160x, 2024, 10, Downloaded from https://advanced.onlinelibrary.wiley.com/doi/10.1002/aelm.202400212 by Universidade Do Minho, Wiley Online Library on [20/04/2026]. See the Terms and Conditions (https://onlinelibrary.wiley.com/terms-and-conditions) on Wiley Online Library for rules of use; OA articles are governed by the applicable Creative Commons License

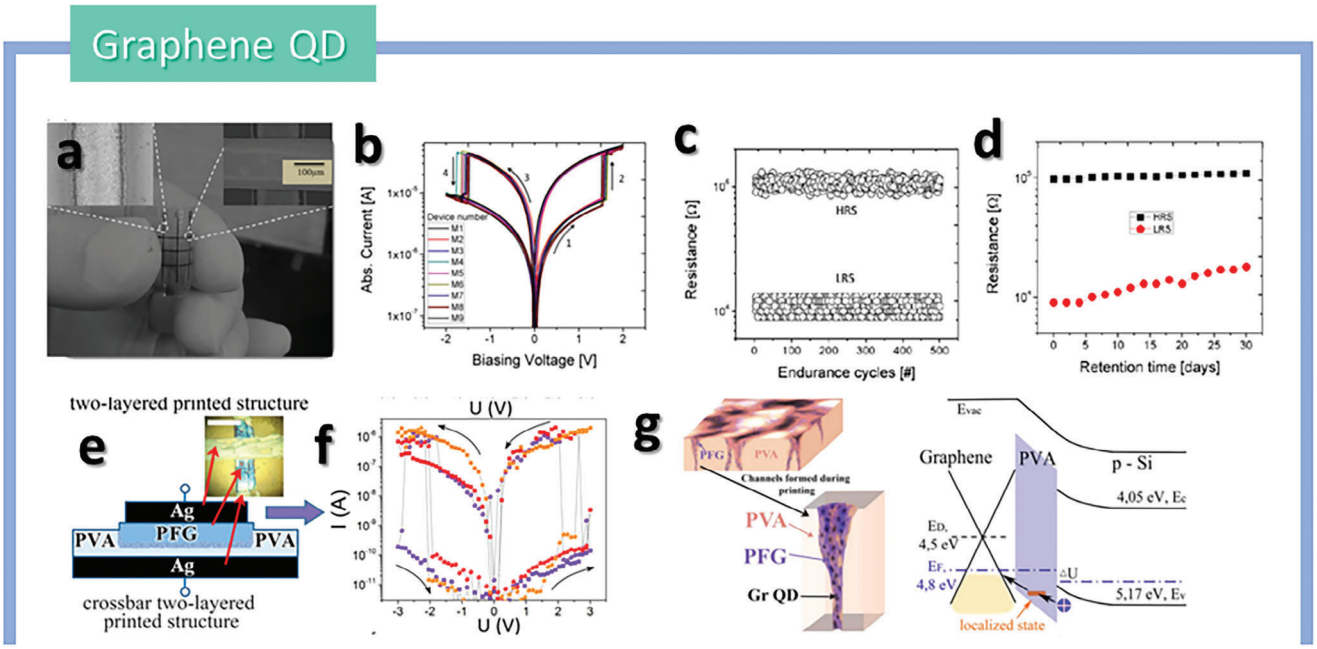


Figure 17. Device characteristics of Ag/ GQD+PVP/Ag: a) photograph of the printed device. b) *I–V* curves. c) Endurance from voltage sweep. d) Retention test. Reproduced with permission.[200] Copyright 2015, Elsevier Ltd. Comparison with Ag/ FGQD+PVP/Ag showing the increase of memory window: e) Schematic of Ag/ FGQD+PVP/Ag crossbars, f) bipolar *I–V* curves showing bipolar RS, g) suggested model to explain the RS nature of Ag/FGP/PVA/Ag memristors. Reproduced with permission.[123c] Copyright 2019, IOP Publishing Ltd.

(ATO),[182] aluminum zinc oxide (AZO),[183] fluorine tin oxide (FTO),[184] gallium zinc oxide (GZO)[185] and indium tin oxide (ITO),[186] and are several examples of doped conductive oxide ceramics. ITO is the most widely used of these materials due to its exceptional conductivity; nevertheless, it is a costly and scarce material.[11a] Metal oxide-based inks are classified into two types: sol–gel and nanoparticle.[187] While the ink made of NPs forms low-density oxide films with higher roughness, the ink based on sol-gel achieves higher conductivity but necessitates very high sintering temperatures. A possible solution to decrease the sintering temperature of these electrodes is using a solution combustion synthesis (SCS) route. This method consists on a self-sustained redox reaction initiated by a source of energy between a fuel and an oxidant in the presence of metal cations.[188] Still, this approach has not been yet explored for the fabrication of fully printed memristors.

Table 5. Printed memristors using 2D in RS layer.

Year	RS Printing technique	T_{max} [°c]	A_{Cell} [μm^2]	BE	RS	TE	V_{SET} [V]	V_{RESET} [V]	Endurance	Retention [s]	t_{Swith} [μs]	R_{On}/R_{off}
2015 [123d]	Inkjet	80	d = 4000	ITO	GO	Ag	0.6	−0.75	10	n.d.	n.d.	3.75
2016*[100b]	EHD	110	30 × 100	Ag	MoS_2 + PVA	Ag	3	−3	10^3	10^5	n.d.	128
2018[221]	EHD	120	d = 42	ITO	h-BN + MoS_2	Ag	1	−1.4	10^3	10^4	n.d.	10^4
2019*[79]	Aerosol	n.d.	100 × 100	Ag	MoS_2	Ag	0.18	−0.3	100	5×10^4	500	10^7
2020*[80a]	Aerosol	0.1 W Laser	70 × 70	Ag	WSe_2	Ag	0.7	0.2	n.d.	n.d.	n.d.	100
2023*[19]	Inkjet	100	d = 60	Ag	h-BN	Ag	2	−1	1.1×10^4	n.d.	10^3	<10
		150				Pt	0.6	−0.4	850 NV 6×10^5 TS	10^1-10^4 NV	10^3	10^5
2023*[54]	Inkjet	60	50 × 50	Ag	h-BN	Ag	0.96	0.12	5×10^4	TS	6	10^5
2023[208]	Metal printing	200	100	Ti	InO_x	Ti	9	−9	100	6×10^3	5×10^3	10
2024*[123a]	Inkjet	150	100 × 100	Ag	MoS_2	G	1	−0.21	100	10^4	10^5	10–100

*Fully printed devices; T_{max}: maximum processing temperature, A_{cell}: cell area (in bold: crossbar arrows; d: diameter); BE: bottom electrode; TE: top electrode; t_{switch}: switching time R_{on}/o_{ff}: resistance on/off ratio; n.d. not defined; TS: Threshold switching; NV: non-volatile.

© 2024 The Author(s). Advanced Electronic Materials published by Wiley-VCH GmbH

2199160x, 2024, 10, Downloaded from https://advanced.onlinelibrary.wiley.com/doi/10.1002/aelm.202400212 by Universidade Do Minho, Wiley Online Library on [20/04/2026]. See the Terms and Conditions (https://onlinelibrary.wiley.com/terms-and-conditions) on Wiley Online Library for rules of use; OA articles are governed by the applicable Creative Commons License

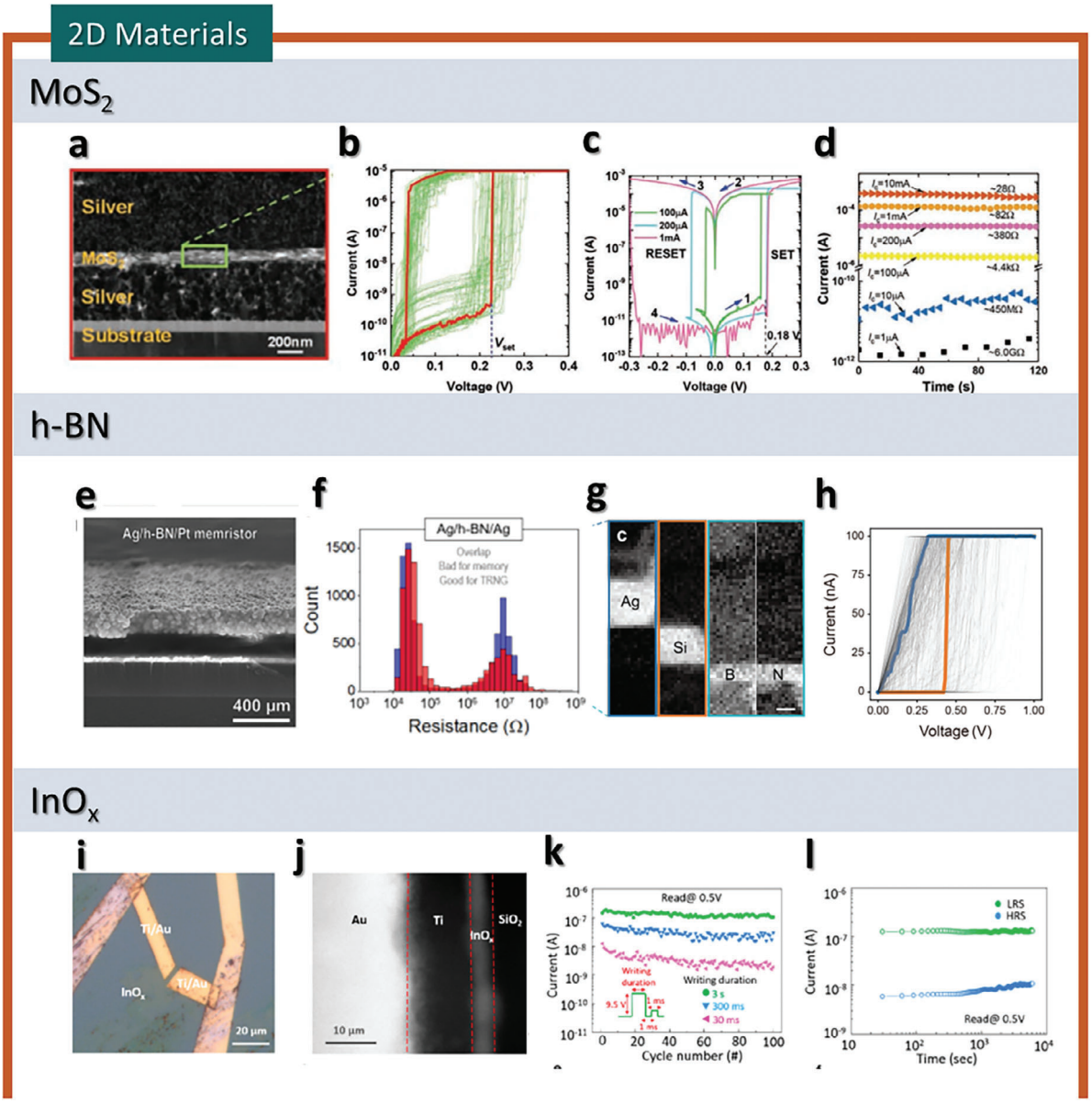


Figure 18. MoS_2 device: a) Cross-sectional TEM image showing the Ag/MoS_2/Ag vertical stack. b) I–V sweeps of a single device with 100 cycles showing volatile behavior. c) Non-volatile RS with CC of 100 μA, 200 μA, and 1 mA d) Multiple states of the resistance recorded with varied CC. Reproduced with permission.[79] Copyright 2019, Wiley-VCH. h-BN performance: e) Cross-sectional SEM image of the Ag/h-BN/Pt memristor, f) overlap of LRS and HRS states showing that the devices can be used as entropy sources for true random number generator (TRNGs). Reproduced with permission.[19] Copyright 2023, Royal Society of Chemistry. g) Energy-dispersive X-ray spectroscopic elemental mappings, showing a 10–20 nm SiO_2 layer deposited between hBN and the top Ag electrode. h) Stochastic *I–V* output characteristics of 20 randomly selected memristors, where each of the memristors is measured with ten sweeping cycles under the same condition. Reproduced with permission.[54] InO_x device: i) Optical image of the 2D-InO_x device with a Ti/Au electrode. j) Scanning transmission electron microscopy (STEM) image of the cross section of the 2D-InO_x device. k) Endurance test of 2D-InO_x memristor demonstrating 100 cycles with different writing duration. (l) Retention test of 2D-InO_x memristor by applying a writing pulse height of 12 V, with a fixed writing duration of 30 ms. Reproduced with permission.[208]

4.2. Materials Used as Resistive Switching Layer

In this subsection, the materials used as RS layers are discussed. **Figure 16** shows that oxides, 2D materials, QDs, organic materials, ferroelectrics, and solid electrolytes have been employed as RS layers. The mechanism, such as oxygen vacancy accumulation or Ag ion redox reactions, may differ based on the electrodes and its RS layers.[189] In the following, the main focus will be on the ink formulations for each type of material, the improvements in performance, and current challenges.

Moreover, Figure 16 shows that 53% of the published works on printed memristors used metal oxides as the RS layer, followed by organics with 18%. Emerging materials such as 2D, QD, and perovskites are still novel areas with just 16%, 7%, and 4%

© 2024 The Author(s). Advanced Electronic Materials published by Wiley-VCH GmbH

2199160x, 2024, 10, Downloaded from https://advanced.onlinelibrary.wiley.com/doi/10.1002/aelm.202400212 by Universidade Do Minho, Wiley Online Library on [20/04/2026]. See the Terms and Conditions (https://onlinelibrary.wiley.com/terms-and-conditions) on Wiley Online Library for rules of use; OA articles are governed by the applicable Creative Commons License

Table 6. Printed memristors using organic materials in RS layer.

Year	RS Printing technique	T_{max} [°c]	A_{Cell} [μm^2]	BE	RS	TE	V_{SET} [V]	V_{RESET} [V]	Endurance	Retention [s]	t_{Swith} [µs]	R_{On}/R_{off}
2012[234]	Inkjet	RT	50 × 50	Pt	PEO+$AgClO_4$	Ag	0.4	−0.15	40	n.d.	1	10^4
2017*[235a]	Inkjet	200	120 × 200	Ag	SOG[a)]	PEDOT:PSS	3	−0.2	10^3	1.6×10^4	n.d.	10^3
2018*[236]	EHD	110	100 x 100	CNT/Ag	PVP	Ag	1	−1	100	3.6×10^3	n.d.	100
2021[142c]	transfer-printed	RT	500 x 500	Au	Fluoropolymer[b)]	Ag	1.5	−1	400	5×10^3	70	10^5
2021*[237]	Inkjet	130	40 x 60	Ag	PEDOT:PSS	Ag	8	WORM	n.d.	2×10^6	10^5	300
2021*[235b]	Inkjet	200	n.d.	Ag	SOG[a)]	Ag	0.1	−0.15	n.d.	n.d.	n.d.	5
2022*[66]	EHD	200	6 × 6	Ag	Nafion	Au	1.5	n.d.	100	TS	10^4	n.d.

Electrochemical memristors			A_{Cell} [mm^2]	S/D	Channel/Electrolyte	Gate						P_{switch} [$Pj.mm^{-2}$]
2022[238]	Aerosol	90	W = 4	Au	chitosan:PANI / PEO	Ag	0.4		40	n.d.	n.d.	n.d.
2022*[94]	(R2R) gravure	120	12 × 20	ITO	s-PEDOT / PEG+BU_4NPF_6	ITO	1	−1	n.d.	n.d.	5×10^5	0.31
2023*[86]	screen printing	120	5.0 x 3.75	Ag	p_6DTP / PEG + Bu_4NPF_6	Ag	0.5	−0.5	n.d.	n.d.	10^5	1

[a)] SOG: a methyl-siloxane polymer from Honeywell; [b)] Novec EGC-1700, 3 M. *Fully printed devices; T_{max}: maximum processing temperature, A_{cell}: cell area (in bold: crossbar arrays); BE: bottom electrode; TE: top electrode; t_{switch}: switching time R_{on}/o_{ff}: resistance on/off ratio; RT room temperature; n.d. not defined; TS: Threshould switching; WORM: Write once read multiples.

respectively. In the current decade it is evident the rise in interest in 2D and organic materials.

4.2.1. 0D Quantum Dots

Quantum dots (QD) are zero-dimensional structures, ranging from 2 nm to 20 nm,[190] and can be categorized into graphene QD, metallic QD, and semiconductor QD. It is conceivable to engineer properties such as gap energy, self-assembly capability, photoluminescence efficiency, and quantum confinement effect by adjusting the composition, size, shape, and surface ligands of the QD.[145e] In storage and neuromorphic applications, QD layers can be incorporated into two-terminal memristive devices as resistive-switching devices[145c,191] or as floating gates, trapping sites, or channel layers in three-terminal flash memories.[145e]

Memristors can also employ metal QD by altering the electrodes or the RS layer. By sputtering metal NPs on the electrode surface, the electrode can be modified to lower the interfacial potential drop and charge injection barrier, increasing the device performance. The surface of the ITO electrode can be modified with sputtered Au NPs, as Sreetosh Goswami and colleagues showed in their study.[143a] With this adjustment, the charge-injection barrier and interface potential drop would be reduced, potentially resulting in a shorter switching time and lower switching voltages. Semiconducting QD exhibits well-defined energy levels for optical processing,[192] allowing the fabrication of electro-photo-sensitive memristors by employing site-controlled QDs.[145b] Its conductance is tuned by applying either optical or electrical signals. Still, most of the solution processed QD-based memristors employ spin-coating techniques to deposit the RS layer.

Graphene QDs (GQDs) are zero-dimensional sp^2 hybridized carbon allotropes. Typically, GQDs have a diameter lower than 20 nm[193] consisting of graphene, either single or multilayer. Since its emergence in 2008, attention has been drawn to GQD because of its optoelectrical characteristics:[194] non-zero bandgap, excellent dispersibility, biocompatibility, and capacity to accept functional groups and dopants. The altered quantum confinement and presence of edge states[195] in GQDs have led to a multitude of proven applications in photonic devices[196] and bioimaging.[197] In the case of memristors, the quantum well structures form charge capture centers, which are useful for regulating the resistance of a device.[198] The quantum well formed in the charge trapping layer can improve the charge trapping efficiency and thus data retention capability.[199] **Table 4** summarizes the device characteristics based on printed QD memristors.

All the reported works in this field used some form of Graphene QD embedded in a polymeric matrix. Ali et al.[201] synthesized graphene QD by grinding and ultra-sonication techniques without the use of any acidic reagents or high-temperature treatments. The ground graphene flakes were dispersed in N-methyl-pyrrolidone (NMP) and 1,2 dichlorobenzene (DCB) and sonicated for 4 h to produce QD. The ratio between Graphene QD and Polyvinylpyrrolidone (PVP) is 1:2.[200–202] The reports on graphene QD indicated a low memory window around 10 and endurance up to 500 cycles (**Figure 17a–d**).

To increase the memory window, Ivanov et al.[123c] developed a method of graphene fluorination in hydrofluoric-acid solution to synthesize fluorinated graphene, few-layer-graphene, and fluorographene suspensions. The RS was analyzed in partially fluorinated graphene-polyvinyl alcohol (PVA) composites and as

© 2024 The Author(s). Advanced Electronic Materials published by Wiley-VCH GmbH

2199160x, 2024, 10, Downloaded from https://advanced.onlinelibrary.wiley.com/doi/10.1002/aelm.202400212 by Universidade Do Minho, Wiley Online Library on [20/04/2026]. See the Terms and Conditions (https://onlinelibrary.wiley.com/terms-and-conditions) on Wiley Online Library for rules of use; OA articles are governed by the applicable Creative Commons License

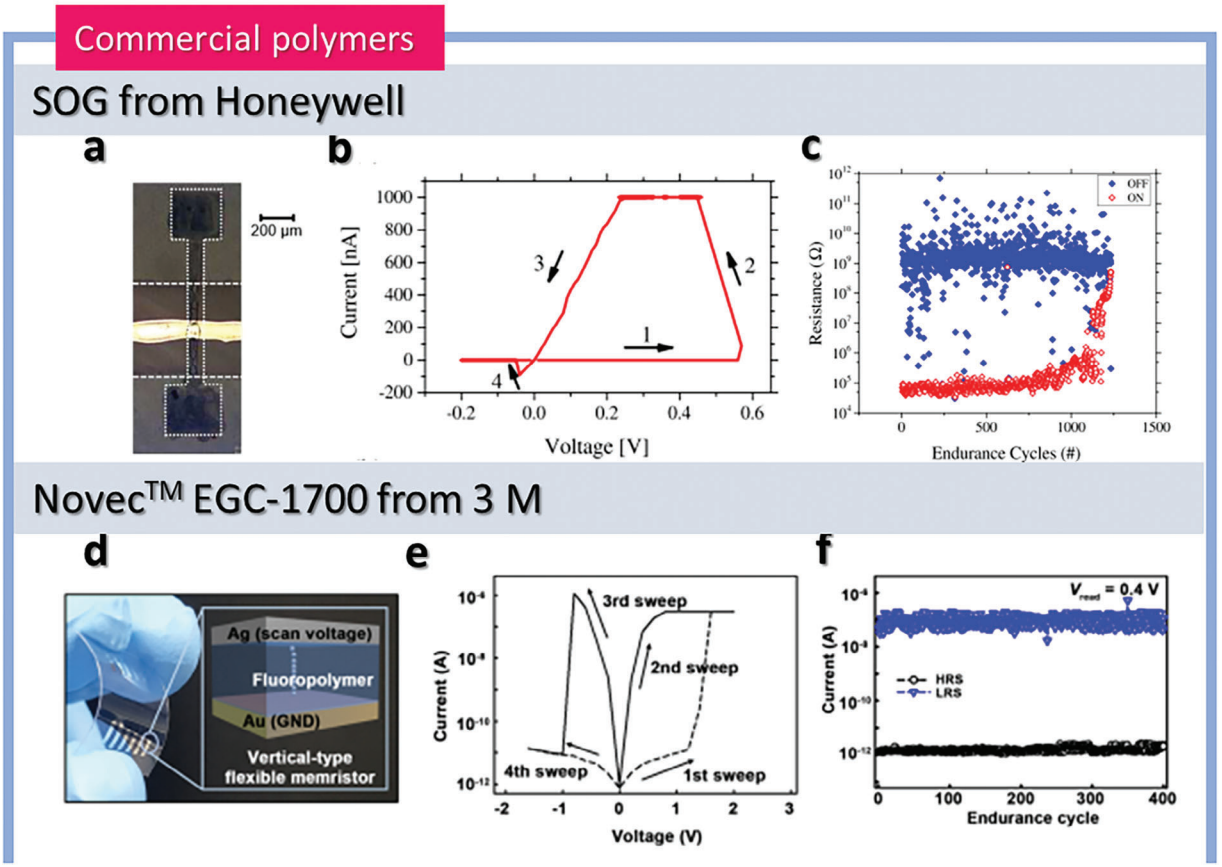


Figure 19. PEDOT: PSS/SOG/Ag memristors: a) Photomicrograph of a cell on PEN foil. b) Current–voltage characteristic. c) Endurance data. Reproduced with permission.[235a] Copyright 2017, AIP Publishing. Ag/Fluoropolymer/Au memristors: d) Photographic image of the vertical-type flexible memristor under bending deformation. e) Current–voltage (*I*–*V*) curves of the device. f) Electrical endurance characteristics of the device. Reproduced with permission.[142c] Copyright 2021, Springer Nature.

stacked layers. The devices shown both threshold switching and bipolar switching achieving a memory window up to 5 orders of magnitude (Figure 17e,f). Moreover, it was confirmed that the reduction in the PVA thickness in combination with an increase in fluorinated graphene thickness leads to a change of the unipolar threshold switching to bipolar RS. The RS mechanism was attributed to the formation of current paths in the partially fluorinated graphene that covered the surface of the porous PVA as a thin film (Figure 17g).

4.2.2. 2D Materials

Since graphene was first produced in 2004,[203] 2D materials have drawn more attention due to their smaller dimensions,[204] high electron confinement,[205] abundance of active sites,[206] and edge polarization.[207] 2D materials have a great deal of potential in microelectronic applications because of their van der Waals nature, which causes them to exhibit low degrees of the lattice mismatch effect in heteroepitaxy.[208]

Due to their electrical properties, 2D materials are considered as a possible solution to produce electronic devices and integrate into circuits beyond the CMOS technology.[209] Nonetheless, the majority of electronic devices based on 2D materials have been created using techniques that are incompatible with wafer-scale circuit technologies.[132] Chemical vapor deposition (CVD) is a scalable technique to produce large-area 2D materials and is used by industry to manufacture graphene sheets. Still, the CVD method has an important drawback: it requires the use of temperatures above 850 °C, which prevents the 2D material from growing directly on wafers that contain CMOS circuits.[210] This fact considerably increases the complexity of the fabrication process, by adding an extra delicate step to transfer the 2D material into the target wafer.[211] During this time-consuming process, the CVD-grown 2D materials may get contaminated and cracked.[211–212]

Another approach to produce 2D layered materials is liquid phase exfoliation (LPE). It is a low-cost process that uses microfluidization or an ultrasonic bath to exfoliate sheets from small bulk crystals in order to create large quantities of 2D sheets. This is conceivable because in-plane covalent bonding is significantly stronger than the van der Waals forces that form the bonds between 2D planes.[213] Moreover, 2D materials synthesized by the LPE process can be deposited using printing techniques on any wafer at a low temperature.[214] A wide range of microelectronic devices have been created using this method, including transistors,[215] photodetectors,[216] capacitors,[217] solar cells,[218] and light-emitting diodes.[219] Due to its low cost,

© 2024 The Author(s). Advanced Electronic Materials published by Wiley-VCH GmbH

2199160x, 2024, 10, Downloaded from https://advanced.onlinelibrary.wiley.com/doi/10.1002/aelm.202400212 by Universidade Do Minho, Wiley Online Library on [20/04/2026]. See the Terms and Conditions (https://onlinelibrary.wiley.com/terms-and-conditions) on Wiley Online Library for rules of use; OA articles are governed by the applicable Creative Commons License

2199160x, 2024, 10, Downloaded from https://advanced.onlinelibrary.wiley.com/doi/10.1002/aelm.202400212 by Universidade Do Minho, Wiley Online Library on [20/04/2026]. See the Terms and Conditions (https://onlinelibrary.wiley.com/terms-and-conditions) on Wiley Online Library for rules of use; OA articles are governed by the applicable Creative Commons License

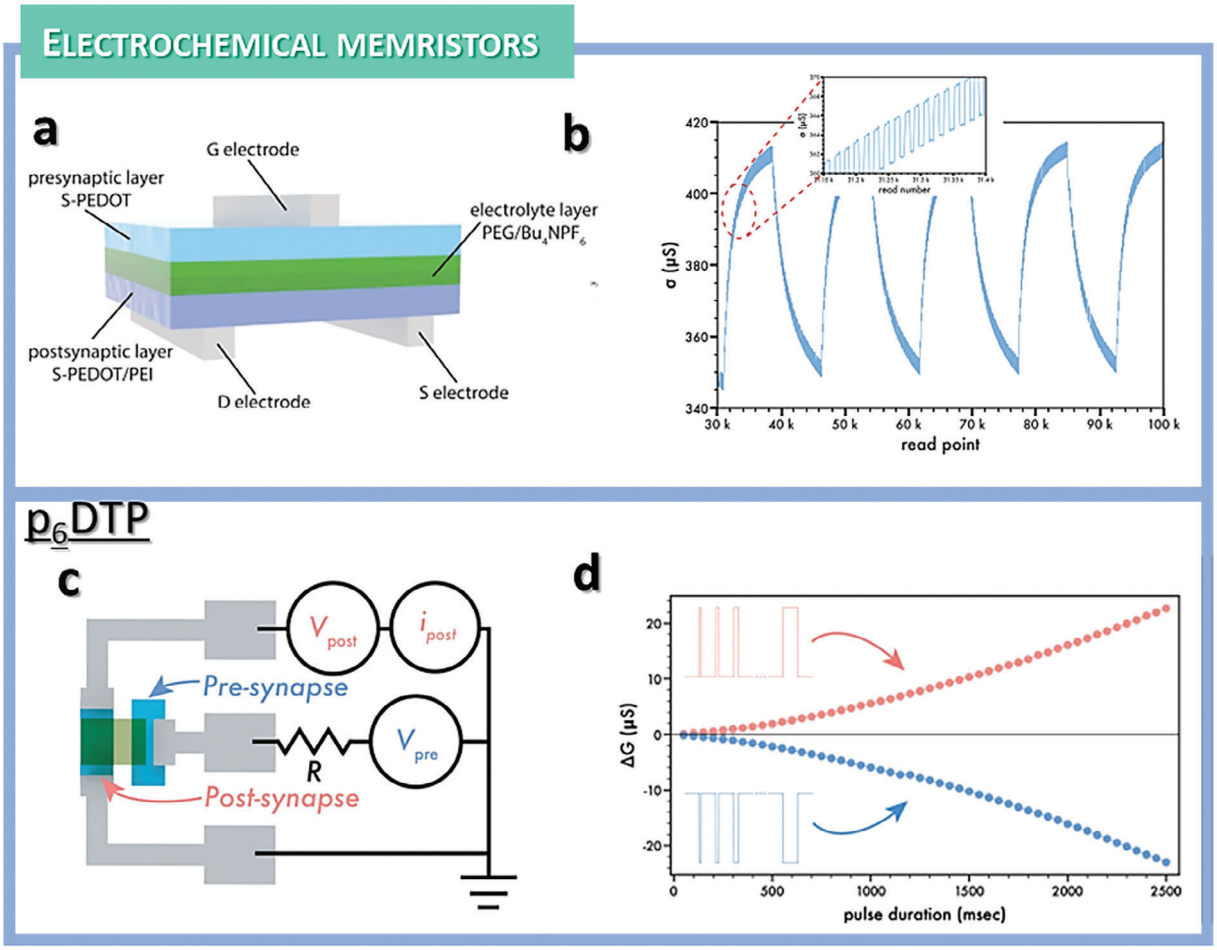


Figure 20. a) Sandwich construction of a conjugated polymer electrochemical memristor. b) Voltage-driven conductance tuning of S-PEDOT electrochemical memristor depicting 500 distinct states per potentiated or depressed cycle. The gate electrode is programmed with a 500 ms voltage pulse of ±1000 mV (V_g) while monitoring the drain current ids with a channel voltage -100 mV (V_{ds}). Reproduced with permission.[94] c) Schematic of the p6DTP-based three-terminal synaptic device circuit. d) Characteristic device response for the post-synaptic terminal based on the pre-synaptic input voltage pulse at a) constant duration (t_{pre} = 100 msec) and b) constant amplitude (V_{pre} = ±500 mV). Reproduced with permission.[86] Copyright 2023, Wiley-VCH.

low crystallinity defects, simple operation, high quality, and the nonexistence of dangling bonds on the surface, 2D materials are promising candidates for realizing improved performance with an energy-efficient operation.[144e] Still, long switching time and short retention time issues need to be addressed.[220] The device characteristics of printed 2D memristors are summarized in **Table 5**.

The first demonstration of printed memristors using 2D materials in RS layers occurred in 2015 by Porro et al.[123d] They inkjet-printed graphene oxide (GO) with a concentration of 1.5 mg mL^{-1} in a mixture of water and ethanol. The *I–V* characteristics exhibit bipolar switching behavior, and the primary physical mechanism for Ag/GO/ITO RS was determined to be oxygen ion drift. This relationship between the electroforming process and a decrease in contact resistance resulting from carbon diffusion in the Ag electrode was also established, and it is supported by the XPS depth profile.

Rehman et al.[100b] used an active layer of an LPE molybdenum disulfide (MoS_2)–polyvinyl alcohol (PVA) composite (90:10 wt%) dispersed in NMP and deposited by EHD. The fabricated device displayed bipolar switching characteristics, demonstrated 1000 cycles at ±3 V, and a memory window of 128. The memory window was improved to 1000 in[221] by using ITO as bottom electrode (instead of Ag) and using a hexagonal boron nitride (h-BN) and MoS_2 composite (1:1 vol). The electrical and thermal characterization results showed that the switching ratio decreases with increasing temperature (300–380 K) or device size (42–100 μm), confirming the formation of a conductive filament through the functional layer. The switching voltage also dropped to less than ±1.4 V. Feng et al.[79] (**Figure 18a–d**) demonstrated an aerosol-jet-printed 4 × 4 Ag/MoS_2/Ag memristor array by developing a 0.5 mg mL^{-1} LPE MoS_2 dispersed in IPA and 2-butanol (9:1 vol%). The devices exhibit an ultra-low switching voltage (0.18 V), a high memory window (10^7), tuneable resistance states ($10–10^{10}$ Ω) for multi-bit data storage (6 states were demonstrated), just 1 fW of standby power consumption and 4.5 fJ of switching energy for each transition set. Furthermore, by regulating the current compliance levels, the MoS_2 memristor

© 2024 The Author(s). Advanced Electronic Materials published by Wiley-VCH GmbH

Table 7. Printed memristors using metal oxides in RS layer.

Year	RS Printing technique	T_{max} [°c]	A_{Cell} [μm^2]	BE	RS	TE	V_{SET} [V]	V_{RESET} [V]	Endurance	Retention [s]	t_{Swith} [μs]	R_{On}/R_{off}
2012*[29b]	EHD	150	100 × 400	Ag	TiO_2	Ag	0.9	−0.5	100	n.d.	n.d.	10^3
2012*[29a]	EHD	450	100 × 200	Cu	TiO_2	Ag	0.7	−0.7	n.d.	n.d.	n.d.	100
2013*[57]	EHD	500	100 × 100	Cu	ZnO	Ag	1	−1	500	n.d.	n.d.	10^3
2013[244]	EHD	135	n.d.	ITO	ZrO_2	Ag	1	−1	50	10^6	n.d.	10
2013*[245]	Inkjet	320	20 × 20	Cu	CuO+AgO	Ag	0.8	−0.8	40	n.d.	n.d.	10
2013*[246]	EHD	150	100 × 100	Ag	ZrO_2	Ag	3	−3	140	n.d.	n.d.	100
2014*[87]	Inkjet	180	n.d.	C	TiO_2	Ag	1	−3	10^3	3×10^4	100	10^3
2016*[58]	EHD	500	0.08 × 0.08	Cu	Cu_XO	Cu	5	12	100	2×10^4	n.d.	10^6
2016*[247]	EHD	500	n.d.	Ag	$ZnSnO_3$	Ag	1	−1	100	8.6×10^5	n.d.	10
2016*[248]	Inkjet	150	60 × 60	Ag	TiO_2	Ag	1.5	−1.5	n.d.	n.d.	n.d.	100
2016[249]	EHD	130	2000 × 100	ITO	$ZnSnO_3$	Ag	8	−8	200	1.2×10^4	n.d.	300
2017*[250]	Inkjet	240	320 × 320	Au	HfO_2	Ag	1	−1.5	120	n.d.	n.d.	10^3
2017*[80b]	Aerosol	280	n.d.	Au	Cu-SiO_2	Cu	3	−3	10^4	10^6	3	100
2019*[251]	Inkjet	RT	60 × 60	Ag	VO_2+FG	Ag	2.5	−2.5	1.3×10^3	n.d	0.1	10^9
2019*[252]	Inkjet	150	20 × 10	Ag	Ag_2O	Ag	-0.4	0.2	100	3×10^3	n.d.	10^8
2019[253]	Inkjet	240	320 × 320	Pt	HfO_2	Ag	0.2	−0.2	450	n.d.	n.d.	10^4
2020[123e]	laser printing	2.4w Laser	n.d.	Pt	CuO	Pt	8	−8	n.d.	n.d.	4x10^5	10^3
2020*[254]	Inkjet	80	150 × 90	Ag	a-TiO_2	Ag	1	n.d.	n.d.	n.d.	200	n.d.
2020*[255]	EHD	n.d.	n.d.	Ag	ZnO	Ag	3.75	−3.75	n.d.	n.d.	n.d.	10^3
2021*[135]	Inkjet	150	250 × 250	ITO	AlO_x	Ag	0.8	−1.2	100	10^5	10^5	50
2021*[123f]	Inkjet	60	200 × 200	PEDOT:PSS	WO_3	PEDOT:PSS	3.5	−3.5	6×10^3	8×10^4	10^5	4
2022[256]	Inkjet	400	50X50	Ag	ZnO	Au	0.7	−0.7	500	10^5	2×10^5	10^7
2022*[123b]	EHD	110	n.d.	Ag	TiO_2 [a]	Ag	1	−1	500	5×10^3	n.d.	2.5×10^3
2022*[181]	Inkjet	80	200 × 200	PEDOT:PSS	ZnO	PEDOT:PSS	5	−5	10^4	2.5×10^5	10^5	2
2022*[257]	Inkjet	120	100 × 100	Ag	a-TiO_2	Ag	1v	n.d.	2×10^3	n.d.	2.5×10^5	n.d.
2023*[258]	Inkjet	400	150 × 150	Ag	ZnO	Ag	2	1	100	10^4	2x10^5	10^7
2023[124]	Inkjet	120	50 × 30	Ag	WO_3	Au	1	−0.45	1.2×10^4	10^5	10^4	100
2023[259]	Inkjet	RT	n.d.	Au	VO_2	Au	n.d.	n.d.	n.d.	n.d.	n.d.	100
2024[260]	Inkjet	200	250 × 250	ITO	IGZO	Ag	2	−3	100	10^5	100	5–200
2024 *[261]	Inkjet	200	n.d.	Ag	ZnO	Ag	0.64	−0.38	n.d.	n.d.	10	10^5

*Fully printed devices; T_{max}: maximum processing temperature, A_{cell}: cell area (in bold: crossbar arrays); BE: bottom electrode; TE: top electrode; t_{switch}: switching time R_{on}/o_{ff}: resistance on/off ratio; RT room temperature, n.d. not defined.

demonstrates both volatile and non-volatile RS behavior, effectively mimicking the short- and long-term plasticity of biological synapses.

H-BN has shown great potential for memristive devices. Zhu et al.[19] fabricated h-BN memristors using inkjet printing technology (Figure 18e,f). The devices show random telegraph noise in addition to volatile TS and non-volatile bipolar RS with a very high cycle-to-cycle variability of state resistances. The devices also show a large variability of the breakdown voltage and initial resistance from device to device. Due to their extreme stability, all of these electronic behaviors can be utilized as entropy sources in physical unclonable function circuits for data encryption as well as true random number generators. These stochastic phenomena are more prominent in these devices than in other types of memristors because of their unpredictable morphology, which is a result of thickness fluctuations and flakes' orientations during the inkjet printing process. Moreover, Song et al.[54] have implemented spiking neurons with neural dynamics using inkjet-printed solution-processed h-BN (Figure 18g,h). The memristors were integrated into RC circuits, which simplified the assembly of LIF neurons and, more intriguingly, enabled two types of key neural dynamics by leveraging their common stochastic switching feature, including Poisson-like spiking and adaptation.

Hsun et al.[208] demonstrated the possibility of fabricating a double-layer InO_x device by liquid metal printing with memristive characteristics with a memory window of 10 (Figure 18i–l). Oxygen migration around the grain boundary drives its conduction mechanism. Furthermore, it was found that the 2D-InO_x memristor's oxygen vacancy dynamics at the grain boundaries resembled the Ca^{2+} dynamics of biological synapses.

© 2024 The Author(s). Advanced Electronic Materials published by Wiley-VCH GmbH

2199160x, 2024, 10, Downloaded from https://advanced.onlinelibrary.wiley.com/doi/10.1002/aelm.202400212 by Universidade Do Minho, Wiley Online Library on [20/04/2026]. See the Terms and Conditions (https://onlinelibrary.wiley.com/terms-and-conditions) on Wiley Online Library for rules of use; OA articles are governed by the applicable Creative Commons License

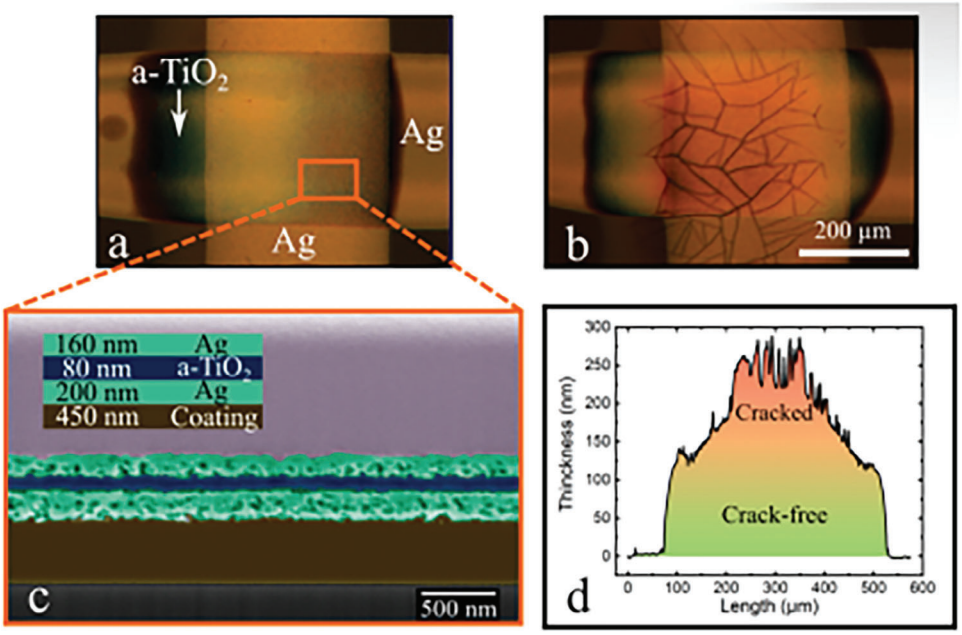


Figure 21. Micrographs of printed polymer coating/Ag/a-TiO_2/Ag devices on glass without (a) and with cracks (b). c) SEM cross-section view of device layers deposited on Si wafer. d) Profilometer results, presenting the relation between active layer thickness and cracks prevalence. Reproduced with permission.[254] Copyright 2019, American Chemical Society.

4.2.3. Organic Materials

Since the invention of the OLED in 1987 by Tang and VanSlyke,[222] organic materials have seen an increasing research interest in electronics. In the electronic field, organic materials have been employed in OLED displays,[223] sensors,[224] solar cells,[225] and organic field-effect transistors (OFETs),[226] among others. Despite the fact that data storage is crucial for electronic applications, the progress in printable organic memory devices has been much slower.[227] Moreover, organic materials have attracted much attention because of the advantages of low cost, high abundance, good mechanical properties, easy to produce on a large scale, and high biodegradability.[228]

In contrast to inorganic materials, organic materials possess the ability to easily add functional groups.[229] The main strength of organic materials includes low cost, scalability, light weight, mechanical flexibility, ductility, and, in many cases, biocompatibility, being particularly suitable for flexible electronic products.[230] The charge carrier concentration and mobility can be adjusted at the atomic level to produce appropriate electrical hysteresis for memristors with different

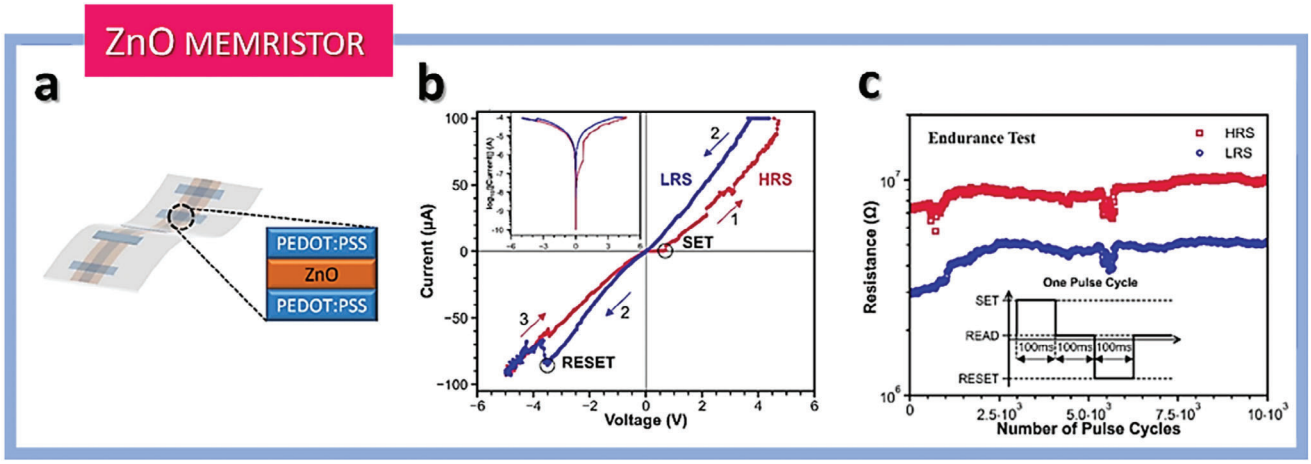


Figure 22. ZnO memristors: a) Schematic of the PEDOT:PSS/ZnO/PEDOT:PSS memory structure, b) current–voltage characteristics of the corresponding memory cell in direct current (DC) sweeping mode, c) endurance measured for 10^4 pulse cycles. Reproduced with permission.[181] Copyright 2022, IOP Publishing Ltd.

© 2024 The Author(s). Advanced Electronic Materials published by Wiley-VCH GmbH

2199160x, 2024, 10, Downloaded from https://advanced.onlinelibrary.wiley.com/doi/10.1002/aelm.202400212 by Universidade Do Minho, Wiley Online Library on [20/04/2026]. See the Terms and Conditions (https://onlinelibrary.wiley.com/terms-and-conditions) on Wiley Online Library for rules of use; OA articles are governed by the applicable Creative Commons License

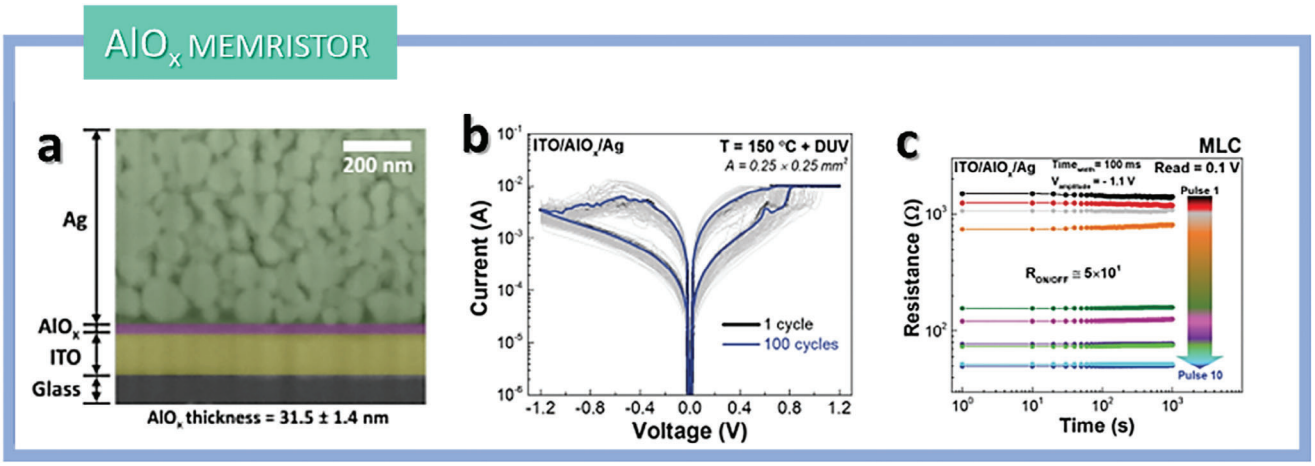


Figure 23. Ag/AlO$_x$/ITO memristors: a) High-resolution SEM-FIB cross-section image of the complete RS device, b) *I–V* sweep endurance showing a bipolar RS behavior during 100 cycles, c) multilevel cell retention characteristics to reach the HRS through the application of 10 pulses. Reproduced with permission.[114a] Copyright 2021, Royal Society of Chemistry.

microscopic mechanisms by adjusting molecular design and synthesis techniques. Organic memristors hold great promise for use in synaptic devices for wearable neural network systems and neuromorphic electronics because of their tunable properties. Nonetheless, there are still several challenges for organic materials: low mobility of charge carriers, low conductivity, and poorer environmental stability, leading to longer switching times, thus not being desirable for high-speed computation tasks.[231] The RS characteristics of organic memristors are mainly caused by the formation of a metallic CF within the device through the application of an electric field.[232] Furthermore, by controlling the device's CF growth, multilevel conductance can be achieved, allowing the emulation of bio-realistic neural networks.[233] Thereby, the development of organic memristors requires an understanding of the electrochemical metallization phenomena for CF dynamics in organic media.[142c] The first concept of printed organic memristor was published in 2012 by Mohapatra et al.[234] using a solid polymer electrolyte: polyethylene oxide (PEO) with 3% (wt.%) of silver perchlorate ($AgClO_4$) in acetonitrile, showing bipolar switching at low voltage. During the current decade, with the rise of neuromorphic computing, the interest in printed organic memristors further increased (**Table 6**).

Three different commercial polymers have been used as the RS layer: SOG from Honeywell,[235] Novec EGC-1700 from 3M,[142c] and Nafion.[66] The first is a methyl-siloxane polymer printable by inkjet, showing 1000 cycles endurance and a memory window of 1000 when using asymmetric electrodes (Ag/SOG/ITO)[235] (**Figure 19**a–c). Using Ag symmetric electrodes it still shows bipolar switching with lower switching voltage (under ±0.15 V) but with a significantly lower memory window of 5.[235b] Novec™ EGC-1700, a hydrophobic fluorinated polymer, has been used by Kim et al.[142c] which deposited the polymer by transfer printing, achieving operating voltages of ≈1.5 and −1.0 V for SET and RESET, respectively, a memory window of 10^5, and 400 cycles endurance (Figure 19d–f). These memristors were applied with the 1T–1R configuration for hardware-based neural network systems. Finally, Nafion, a sulfonated tetrafluoroethylene-based fluoropolymer-copolymer with ionic characteristics was printed by[66] in a printed 6 × 6 μm^2 Ag/Nafion/Au crossbar array, showing TS volatile characteristics that were implemented as Leaky Integrate and Fire Neuron.

In recent years, it has been an increase of interest in redox-active conjugated polymers and functionalized organic molecules.[143] Based on a three-terminal transistor configuration, an organic electrochemical memristor is focused on a counter redox-stacked reaction.[239] Through the use of voltage- or current-driven programming stimuli via the oxidized gate, this device modifies the conductivity of the reduced channel by electronically (de)doping the redox state of the electrochemical memristor.[94] Based on heterocyclic dithienopyrrole (DTP), Grant et al.[86] were able to achieve a continuous analog RS, capable of synaptic emulation with 100 fJ per programmed stimulus using poly(4-(6-hexyl)−4*H*-dithieno[3,2-*b*:2′,3′-*d*]pyrrole) (p6DTP) (**Figure 20**a,b). Also in another work[94] (Figure 20c,d) a fully water-soluble, self-doped PEDOT electrochemical memristors was developed, that demonstrates high conductivity, linearity over 500 distinct states per potentiated or depressed cycle, and low energy consumption (0.31 pJ mm^{-2}).

4.2.4. Metal Oxides

Amorphous metal oxide semiconductor (AOS) materials have been extensively researched and used in TFTs[240] for display applications as switches and LED drivers because of their high transparency, carrier mobility, and environmental stability.[240b,241] Just one year after the advent of the memristor,[27] publications on RS devices made of metal oxide thin films began to appear.[114a] The use of metal oxides as the RS of memristor have attracted attention in the electronics field by its capability to tune its stoichiometric, low cost, high switching speed, high retention time, and compatibility with conventional processes, making it simple to integrate into CMOS circuits.[242] Due to its remarkable properties, AOS is the most used material in

© 2024 The Author(s). Advanced Electronic Materials published by Wiley-VCH GmbH

2199160x, 2024, 10, Downloaded from https://advanced.onlinelibrary.wiley.com/doi/10.1002/aelm.202400212 by Universidade Do Minho, Wiley Online Library on [20/04/2026]. See the Terms and Conditions (https://onlinelibrary.wiley.com/terms-and-conditions) on Wiley Online Library for rules of use; OA articles are governed by the applicable Creative Commons License

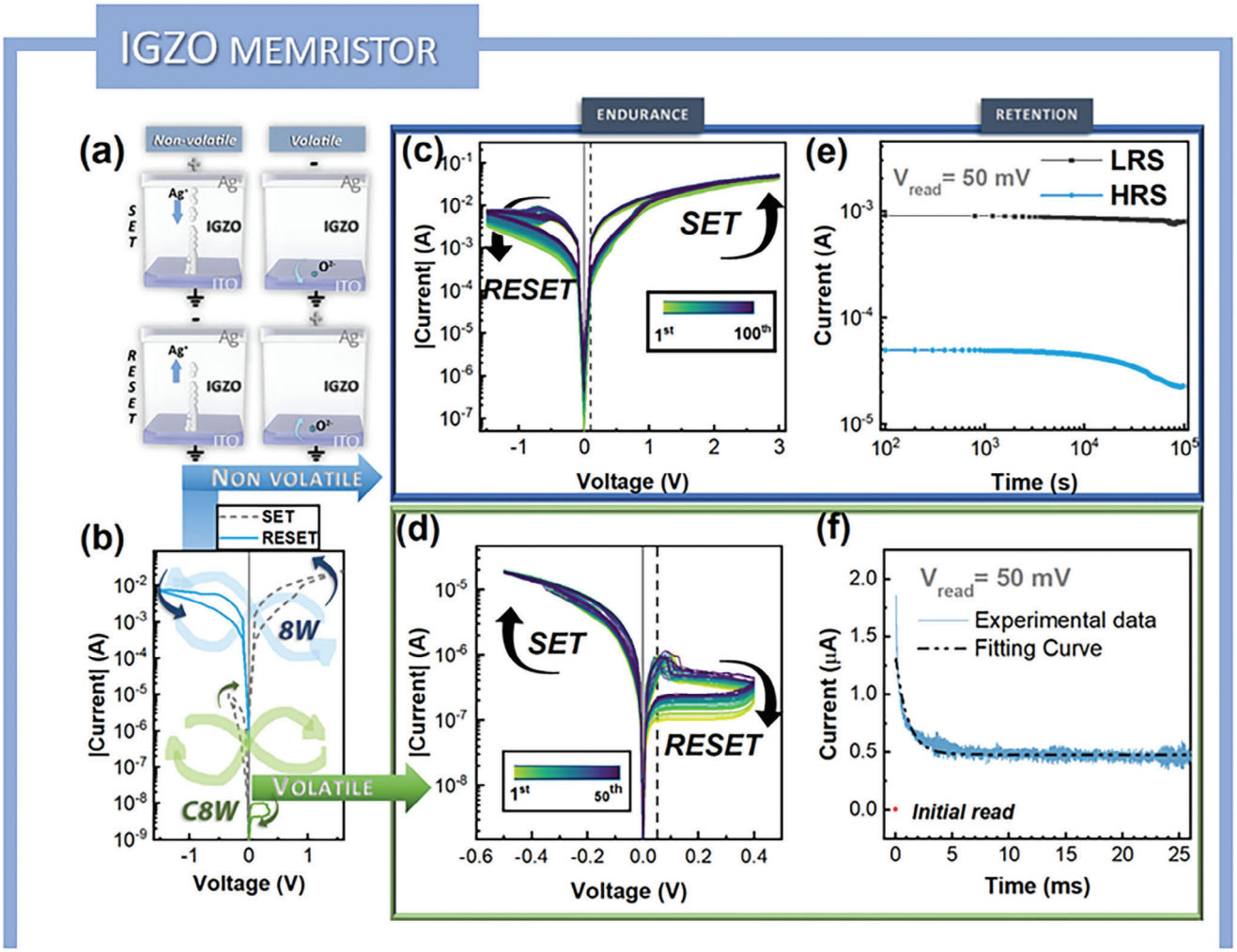


Figure 24. a) Schematic of Ag/IGZO/ITO devices emphasizing the coexistence of two distinctive switching mechanisms. b) Different *I–V* characteristics of the memristors taken from voltage sweeps: at a larger current, it follows a counter8wise switching (non-volatile) while for a low current it follows an 8-wise switching (volatile). c) 100 cycles endurance voltage sweep for non-volatile programming. d) Fifty cycles endurance voltage sweep for volatile programming. e) Retention test for 105 s at 0.1 V. f) Current decay in IGZO memristor after being programmed by 1 write pulse (−0.65 V, 0.1 ms); the current was then monitored by read pulses at 0.05 V for 25 ms. Reproduced with permission.[260] Copyright 2024, Springer Nature.

memristors. Yet, it is a challenge to obtain a stable operation with a low power consumption due to the local crystallinity imperfections, inducing leakage currents.[144e]

Solution-based AOS has been developed and used for diverse applications, mostly in TFTs.[243] Notwithstanding, solution synthesis parameters need to be taken into account to ensure a higher quality of the synthesized metal oxide structures for use in RS devices. The synthesis process, molar ratio, doping, metal salt precursor, solvent, film thickness, and environmental factors are crucial variables to regulate in order to achieve optimal performance from a solution-based memristor.[114a] **Table 7** summarizes all the published works using printed metal oxides as RS layer.

Titanium dioxide (TiO_2) is the most used metal oxide for the RS layer of printed memristors. The electronic and transport characteristics of amorphous TiO_2 are similar to those of its bulk crystalline phases,[262] representing a low cost and abundant[263] option for RS layer. Two distinctive methods have been used to form TiO_2 films: by TiO_2 NPs-based ink[87] or by a metal alkoxide complex (Titanium isopropoxide),[29a,123b,248,254,257,264] The latter approach shows more potential since precursor inks are easier to stabilize and avoid clogging the nozzles. Salonikidou et al.[254] developed a Ti(IV) isopropoxide precursor ink using 1-methoxy-2-propanol as the main solvent. They used a condensed version of the sol-gel and Pechini procedures,[265] which eliminates the need for a high temperature and an aqueous precursor. However, the formation of cracks that subsequently lead to pinholes is one of the most frequent fabrication challenges of solution-based TiO_2. It was demonstrated the prevalence of cracks at layer thickness above 120 nm (**Figure 21**). To minimize the issue, the formulation was changed[257] by adding stabilizing agents (acetic acid and acetylacetone) in propylene glycol methyl ether and ethylene glycol. The addition of acetylacetone prevented the pressure gradient in the printed layer and reduced the rate where the solution evaporated, which would have otherwise caused the inner and

 © 2024 The Author(s). Advanced Electronic Materials published by Wiley-VCH GmbH

2199160x, 2024, 10, Downloaded from https://advanced.onlinelibrary.wiley.com/doi/10.1002/aelm.202400212 by Universidade Do Minho, Wiley Online Library on [20/04/2026]. See the Terms and Conditions (https://onlinelibrary.wiley.com/terms-and-conditions) on Wiley Online Library for rules of use; OA articles are governed by the applicable Creative Commons License

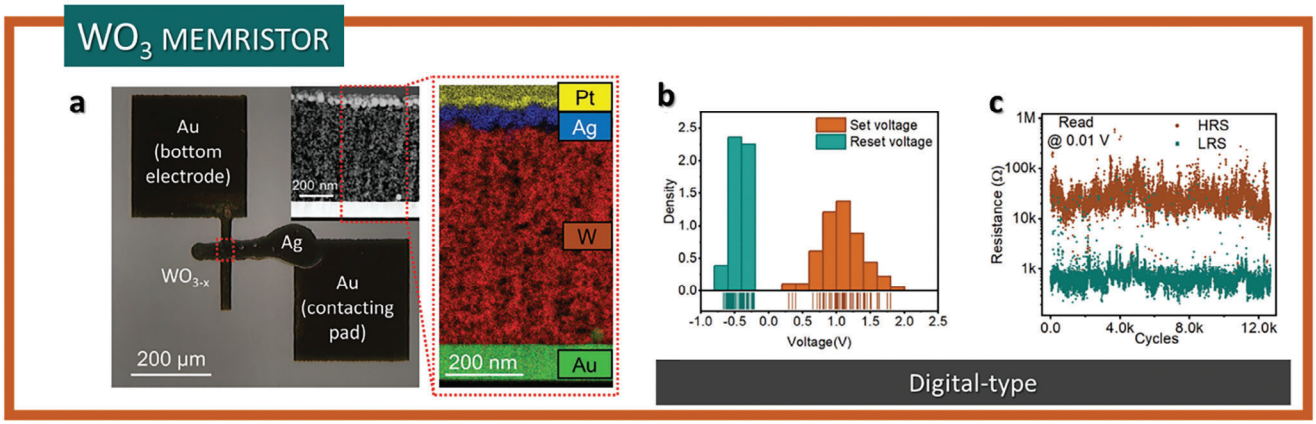


Figure 25. Ag/ WO_3/Au memristors: a) Optical image of the inkjet-printed memristor from a top view. The effective area of the device is formed at the overlapping area of top and bottom electrodes, which is marked with a red dashed rectangle with a size of 50 μm × 30 μm. Inset: cross-sectional STEM HAADF micrograph of the inkjet-printed memristor. An EDS elemental map of selected area in STEM is shown in the zoom-in box. The elemental lines selected for the map are Pt_Lα, Ag_Kα, W_Lα, and Au_Lα., b) view Distribution of SET and RESET voltage values extracted over 100 switching cycles visualized as histograms. c) Endurance performance of the memristor, operated under pulse mode. Reproduced with permission.[124] Copyright 2023, Wiley-VCH.

outer layer regions to shrink at different rates and resulted in cracks. Overall, it was demonstrated a low power fully printed Ag/a-TiO_2/Ag electronic synapses with RS properties that emulate synaptic plasticity properties achieving an endurance of 2000 cycles.[254]

Zinc oxide (ZnO) has been also widely used as an RS layer. The majority of printed ZnO memristors used an NP-based ink dispersed in ethanol,[57,255] a mixture of terpineol and n-butanol[181] or acetone and isopropanol.[258] Delfag et al.[181] reported the fabrication of flexible, transparent, and fully inkjet-printed PEDOT:PSS/ZnO/PEDOT:PSS cells with bipolar RS, showing 10^4 endurance cycles, retention of 10^5 s but with a memory window of 2 (**Figure 22**). Using a Au/ZnO/Ag structure greatly increases the memory window up to 10^7.[256] Moreover, this work adopted a zinc nitrate-based salt precursor ink. However, the high sintering temperature of 400 °C makes it incompatible with flexible or paper substrates. Recently, Chen et al. fabricated a fully inkjet-printed 3 × 3 memristor crossbar using Ag as an electrode, exhibiting synaptic plasticity under a compliance current of 1 μA.[261] The formulated ZnO ink was NP based in a glycerol solution.

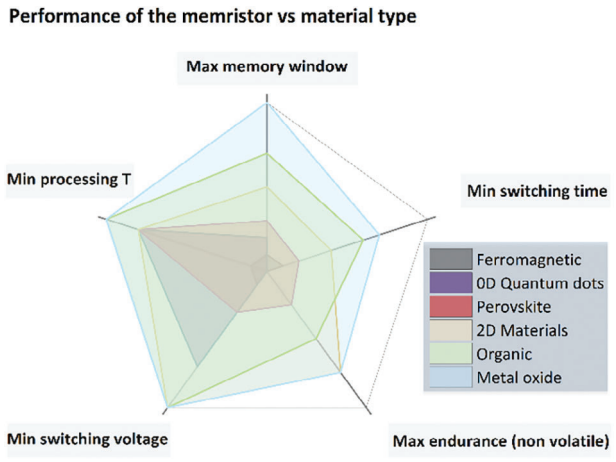


Figure 26. Comparison of the performance of memristors based on different classes of materials.

As explained in the previous section, employing a SCS route greatly decreases the sintering temperature. This approach was utilized by Carlos et al.[188] on aluminum oxide (AlO_x) memristors (**Figure 23**). The precursor ink used aluminium nitrate as precursor dissolved in 2-methoxyethanol and urea which acts as a fuel. The Ag/ AlO_x/ITO memristors show bipolar RS with high yield (95%) at low temperature (150 °C), retention time (10^5 s), and sufficient ON/OFF ratio of 50 to achieve a multilevel cell (MLC) with up to 4 states. About the switching mechanism, the temperature dependence of the resistance did not support the metallic filament as the main conduction mechanism of the device.

A similar approach was adopted by Franco et al. using indium gallium zinc oxide (IGZO). The precursor ink, composed of indium nitrate, gallium nitrate, and zinc nitrate, was separately dissolved in a mixture of 2-methoxyethanol and ethylene glycol (95:5).[260] The IGZO thickness has a great influence on the memory window, rising from 5 to 200 with the increase in thickness from 150 to 550 nm. The inkjet Ag/IGZO/ITO devices show both volatile counter8wise (c8w) and non-volatile 8wise (8w) switching . It has been found that variable range hopping determines the LRS charge transport, and that the origin of defects on IGZO is most likely related to the diffusion of Ag ions in the form of filaments. Furthermore, the volatile characteristics were tested on different 4-bit pulse sequences (**Figure 24**).

Printed tungsten oxide (WO_3) memristors have been also developed with endurance above 5000 cycles.[123f,124] Both works used commercial WO_3 dispersions in 2-propanol with low sintering temperature. Hu et al.[124] fabricated inkjet printed Ag/WO_3/Au memristors with coexistence of two distinctive switching types (**Figure 25**). This device can then be used as a digital-type memristor that can be switched between an LRS

© 2024 The Author(s). Advanced Electronic Materials published by Wiley-VCH GmbH

2199160x, 2024, 10, Downloaded from https://advanced.onlinelibrary.wiley.com/doi/10.1002/aelm.202400212 by Universidade Do Minho, Wiley Online Library on [20/04/2026]. See the Terms and Conditions (https://onlinelibrary.wiley.com/terms-and-conditions) on Wiley Online Library for rules of use; OA articles are governed by the applicable Creative Commons License

Table 8. Relevant printed memristor parameters: current state, challenges, and perspectives.

Parameter		Current status	Challenges/Perspectives
Materials	RS layer	A large range of materials have been explored and matured namely organic and metal oxides	Printed Organic molecules and Mxenes can be further explored
		Still some works use toxic solvents as NMP	Use environmentally friendlier solvents on ink formulation, if possible, water or a low toxic solvent (Cyrene as an NMP alternative)
	Electrodes	72% of the printed memristors used Ag as an electrode	Lack of a wide range of commercial conductive inks. Inert metals (e.g., Pt) have a high sintering temperature. Au is a good alternative.
			Carbon-based inks for contact needs to be explored since it has low sintering temperature and decent conductivity
Device architecture		25% of the papers used common bottom electrode	Crossbar architecture avoids device damage caused by the tips
		48% of the papers used symmetric electrodes	Asymmetric electrodes are recommended for VCM memories
Device fabrication	Printing techniques	Printing equipment needs to be matured/evolved to face miniaturization challenges	The biggest handicap of printing equipment is the accuracy alignment that limits the feature size of multilayer devices to no lower than 1 µm
	Printing conditions	Environmental conditions (temperature and humidity) should be reported	Devices can be sensitive to humidity
			Passivation can avoid device variation caused by external environmental factors
Device characterization	Yields	Only few works report yields	Yields should be reported to evaluate the potential of the fabrication technique as well the materials employed
	Device to device variation	Few works report the device-to-device variation (switching voltage; HRS and LRS state)	Failure analysis or challenges during fabrication should be incentivized to report in order to reduce device variation
	Performance	Only few works reported endurance higher than 10^4	10^9 is the minimum number of cycles recommended for computational applications
		Still a few works have their endurance claims with poor data quality	
Circuit design		Device area still larger than 10 µm^2	Miniaturization improve switching speed and might improve device to device variation
			Use 1T1R or 1D1R to reduce sneak path on crossbar devices

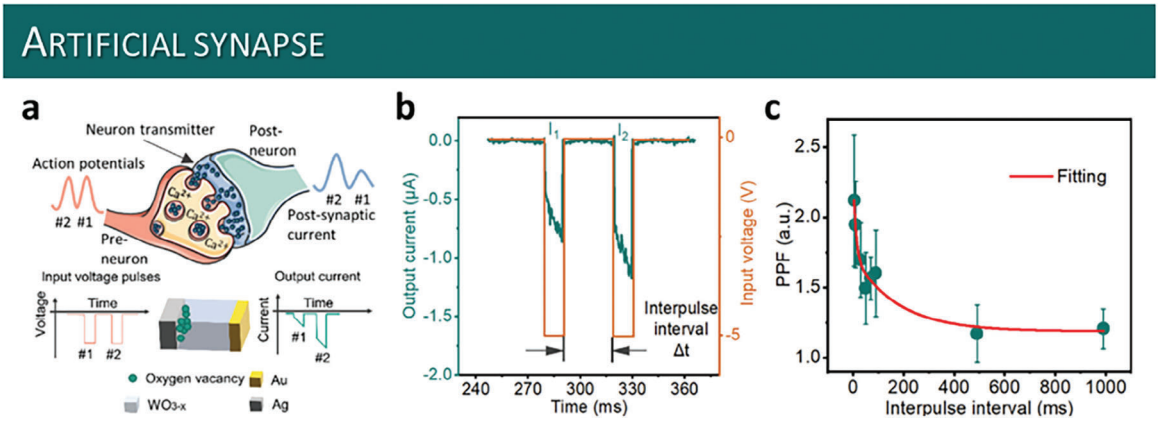


Figure 27. Paired-pulse facilitation (PPF) of the artificial memristive synapse. a) Schematic illustration of PPF in a biological synapse and emulation of the PPF using a memristor. b) Experimental result of the inkjet-printed memristor by applying two consecutive identical voltage pulses. c) Measured decay of the PPF with increasing time intervals between voltage pulses. Reproduced with permission.[124] Copyright 2023, Wiley-VCH.

© 2024 The Author(s). Advanced Electronic Materials published by Wiley-VCH GmbH

2199160x, 2024, 10, Downloaded from https://advanced.onlinelibrary.wiley.com/doi/10.1002/aelm.202400212 by Universidade Do Minho, Wiley Online Library on [20/04/2026]. See the Terms and Conditions (https://onlinelibrary.wiley.com/terms-and-conditions) on Wiley Online Library for rules of use; OA articles are governed by the applicable Creative Commons License

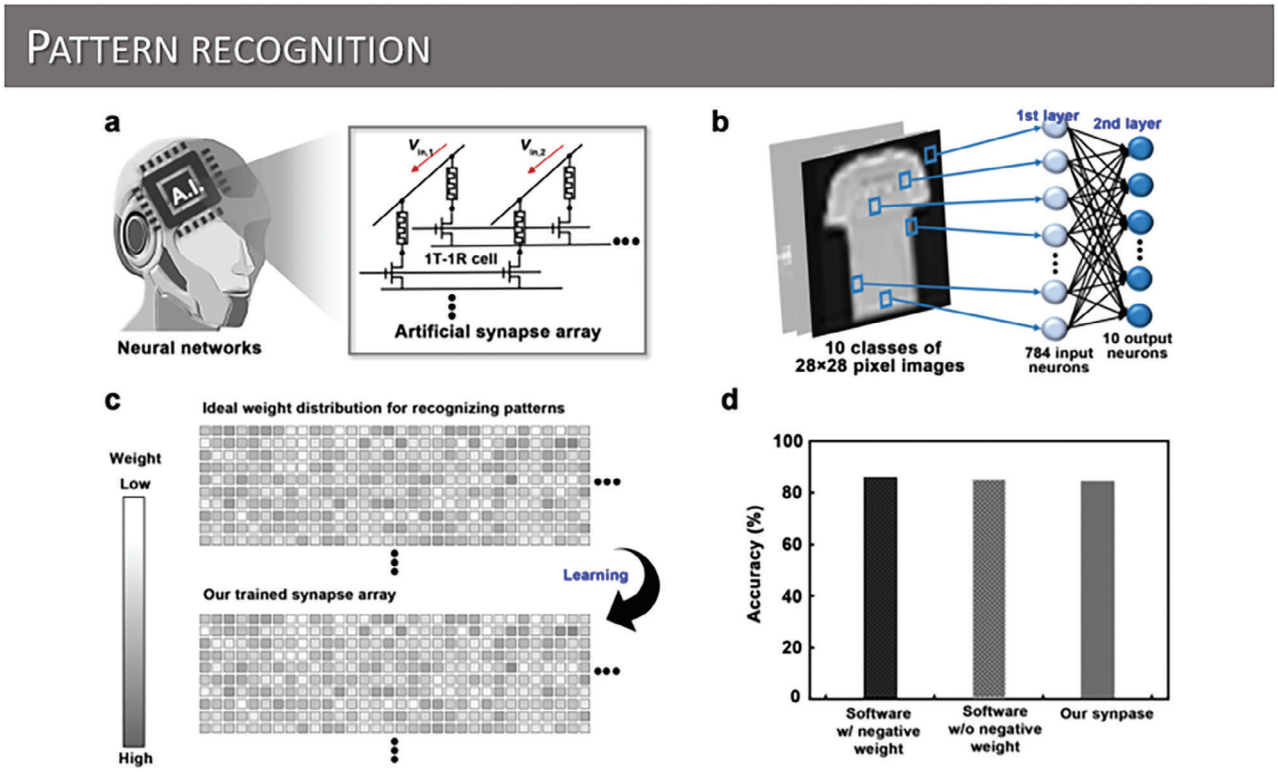


Figure 28. Pattern recognition in neural networks based on the developed synapse array. A) Schematics presenting the 1T–1R structured crossbar array and its applications. B) A fully connected one-layer neural network for the recognition of labelled fashion images. The input (784 neurons for input images with 28 × 28 pixels) and output (10 neurons for 10 classes of images) neurons were used. C) Distributions of ideal synaptic weights for accurate pattern recognition (top) and the weights of the trained synapse arrays after the learning process (bottom). D) Recognition accuracy after training 10 epochs for an ideal software and the developed synapse-based neural networks. Reproduced with permission.[142c] Copyright 2021, Springer Nature.

and an HRS for digital information storage, due in part to the formation of a conducting Ag filament within the tungsten oxide layer. Under device programming for digital type memristor, it allows low-voltage switching with a SET and RESET voltage of 1.05 V and −0.45 V respectively, a memory window of 10, with the longest endurance of any printed memristor ever published (12672 cycles). By switching the device in negative bias, the device works as volatile analog RS. The reported dynamic transition between Schottky and Ohmic-like contact at the Ag/WO_3 interface results from the stoichiometric change of oxygen in the tungsten oxide semiconductor. As a result, the device is able to simulate biological synaptic properties like short-term plasticity and memory formation after repeated stimulation.

4.3. Overview of the Performance Metrics Based on Different Class of Materials: Challenges and Opportunities

In the field of printed memristors a remarkable progress has occurred during the past decade, from a simple proof of concept to the integration in circuits for neural networks. Over the years, a wide variety of materials were tested as RS layers. **Figure 26** compares the performance of different classes of materials used in memristors. Five key metrics were selected to compare: Processing temperature, memory window, switching time, endurance, and switching voltage. It needs to be remembered that the correct characterization method of endurance measurement should be one data point per cycle, as explained in ref. [136].

Metal oxide seems the most promising class of material showing the best endurance for non-volatile RS (currently the endurance record is at 12672 cycles),[124] the fastest switching time (100 ns),[251] memory window up to 10^9.[251] Aligned with the performance metrics allied with the simple integration into CMOS circuits[242] makes metal oxides the most studied and implemented class of materials in printed memristors. 2D and organic materials are also very promising for distinctive reasons: the 2D h-BN shows volatile TS with robust performance with reported endurance of 600 000 cycles,[19] making an interesting approach for spiking neural networks or in hardware security applications. By the other side, organic materials show low switching power and analog non-volatile RS, making it promising to neuromorphic computing. Nonetheless redox-based metal-coordinated organic molecules as RS layer are an emerging approach with state-of-the-art performance.[143] Yet, all the works were spin-coated, making a field that can largely benefit from using printing techniques.

Table 8 summarizes the current status with respective challenges and perspectives of printed memristors. The biggest challenge in performance that printed memristors need to overcome is still endurance. The recommended endurance for memristors to be implemented in neuromorphic applications is 10^9 cycles,[230] 5 orders of magnitude higher than the best-printed

© 2024 The Author(s). Advanced Electronic Materials published by Wiley-VCH GmbH

2199160x, 2024, 10, Downloaded from https://advanced.onlinelibrary.wiley.com/doi/10.1002/aelm.202400212 by Universidade Do Minho, Wiley Online Library on [20/04/2026]. See the Terms and Conditions (https://onlinelibrary.wiley.com/terms-and-conditions) on Wiley Online Library for rules of use; OA articles are governed by the applicable Creative Commons License

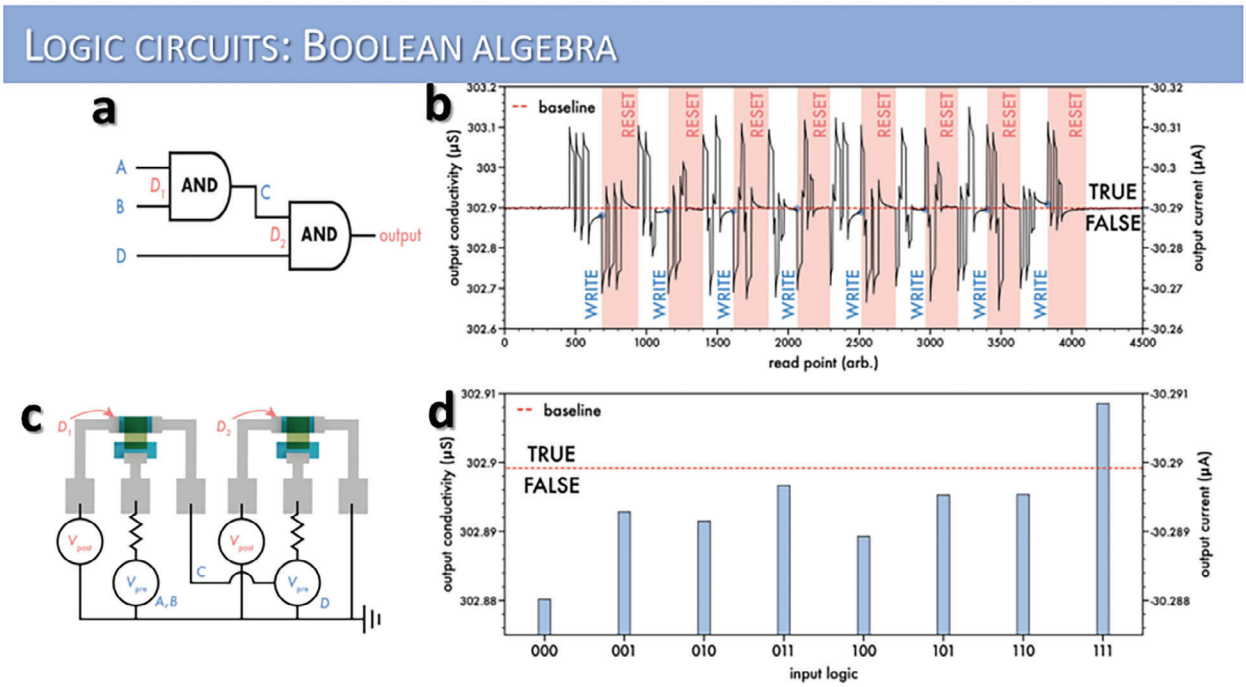


Figure 29. An implementation of Boolean algebra for logic circuits: a) Cascaded combinational logic gate of two AND gates. b) Output data after applying all cases of logical inputs and reset operations. The dashed line (red) represents the baseline conductivity and current prior to any programmed logical input. The circles (blue) indicate the final logical output after applying each input series. c) Schematic for the p6DTP-based combinational logic gate circuit. d) Extrapolated data showing the logical outputs for the device after the combinational programming sequence. The dashed line (red) represents the baseline conductivity and current prior to any programmed logical input. Reproduced with permission.[86] Copyright 2023, Wiley-VCH.

metal oxide and 2D-based memristor can achieve. The low endurance performance can be attributed to the lack of variety of printed inks for electrode as well as the device size which also impacts on the switching time. The smallest printed memristor has a device area of 6 × 6 μm^2[66] and 80 × 80 nm^2 when using nanowires,[58] still far away to the state-of-the-art lithography nodes. To shrink the device size to sub micrometre it requires an improvement of printing machines, specifically on the motor and alignment accuracy.

The key challenges of printed memristors are transversal to printed circuits, which includes:[266]

1) Device miniaturization, a smaller feature size is desired to reduce the parasitic impedance and improve device performance especially the switching time.
2) Layer alignment and layer interaction. A poor alignment can cause a larger device-to-device variation. Since additive printing electronics rely on inks, it is important to formulate/choose inks where the solvent does not interact with the previous printed layer.
3) Printing uniformity and variations. Nonuniform layers might increase the probability of pinholes and cause a larger device-to-device variation and/or lower yields.

Consequently, fully printed memristors can make a huge forward leap once there is a bigger choice of conductive inks for electrodes and high-resolution printing equipment.

4.4. Applications Prospects

During the last few years applications have been reported where printed memristors were integrated.[19,54,66,79,86,94,124,142c,202,248] The analog non-volatile RS characterized by the gradual switching of the device have great potential on artificial synapses towards neuromorphic computing.[267] Hu et al.[124] reported Ag/Wo_3/Au memristors being able to emulate processes carried out by biological synapses, including memory formation and short-term plasticity after repeated stimulation. The device exhibited facilitation (10–177 ms), augmentation (10s), and potentiation (35s) (**Figure 27**a–c). Also, Feng et al.[79] reported a printed MoS_2 memristors allowing a successful emulation of both short- and long-term synaptic plasticity functions including paired-pulse facilitation (PPF), relaxation, long-term potentiation/depression (LTP)/(LTD), and spike-rate-dependent plasticity SRDP within one single device with a switching energy of 4.5 fJ.

The fluoropolymer-based organic memristor developed by Kim et al.[142c] showed the capability for realizing hardware-based neural networks. For complex image recognition, neural networks based on the developed synapse achieved approximately 85% accuracy, resembling the ideal software system (**Figure 28**a–d).

Another potential of neuromorphic computing is the ability to perform information processing (mathematical and logical operations). Grant et al.[86] demonstrated the first implementation of a memristive device as a cascaded combinational logic circuit

© 2024 The Author(s). Advanced Electronic Materials published by Wiley-VCH GmbH

2199160x, 2024, 10, Downloaded from https://advanced.onlinelibrary.wiley.com/doi/10.1002/aelm.202400212 by Universidade Do Minho, Wiley Online Library on [20/04/2026]. See the Terms and Conditions (https://onlinelibrary.wiley.com/terms-and-conditions) on Wiley Online Library for rules of use; OA articles are governed by the applicable Creative Commons License

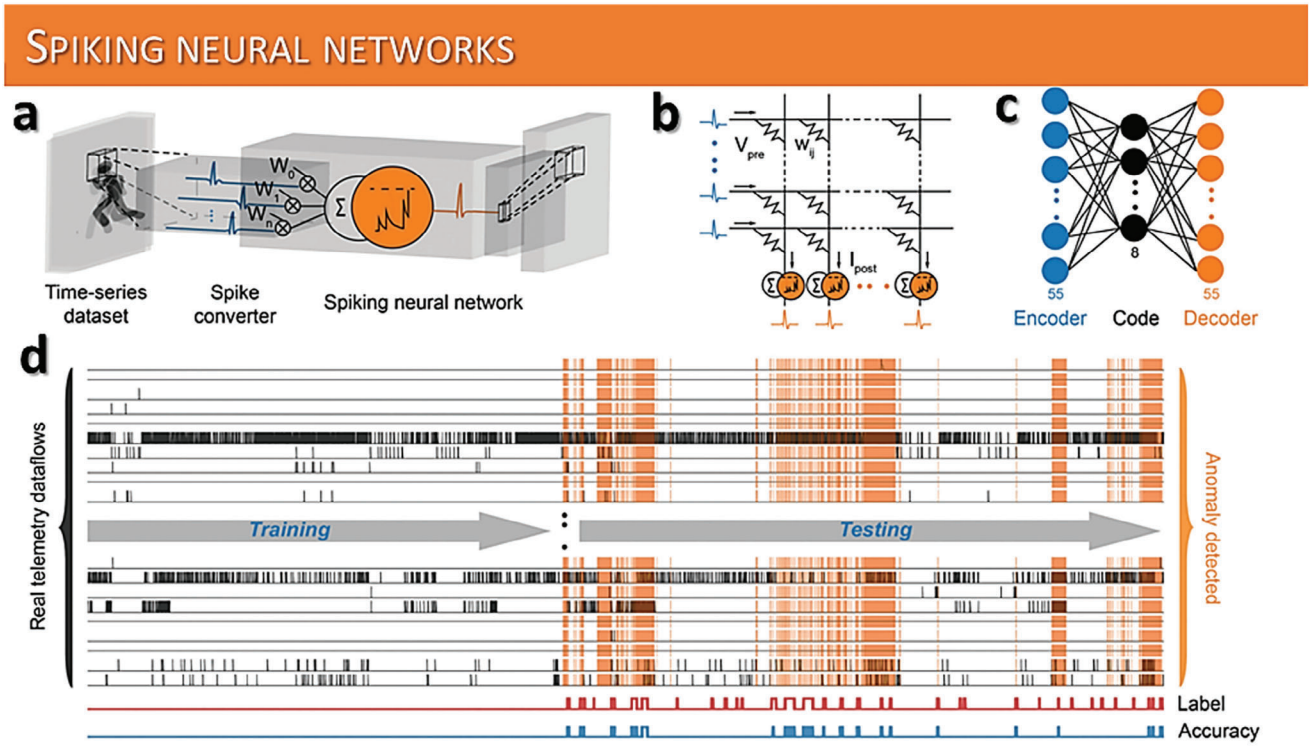


Figure 30. An example of an SNN implementation made by printed memristors: a) Working principle of the autoencoder for anomaly detection in simulation, showing the time-series input encoded and processed in the SNN framework. The spike converter encodes the input into Poisson spike trains via rate coding to fit the subsequent Poisson-like spiking of the neurons. b) Hardware in a crossbar design in this simulation, consisting of non-volatile memories as the synapses and the spiking neurons as the neurons. c) The network topology of a 3-layer fully-connected autoencoder, consisting of an encoder for compressing the input, a code for storing abstracted features, and a decoder for reconstructing information from the code. d) Anomaly detection for 55 flows of time-series real spacecraft telemetry data collected from the Curiosity rover on Mars, showing the feature learning and anomaly detection stages. The orange "Anomaly detected" flows represent the anomalies detected. The red "Label" flow represents the actual anomalies labeled in the dataset. The blue "Accuracy" flow represents the accuracy of the anomalies detected with respect to the anomalies labeled. Reproduced with permission.[54] Copyright 2023, Wiley-VCH.

(**Figure 29**a–d). The presented analog p6DTP-based device performed various mathematical operations of addition and subtraction, multiplication, and division.

On the other side, volatile memristors can be also applied in neuromorphic computing. The self-reset threshold switching fit the leaky integrate-and fire (LIF) neuron design while avoiding peripheral threshold and reset circuits for spike generation and resetting,[66,268] suitable for Spiking neural network (SNN). Time-series tasks like temporal pattern recognition, action localization, and anomaly detection are tasks that the SNNs excel at.[269] Song et al.[54] have implemented SNN using inkjet printed solution-h-BN stochastic memristors. The network demonstrated its capabilities by testing anomaly detection on a publicly available dataset that included time-series real spacecraft telemetry data gathered from the Curiosity rover on Mars (**Figure 30**a–d).

The digital operation of a non-volatile memristor, characterized by an abrupt switching between conductive states is suitable for data storage applications.[270] Ali et al.[202] printed GQDs/PVP memristors and GQDs/PVP capacitors to be implemented as low pass, high pass, and band pass filters (**Figure 31**a). The cut-off frequencies of the filters were controlled through resistive states of the memristor (HRS/LRS), as the cut-off frequency is shifted by a change in resistance value. Zhu et al.[19] printed h-BN memristors that exhibit multiple stochastic phenomena, which it was demonstrated suitable as entropy sources in electronic circuits for data encryption (physical unclonable functions and true random number generators (Figure 31b). Vilmi et al.[248] demonstrated the functionality of the Ag/TiO_2/Ag memristor, which was integrated into a circuit that included a printed voltage doubler acting as a rectifier and a piezoelectric element serving as a pulse source. The memristor was able to switch between high and low resistive states by means of the mechanical impact, which was converted into an electrical signal by the piezoelectric element (Figure 31c).

5. Conclusions and Outlook

This review has given a thorough and critical overview of PE for memristor fabrication. Despite being a novel area that started in 2012 from solely device DC characteristics, it evolved at a rapid pace and fully printed memristive circuits are already being demonstrated. Metal oxides are the most studied and implemented class of materials in printed memristors with leading performance. 2D and organic materials show great promise, although they are among the least studied for neuromorphic computing.

© 2024 The Author(s). Advanced Electronic Materials published by Wiley-VCH GmbH

2199160x, 2024, 10, Downloaded from https://advanced.onlinelibrary.wiley.com/doi/10.1002/aelm.202400212 by Universidade Do Minho, Wiley Online Library on [20/04/2026]. See the Terms and Conditions (https://onlinelibrary.wiley.com/terms-and-conditions) on Wiley Online Library for rules of use; OA articles are governed by the applicable Creative Commons License

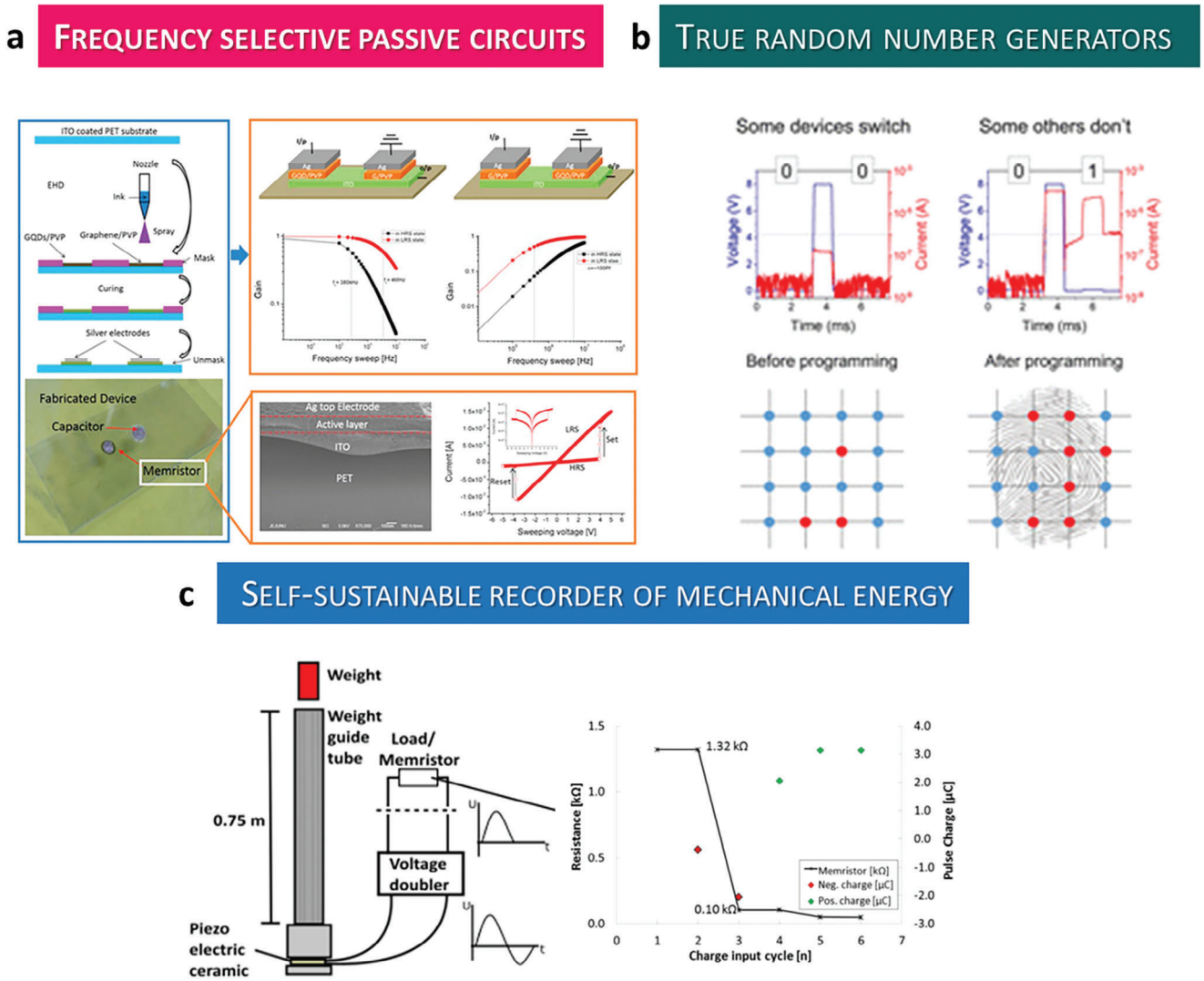


Figure 31. Another demonstration of applications where printed memristors were implemented: a) flexible EHD printed memristor-capacitor circuit for low pass, high pass, and band pass filters. Reproduced with permission.[202] Copyright 2017, Elsevier Ltd. b) True random number generator for security applications by using stochastic memristors. Reproduced with permission.[19] Copyright 2023, Royal Society of Chemistry. c) Self-sustainable recorder of mechanical energy: the resistance value altered once significantly and decreased after that subsequently with each electrical pulse. Reproduced with permission.[248] Copyright 2016, IOP Publishing Ltd.

While the outlook for printed memristors is particularly promising, numerous challenges still need to be addressed. At the materials level, it needs to focus on asymmetric structures. Symmetric Ag electrodes are not the most suitable architecture for memristors. Since the combination of the electrode material heavily influences the RS characteristics, it is recommended to study the device RS characteristics by changing the electrode material. To the current date, a significant range of conductive inks is commercially available. It needs to be reminded that there are areas that can be improved in conductive inks, namely on formulating low-temperature sintering and environmentally friendlier formulations. Also, for droplet-based inks, precursor-based inks are more promising than NP-based inks due to the fact it generates films with lower roughness.

Still, significant challenges lie at the fabrication level, which to improve device performance, it needs to shrink the memristor size. To achieve sub-micrometer feature size, it is required the development of novel printing setups, particularly with improved motor and alignment accuracy. Moreover, more reports should start to emphasize the fabrication optimization of the device (device area, layer thickness, sintering conditions) in order to achieve high yields and low device-to-device variation.

With those aspects in mind, fully printed memristors can achieve an important forward leap in performance in the next years where PE should expect a large increase in market cap. It is anticipated that the field of printed memristors will expand in both academic and industrial research over the next years. Printed memristors will also directly benefit new and

© 2024 The Author(s). Advanced Electronic Materials published by Wiley-VCH GmbH

2199160x, 2024, 10, Downloaded from https://advanced.onlinelibrary.wiley.com/doi/10.1002/aelm.202400212 by Universidade Do Minho, Wiley Online Library on [20/04/2026]. See the Terms and Conditions (https://onlinelibrary.wiley.com/terms-and-conditions) on Wiley Online Library for rules of use; OA articles are governed by the applicable Creative Commons License

exciting fields like large-area sensing, soft robotics, and wearable electronics.

Acknowledgements

This work was financed by national funds from FCT - Fundação para a Ciência e Tecnologia, I.P., in the scope of the projects LA/P/0037/2020, UIDP/50025/2020 and UIDB/50025/2020 of the Associate Laboratory Institute of Nanostructures, Nanomodelling and Nanofabrication - i3N. The authors also thank FCT for financial support under the framework of Strategic Funding grants UID/FIS/04650/2020 and grant SFRH/BD/145741/2019. Financial support from the Basque Government Industry Department under the ELKARTEK program is acknowledged. E. Carlos and A. Kiazadeh acknowledge the Individual Call to Scientific Employment Stimulus – 4th Edition (2021. 03825.CEECIND), (2021. 03386.CEECIND) through FCT. The authors further acknowledge the Horizon Europe (HE) projects TERRAMETA (no 101097101) and SUPERIOT (no 101096021).

Conflict of Interest

The authors declare no conflict of interest.

Keywords

deposition techniques, memristors, printed electronics, resistive switching

Received: March 13, 2024
Revised: May 15, 2024
Published online: August 2, 2024

[1] a) R. Wang, J.-Q. Yang, J.-Y. Mao, Z.-P. Wang, S. Wu, M. Zhou, T. Chen, Y. Zhou, S.-T. Han, *Adv. Intell. Systems* **2020**, *2*, 2000055; b) A. Gandomi, M. Haider, *Int. J. Inform. Manag.* **2015**, *35*, 137; c) P. Zikopoulos, C. Eaton, *Understanding big data: Analytics for Enterprise Class Hadoop and Streaming Data*, McGraw-Hill Osborne Media, New York **2011**; d) C. P. Chen, C.-Y. Zhang, *Inform. Sci.* **2014**, *275*, 314; e) J. Fan, F. Han, H. Liu, *Natl. Sci. Rev.* **2014**, *1*, 293; f) V. Marx, *Nature* **2013**, *498*, 255.

[2] a) D. C. Brock, Understanding Moore's law: four decades of innovation, *Chemical Heritage Foundation* **2006**; b) M. Lundstrom, *Science* **2003**, *299*, 210; c) C. A. Mack, *IEEE Trans. Semiconductor Manuf.* **2011**, *24*, 202.

[3] J. Shalf, *Phil. Trans. R. Soc. A* **2020**, *378*, 20190061.

[4] L. Chua, *IEEE Trans. Circuit Theory* **1971**, *18*, 507.

[5] Z. Q. Wang, H. Y. Xu, X. H. Li, H. Yu, Y. C. Liu, X. J. Zhu, *Adv. Funct. Mater.* **2012**, *22*, 2759.

[6] S. Hong, O. Auciello, D. Wouters, *Emerging Non-Volatile Memories*, Springer, Berlin **2014**.

[7] C. Xu, X. Dong, N. P. Jouppi, Y. Xie, presented at *2011 Design, Automation & Test in Europe*, Grenoble, France, March **2011**.

[8] G. W. Burr, R. M. Shelby, A. Sebastian, S. Kim, S. Kim, S. Sidler, K. Virwani, M. Ishii, P. Narayanan, A. Fumarola, *Adv. Phys.: X* **2017**, *2*, 89.

[9] a) F. Liu, X. Qiu, J. Xu, J. Huang, D. Chen, G. Chen, *Prog. Org. Coat.* **2019**, *133*, 125; b) S. Zulfiqar, A. A. Saad, M. F. M. Sharif, Z. Samsudin, M. Y. T. Ali, F. C. Ani, Z. Ahmad, M. K. Abdullah, *Microelectron. Reliability* **2021**, *127*, 114373.

[10] a) J. Oliveira, V. Correia, H. Castro, P. Martins, S. Lanceros-Mendez, *Addit. Manuf.* **2018**, *21*, 269; b) H. Li, S. Wang, X. Dong, X. Ding, Y. Sun, H. Tang, Y. Lu, Y. Tang, X. Wu, *Nano Energy* **2022**, *101*, 107585.

[11] a) J. Wiklund, A. Karakoç, T. Palko, H. Yiğitler, K. Ruttik, R. Jäntti, J. Paltakari, *J. Manuf. Mater. Process.* **2021**, *5*, 89; b) R. A. Patil, S. Ramakrishna, *Environ. Sci. Pollut. Res.* **2020**, *27*, 14412.

[12] M. Heacock, C. B. Kelly, K. A. Asante, L. S. Birnbaum, Å. L. Bergman, M.-N. Bruné, I. Buka, D. O. Carpenter, A. Chen, X. Huo, M. Kamel, P. J. Landrigan, F. Magalini, F. Diaz-Barriga, M. Neira, M. Omar, A. Pascale, M. Ruchirawat, L. Sly, P. D. Sly, M. V. d. Berg, W. A. Suk, *Environ. Health Perspect.* **2016**, *124*, 550.

[13] a) S. Arya, S. Kumar, *J. Cleaner Prod.* **2020**, *271*, 122707; b) W. Li, V. Achal, *Sci. Total Environ.* **2020**, *737*, 139745; c) D. Lee, D. Offenhuber, F. Duarte, A. Biderman, C. Ratti, *Waste Manage.* **2018**, *72*, 362.

[14] a) M. Zabihipour, R. Lassnig, J. Strandberg, M. Berggren, S. Fabiano, I. Engquist, P. Andersson Ersman, *npj Flexible Electron.* **2020**, *4*, 15; b) R. R. Søndergaard, M. Hösel, F. C. Krebs, *J. Polym. Sci., Part B: Polym. Phys.* **2013**, *51*, 16.

[15] M. Berggren, D. T. Simon, D. Nilsson, P. Dyreklev, P. Norberg, S. Nordlinder, P. A. Ersman, G. Gustafsson, J. J. Wikner, J. Hederén, H. Hentzell, *Adv. Mater.* **2016**, *28*, 1911.

[16] J. G. Lee, Z. Gao, D. Fu, X. Yan, *Dig. Tech. Pap. - Soc. Inf. Disp. Int. Symp.* **2022**, *53*, 993.

[17] Y.-Q.-Q. Yi, W. Su, in *Solution-Processed Organic Light-emitting Devices* (Ed: G. Xie), Woodhead Publishing, Sawston, UK **2024**.

[18] Visiongain, **2023**.

[19] K. Zhu, G. Vescio, S. González-Torres, J. López-Vidrier, J. L. Frieiro, S. Pazos, X. Jing, X. Gao, S.-D. Wang, J. Ascorbe-Muruzábal, J. A. Ruiz-Fuentes, A. Cirera, B. Garrido, M. Lanza, *Nanoscale* **2023**, *15*, 9985.

[20] A. C. Hübler, G. C. Schmidt, H. Kempa, K. Reuter, M. Hambsch, M. Bellmann, *Org. Electron.* **2011**, *12*, 419.

[21] C. Yang, H. Wang, Z. Cao, X. Chen, G. Zhou, H. Zhao, Z. Wu, Y. Zhao, B. Sun, *Small* **2023**, *20*, 2308918.

[22] M. Soni, R. Dahiya, *Philos. Trans. R. Soc., A* **2020**, *378*, 20190156.

[23] H. Adachi, Y. Kuroda, T. I. Takuya Imahashi, K. Y. Kazuhisa Yanagisawa, *Jpn. J. Appl. Phys.* **1997**, *36*, 1159.

[24] T. R. Hebner, C. C. Wu, D. Marcy, M. H. Lu, J. C. Sturm, *Appl. Phys. Lett.* **1998**, *72*, 519.

[25] H. Sirringhaus, T. Kawase, R. H. Friend, T. Shimoda, M. Inbasekaran, W. Wu, E. P. Woo, *Science* **2000**, *290*, 2123.

[26] J.-U. Park, M. Hardy, S. J. Kang, K. Barton, K. Adair, D. k. Mukhopadhyay, C. Y. Lee, M. S. Strano, A. G. Alleyne, J. G. Georgiadis, P. M. Ferreira, J. A. Rogers, *Nat. Mater.* **2007**, *6*, 782.

[27] D. B. Strukov, G. S. Snider, D. R. Stewart, R. S. Williams, *Nature* **2008**, *453*, 80.

[28] S. H. Jo, T. Chang, I. Ebong, B. B. Bhadviya, P. Mazumder, W. Lu, *Nano Lett.* **2010**, *10*, 1297.

[29] a) N. Duraisamy, N. M. Muhammad, H.-C. Kim, J.-D. Jo, K.-H. Choi, *Thin Solid Films* **2012**, *520*, 5070; b) K. Rahman, M. Mustafa, N. Muhammad, K. Choi, *Electron. Lett.* **2012**, *48*, 1261.

[30] H. Wang, Q. Zhao, Z. Ni, Q. Li, H. Liu, Y. Yang, L. Wang, Y. Ran, Y. Guo, W. Hu, Y. Liu, *Adv. Mater.* **2018**, *30*, 1803961.

[31] F. Molina-Lopez, T. Gao, U. Kraft, C. Zhu, T. Öhlund, R. Pfattner, V. Feig, Y. Kim, S. Wang, Y. Yun, *Nat. Commun.* **2019**, *10*, 2676.

[32] S. Logothetidis, *Mater. Sci. Eng., B* **2008**, *152*, 96.

[33] P. F. Moonen, I. Yakimets, J. Huskens, *Adv. Mater.* **2012**, *24*, 5526.

[34] a) S. Zhu, Y. Tang, C. Lin, X. Y. Liu, Y. Lin, *Small Methods* **2021**, *5*, 2001060; b) R. Xiong, J. Luan, S. Kang, C. Ye, S. Singamaneni, V. V. Tsukruk, *Chem. Soc. Rev.* **2020**, *49*, 983.

[35] S. H. Kim, S. Jung, I. S. Yoon, C. Lee, Y. Oh, J.-M. Hong, *Adv. Mater.* **2018**, *30*, 1800109.

© 2024 The Author(s). Advanced Electronic Materials published by Wiley-VCH GmbH

2199160x, 2024, 10, Downloaded from https://advanced.onlinelibrary.wiley.com/doi/10.1002/aelm.202400212 by Universidade Do Minho, Wiley Online Library on [20/04/2026]. See the Terms and Conditions (https://onlinelibrary.wiley.com/terms-and-conditions) on Wiley Online Library for rules of use; OA articles are governed by the applicable Creative Commons License

[36] a) H. Yu, D. Fang, M. Dirican, R. Wang, Y. Tian, L. Chen, H. Liu, J. Wang, F. Tang, A. M. Asiri, X. Zhang, J. Tao, *ACS Appl. Mater. Interfaces* **2019**, *11*, 20281; b) M. Serpelloni, E. Cantù, M. Borghetti, E. Sardini, *Sensors* **2020**, *20*, 841; c) M. Rincón-Iglesias, A. Delgado, N. Peřinka, E. Lizundia, S. Lanceros-Méndez, *Carbohydr. Polym.* **2020**, *233*, 115855; d) R. Brito-Pereira, A. Silva Macedo, C. Ribeiro, V. F. Cardoso, S. Lanceros-Méndez, *ACS Appl. Mater. Interfaces* **2023**, *15*, 46747.
[37] S. Pradhan, K. M. Moore, K. M. Ainslie, V. K. Yadavalli, *J. Mater. Chem. B* **2019**, *7*, 5328.
[38] J. M. Lee, S. K. Q. Suen, W. L. Ng, W. C. Ma, W. Y. Yeong, *Macromol. Biosci.* **2021**, *21*, 2000280.
[39] T. Posati, A. Aluigi, A. Donnadio, G. Sotgiu, M. Mosconi, M. Muccini, G. Ruani, R. Zamboni, M. Seri, *Adv. Sustainable Syst.* **2019**, *3*, 1900080.
[40] a) G. Chen, N. Matsuhisa, Z. Liu, D. Qi, P. Cai, Y. Jiang, C. Wan, Y. Cui, W. R. Leow, Z. Liu, S. Gong, K.-Q. Zhang, Y. Cheng, X. Chen, *Adv. Mater.* **2018**, *30*, 1800129; b) M. Jo, K. Min, B. Roy, S. Kim, S. Lee, J.-Y. Park, S. Kim, *ACS Nano* **2018**, *12*, 5637.
[41] C. Wang, T. Yokota, T. Someya, *Chem. Rev.* **2021**, *121*, 2109.
[42] a) N. J. Wilkinson, M. A. A. Smith, R. W. Kay, R. A. Harris, *Int. J. Adv. Manuf. Technol.* **2019**, *105*, 4599; b) H. Abdolmaleki, P. Kidmose, S. Agarwala, *Adv. Mater.* **2021**, *33*, 2006792; c) J. Zikulnig, S. Chang, J. Bito, L. Rauter, A. Roshanghias, S. Carrara, J. Kosel, *Adv. Sens. Res.* **2023**, *2*, 2200073.
[43] a) G. Miskovic, R. Kaufhold, *IEEE Open J. Nanotechnol.* **2022**, *3*, 191; b) W. Zou, H. Yu, P. Zhou, L. Liu, *Mater. Des.* **2019**, *166*, 107609; c) N. Mkhize, H. Bhaskaran, *Small Sci.* **2022**, *2*, 2100073; d) D. Wang, X. Zhao, Y. Lin, J. Liang, T. Ren, Z. Liu, J. Li, *Nanoscale* **2018**, *10*, 9867.
[44] a) K.-H. Shin, H. A. D. Nguyen, J. Park, D. Shin, D. Lee, *J. Coat. Technol. Res.* **2017**, *14*, 95; b) Y. Y. Kim, T.-Y. Yang, R. Suhonen, M. Välimäki, T. Maaninen, A. Kemppainen, N. J. Jeon, J. Seo, *Adv. Sci.* **2019**, *6*, 1802094; c) G. Grau, J. Cen, H. Kang, R. Kitsomboonloha, W. J. Scheideler, V. Subramanian, *Flexible Printed Electron.* **2016**, *1*, 023002.
[45] a) A. Sneck, H. Ailas, F. Gao, J. Leppäniemi, *ACS Appl. Mater. Interfaces* **2021**, *13*, 41782; b) Y. T. Cho, Y. Jeong, Y. J. Kim, S. Kwon, S.-H. Lee, K. Y. Kim, D. Kang, T.-M. Lee, *Appl. Sci.* **2017**, *7*, 1302.
[46] T. Wenzel, A. Lorenz, E. Lohmüller, S. Auerbach, K. Masuri, Y. C. Lau, S. Tepner, F. Clement, *Sol. Energy Mater. Sol. Cells* **2022**, *244*, 111804.
[47] V. Beedasy, P. J. Smith, *Materials* **2020**, *13*, 704.
[48] a) G. Mattana, A. Loi, M. Woytasik, M. Barbaro, V. Noël, B. Piro, *Adv. Mater. Technol.* **2017**, *2*, 1700063; b) L. Nayak, S. Mohanty, S. K. Nayak, A. Ramadoss, *J. Mater. Chem. C* **2019**, *7*, 8771.
[49] W. Zapka, *Handbook of Industrial Inkjet Printing: A Full System Approach*, John Wiley & Sons, Hoboken, NJ **2017**.
[50] J. Eggers, at *Nonsmooth Mechanics and Analysis* (Eds: P. Alart, O. Maisonneuve, R. Tyrrell Rockafellar), Springer, Boston, MA **2006**.
[51] T. Driessen, R. Jeurissen, in *Fundamentals of Inkjet Printing* (Ed: S. D. Hoath), Wiley, Hoboken, NJ **2016**.
[52] S. Jung, S. D. Hoath, G. D. Martin, I. M. Hutchings, in *Large Area and Flexible Electronics* (Eds: M. Caironi, Y. Y. Noh), Wiley, Hoboken, NJ **2015**.
[53] N. Morita, A. A. Khalate, A. M. v. Buul, H. Wijshoff, in *Fundamentals of Inkjet Printing* (Ed: S. D. Hoath), Wiley, Hoboken, NJ **2016**.
[54] L. Song, P. Liu, J. Pei, F. Bai, Y. Liu, S. Liu, Y. Wen, L. W. T. Ng, K.-P. Pun, S. Gao, M. Q.-H. Meng, T. Hasan, G. Hu, *Adv. Electron. Mater.* **2024**, *10*, 2300564.
[55] J. Lin, in *Printed Electronics* (Ed: Z. Cui), Wiley, Hoboken, NJ **2016**.
[56] O. A. Basaran, R. T. Collins, M. T. Harris, *J. Fluid Mech.* **2007**, *588*, 75.
[57] N. M. Muhammad, N. Duraisamy, K. Rahman, H. W. Dang, J. Jo, K. H. Choi, *Curr. Appl. Phys.* **2013**, *13*, 90.
[58] W. Xu, Y. Lee, S.-Y. Min, C. Park, T.-W. Lee, *Adv. Mater.* **2016**, *28*, 527.
[59] A. Reizabal, B. Tandon, S. Lanceros-Méndez, P. D. Dalton, *Small* **2023**, *19*, 2205255.
[60] D. Gao, J. G. Zhou, *IJB* **2018**, 5.
[61] A. Khan, K. Rahman, D. S. Kim, K. H. Choi, *J. Mater. Process. Technol.* **2012**, *212*, 700.
[62] G. I. Taylor, M. D. Van Dyke, *Proc R Soc Lond A Math Phys Sci* **1969**, *313*, 453.
[63] H. F. Poon, D. A. Saville, I. A. Aksay, *Appl. Phys. Lett.* **2008**, 93.
[64] M. S. Onses, E. Sutanto, P. M. Ferreira, A. G. Alleyne, J. A. Rogers, *Small* **2015**, *11*, 4237.
[65] C. Wei, H. Qin, N. A. Ramírez-Iglesias, C.-P. Chiu, Y.-s. Lee, J. Dong, *J. Micromech. Microeng.* **2014**, *24*, 045010.
[66] Y. Xu, H. Wang, D. Ye, R. Yang, Y. Huang, X. Miao, *IEEE Electron Device Lett.* **2022**, *43*, 116.
[67] P. Galliker, J. Schneider, H. Eghlidi, S. Kress, V. Sandoghdar, D. Poulikakos, *Nat. Commun.* **2012**, *3*, 890.
[68] Z. Cui, Y. Han, Q. Huang, J. Dong, Y. Zhu, *Nanoscale* **2018**, *10*, 6806.
[69] Y. Han, J. Dong, *Proc. Manufac.* **2017**, *10*, 845.
[70] M. Yu, K. H. Ahn, S. J. Lee, *Mater. Des.* **2016**, *89*, 109.
[71] K.-S. Kwon, M. K. Rahman, T. H. Phung, S. D. Hoath, S. Jeong, J. S. Kim, *Flexible Printed Electron.* **2020**, *5*, 043003.
[72] A. Khan, K. Rahman, M.-T. Hyun, D.-S. Kim, K.-H. Choi, *Appl. Phys. A* **2011**, *104*, 1113.
[73] M. Maher, A. Smith, J. Margiotta, *Laser 3D Manufacturing*, Vol. *8970*, SPIE, Bellingham, WA **2014**, 897002.
[74] G. J. Marquez, M. J. Renn, W. D. Miller, *MRS Online Proc. Libr.* **2011**, *698*, 521.
[75] J. G. Tait, E. Witkowska, M. Hirade, T.-H. Ke, P. E. Malinowski, S. Steudel, C. Adachi, P. Heremans, *Org. Electron.* **2015**, *22*, 40.
[76] R. Herbert, H.-R. Lim, S. Park, J.-H. Kim, W.-H. Yeo, *Adv. Healthcare Mater.* **2021**, *10*, 2100158.
[77] I. Grunwald, E. Groth, I. Wirth, J. Schumacher, M. Maiwald, V. Zoellmer, M. Busse, *Biofabrication* **2010**, *2*, 014106.
[78] M. Smith, Y. S. Choi, C. Boughey, S. Kar-Narayan, *Flexible Printed Electron.* **2017**, *2*, 015004.
[79] X. Feng, Y. Li, L. Wang, S. Chen, Z. G. Yu, W. C. Tan, N. Macadam, G. Hu, L. Huang, L. Chen, X. Gong, D. Chi, T. Hasan, A. V.-Y. Thean, Y.-W. Zhang, K.-W. Ang, *Adv. Electron. Mater.* **2019**, *5*, 1900740.
[80] a) Y. Li, X. Feng, M. Sivan, J. F. Leong, B. Tang, X. Wang, J. N. Tey, J. Wei, K. W. Ang, A. V. Y. Thean, *IEEE Sens. J.* **2020**, *20*, 4653; b) M. J. Catenacci, P. F. Flowers, C. Cao, J. B. Andrews, A. D. Franklin, B. J. Wiley, presented at *2017 75th Annual Device Research Conference (DRC)*, South Bend, IN, June **2017**.
[81] X. Cao, H. Chen, X. Gu, B. Liu, W. Wang, Y. Cao, F. Wu, C. Zhou, *ACS Nano* **2014**, *8*, 12769.
[82] C. F. Coombs, H. Holden, Printed Circuits Handbook, Seventh Edition, McGraw-Hill Education, **2016**.
[83] C. Chen, C. Ran, Q. Yao, J. Wang, C. Guo, L. Gu, H. Han, X. Wang, L. Chao, Y. Xia, Y. Chen, *Adv. Sci.* **2023**, *10*, 2303992.
[84] W. J. Hyun, E. B. Secor, M. C. Hersam, C. D. Frisbie, L. F. Francis, *Adv. Mater.* **2015**, *27*, 109.
[85] Y. Khan, A. Thielens, S. Muin, J. Ting, C. Baumbauer, A. C. Arias, *Adv. Mater.* **2020**, *32*, 1905279.
[86] B. Grant, T. Wanless, Y. Bandera, H. Noor, N. Poole, S. Chang, S. H. Foulger, *Adv. Mater. Technol.* **2023**, *8*, 2202091.
[87] D.-H. Lien, Z.-K. Kao, T.-H. Huang, Y.-C. Liao, S.-C. Lee, J.-H. He, *ACS Nano* **2014**, *8*, 7613.
[88] S. Tepner, L. Ney, M. Linse, A. Lorenz, M. Pospischil, K. Masuri, F. Clement, *Prog. Photovoltaics* **2020**, *28*, 1054.
[89] S.-J. Potts, C. Phillips, E. Jewell, B. Clifford, Y. C. Lau, T. Claypole, *J. Coat. Technol. Res.* **2020**, *17*, 447.
[90] S. Tepner, N. Wengenmeyr, M. Linse, A. Lorenz, M. Pospischil, F. Clement, *Adv. Mater. Technol.* **2020**, *5*, 2000654.

© 2024 The Author(s). Advanced Electronic Materials published by Wiley-VCH GmbH

2199160x, 2024, 10, Downloaded from https://advanced.onlinelibrary.wiley.com/doi/10.1002/aelm.202400212 by Universidade Do Minho, Wiley Online Library on [20/04/2026]. See the Terms and Conditions (https://onlinelibrary.wiley.com/terms-and-conditions) on Wiley Online Library for rules of use; OA articles are governed by the applicable Creative Commons License

[91] A. E. Ostfeld, I. Deckman, A. M. Gaikwad, C. M. Lochner, A. C. Arias, *Sci. Rep.* **2015**, *5*, 15959.
[92] a) A. A. Bessonov, M. N. Kirikova, D. I. Petukhov, M. Allen, T. Ryhänen, M. J. A. Bailey, *Nat. Mater.* **2015**, *14*, 199; b) M. Patel, D. D. Kumbhar, J. Gosai, M. R. Sekhar, A. T. Mallajosyula, A. Solanki, *Adv. Electron. Mater.* **2023**, *9*, 2200908; c) A. R. Patil, T. D. Dongale, L. D. Namade, S. V. Mohite, Y. Kim, S. S. Sutar, R. K. Kamat, K. Y. Rajpure, *J. Colloid Interface Sci.* **2023**, *642*, 540.
[93] E. B. Secor, S. Lim, H. Zhang, C. D. Frisbie, L. F. Francis, M. C. Hersam, *Adv. Mater.* **2014**, *26*, 4533.
[94] B. Grant, Y. Bandera, S. H. Foulger, J. Vilčáková, P. Sáha, J. Pfleger, *Adv. Mater. Technol.* **2022**, *7*, 2101108.
[95] a) A. Sneck, T. Mäkelä, A. Alastalo, *Flexible Printed Electron.* **2018**, *3*, 014001; b) N. Choi, H. Wee, S. Nam, J. Lavelle, M. Hatalis, *Microelectron. Eng.* **2012**, *91*, 93.
[96] Y. Kusaka, H. Fukushima, D. Shiratori, Y. Takebuchi, K. Igashira, D. Nakauchi, T. Kato, N. Kawaguchi, T. Yanagida, *Jpn. J. Appl. Phys.* **2020**, *59*, 112005.
[97] Y. Kusaka, N. Fukuda, H. Ushijima, *Jpn. J. Appl. Phys.* **2020**, *59*, SG0802.
[98] J. Zikulnig, J. Kosel, *Reference Module in Biomedical Sciences* **2021**.
[99] M. A. U. Khalid, S. W. Kim, J. Lee, A. M. Soomro, M. M. Rehman, B.-G. Lee, K. H. Choi, *Polymer* **2020**, *189*, 122183.
[100] a) G. U. Siddiqui, M. M. Rehman, K. H. Choi, *Polymer* **2016**, *100*, 102; b) M. M. Rehman, G. U. Siddiqui, J. Z. Gul, S.-W. Kim, J. H. Lim, K. H. Choi, *Sci. Rep.* **2016**, *6*, 36195.
[101] H. Kim, E. Lee, Y.-M. Choi, S. Kwon, S. Lee, J. Jo, T.-M. Lee, D. Kang, *Rev. Sci. Instrum.* **2016**, 87.
[102] Y. Kusaka, K. Sugihara, H. Ushijima, *Flexible Printed Electron.* **2016**, *1*, 045004.
[103] J. Leppäniemi, A. Sneck, Y. Kusaka, N. Fukuda, A. Alastalo, *Adv. Electron. Mater.* **2019**, *5*, 1900272.
[104] A. C. Torrezan, J. P. Strachan, G. Medeiros-Ribeiro, R. S. Williams, *Nanotechnology* **2011**, *22*, 485203.
[105] M. P. Sah, C. Yang, H. Kim, B. Muthuswamy, J. Jevtic, L. Chua, *IEEE Trans. Circuits Syst. I Regul. Pap.* **2015**, *62*, 891.
[106] G. Vescio, J. L. Frieiro, A. F. Gualdrón-Reyes, S. Hernández, I. Mora-Seró, B. Garrido, A. Cirera, *Adv. Mater. Technol.* **2022**, *7*, 2101525.
[107] a) P. Escobedo, M. M. Erenas, N. López-Ruiz, M. A. Carvajal, S. Gonzalez-Chocano, I. de Orbe-Payá, L. F. Capitán-Valley, A. J. Palma, A. Martínez-Olmos, *Anal. Chem.* **2017**, *89*, 1697; b) J. M. Nassar, S. M. Khan, D. R. Villalva, M. M. Nour, A. S. Almuslem, M. M. Hussain, *npj Flexible Electron.* **2018**, *2*, 24; c) M. Franco, V. Correia, P. Marques, F. Sousa, R. Silva, B. R. Figueiredo, A. Bernardes, R. P. Silva, S. Lanceros-Mendez, P. Costa, *Adv. Mater. Interfaces* **2021**, *8*, 2100578.
[108] a) T. Sekine, A. Gaïtis, J. Sato, K. Miyazawa, K. Muraki, R. Shiwaku, Y. Takeda, H. Matsui, D. Kumaki, F. Domingues Dos Santos, A. Miyabo, M. Charbonneau, S. Tokito, *ACS Appl. Electron. Mater.* **2019**, *1*, 246; b) C.-Y. Yang, D. Tu, T.-P. Ruoko, J. Y. Gerasimov, H.-Y. Wu, P. C. Harikesh, M. Massetti, M.-A. Stoeckel, R. Kroon, C. Müller, M. Berggren, S. Fabiano, *Adv. Electron. Mater.* **2022**, *8*, 2100907.
[109] H. F. Castro, V. Correia, E. Sowade, K. Y. Mitra, J. G. Rocha, R. R. Baumann, S. Lanceros-Méndez, *Org. Electron.* **2016**, *38*, 205.
[110] a) Z. Hu, Y. Yin, M. U. Ali, W. Peng, S. Zhang, D. Li, T. Zou, Y. Li, S. Jiao, S.-j. Chen, C.-Y. Lee, H. Meng, H. Zhou, *Nanoscale* **2020**, *12*, 2103; b) J. Sun, A. Sapkota, H. Park, P. Wesley, Y. Jung, B. B. Maskey, Y. Kim, Y. Majima, J. Ding, J. Ouyang, C. Guo, J. Lefebvre, Z. Li, P. R. L. Malenfant, A. Javey, G. Cho, *Adv. Electron. Mater.* **2020**, *6*, 1901431; c) F. Ma, Y. Lin, W. Yuan, C. Ding, W. Su, X. Meng, Z. Cui, *ACS Appl. Electron. Mater.* **2021**, *3*, 1747.
[111] Z. Liang, Y. Pei, C. Chen, B. Jiang, Y. Yao, H. Xie, M. Jiao, G. Chen, T. Li, B. Yang, L. Hu, *ACS Nano* **2019**, *13*, 12653.
[112] Y. Jang, J. Kim, D. Byun, *Journal of Physics D: Applied Physics* **2013**, *46*, 155103.
[113] M. Mosberg, presented at *Novel Patterning Tachnologies*, **2024**, 2024.
[114] a) E. Carlos, R. Branquinho, R. Martins, A. Kiazadeh, E. Fortunato, *Adv. Mater.* **2021**, *33*, 2004328; b) X. Chen, X. Wang, Y. Pang, G. Bao, J. Jiang, P. Yang, Y. Chen, T. Rao, W. Liao, *Small Methods* **2023**, *7*, 2201156.
[115] M. Franco, R. Alves, N. Perinka, C. Tubio, P. Costa, S. Lanceros-Mendéz, *ACS Appl. Electron. Mater.* **2020**, *2*, 2857.
[116] Y. Gao, L. Yu, J. C. Yeo, C. T. Lim, *Adv. Mater.* **2020**, *32*, 1902133.
[117] A. M. Gaikwad, Y. Khan, A. E. Ostfeld, S. Pandya, S. Abraham, A. C. Arias, *Org. Electron.* **2016**, *30*, 18.
[118] C. Tong, in *Advanced Materials for Printed Flexible Electronics* (Ed: C. Tong), Springer International Publishing, Cham **2022**.
[119] a) M. Gao, L. Li, Y. Song, *J. Mater. Chem. C* **2017**, *5*, 2971; b) H. C. Nallan, J. A. Sadie, R. Kitsomboonloha, S. K. Volkman, V. Subramanian, *Langmuir* **2014**, *30*, 13470.
[120] Y. Aleeva, B. Pignataro, *J. Mater. Chem. C* **2014**, *2*, 6436.
[121] E. Carlos, R. Branquinho, P. Barquinha, R. Martins, E. Fortunato, in *Chemical Solution Synthesis for Materials Design and Thin Film Device Applications* (Eds: S. Das, S. Dhara), Elsevier, Cham **2021**.
[122] C. Larsen, P. Lundberg, S. Tang, J. Ràfols-Ribé, A. Sandström, E. Mattias Lindh, J. Wang, L. Edman, *Nat. Commun.* **2021**, *12*, 4510.
[123] a) Z. Peng, A. Grillo, A. Pelella, X. Liu, M. Boyes, X. Xiao, M. Zhao, J. Wang, Z. Hu, A. Di Bartolomeo, C. Casiraghi, *Mater. Horiz.* **2024**, *11*, 1344; b) M. Khan, H. M. Mutee Ur Rehman, R. Tehreem, M. Saqib, M. M. Rehman, W.-Y. Kim, *Nanomaterials* **2022**, *12*, 2289; c) A. I. Ivanov, N. A. Nebogatikova, I. A. Kotin, S. A. Smagulova, I. V. Antonova, *Nanotechnology* **2019**, *30*, 255701; d) S. Porro, C. Ricciardi, *RSC Adv.* **2015**, *5*, 68565; e) H. Liu, Y. Liu, W. Guo, X. Zhou, L. Lin, P. Peng, *Mater. Lett.* **2020**, *261*, 127097; f) M. Delfag, R. Katoch, J. Jehn, Y. Gonzalez, C. Schindler, A. Ruediger, *Flexible Printed Electron.* **2021**, *6*, 035011.
[124] H. Hu, A. Scholz, C. Dolle, A. Zintler, A. Quintilla, Y. Liu, Y. Tang, B. Breitung, G. C. Marques, Y. M. Eggeler, J. Aghassi-Hagmann, *Adv. Funct. Mater.* **2023**, *n/a*, 2302290.
[125] V. Subramanian, J. Cen, A. d. l. F. Vornbrock, G. Grau, H. Kang, R. Kitsomboonloha, D. Soltman, H. Y. Tseng, *Proc IEEE Inst Electr Electron Eng* **2015**, *103*, 567.
[126] J. E. Fromm, *IBM J. Res. Dev.* **1984**, *28*, 322.
[127] N. Reis, B. Derby, *MRS Online Proc. Libr.* **2000**, *625*, 117.
[128] D. Jang, D. Kim, J. Moon, *Langmuir* **2009**, *25*, 2629.
[129] B. Derby, *Engineering* **2015**, *1*, 113.
[130] M. Franco, A. Motealleh, C. M. Costa, N. Perinka, C. Ribeiro, C. R. Tubio, S. A. C. Carabineiro, P. Costa, S. Lanceros-Méndez, *ACS Appl. Polym. Mater.* **2023**, *5*, 7144.
[131] S. D. Hoath, *Fundamentals of Inkjet Printing: The Science of Inkjet and Droplets*, John Wiley & Sons, Hoboken, NJ **2016**.
[132] C. Backes, A. M. Abdelkader, C. Alonso, A. Andrieux-Ledier, R. Arenal, J. Azpeitia, N. Balakrishnan, L. Banszerus, J. Barjon, R. Bartali, S. Bellani, C. Berger, R. Berger, M. M. B. Ortega, C. Bernard, P. H. Beton, A. Beyer, A. Bianco, P. Bøggild, F. Bonaccorso, G. B. Barin, C. Botas, R. A. Bueno, D. Carriazo, A. Castellanos-Gomez, M. Christian, A. Ciesielski, T. Ciuk, M. T. Cole, J. Coleman, et al., *2D Mater.* **2020**, *7*, 022001.
[133] D. Li, W.-Y. Lai, Y.-Z. Zhang, W. Huang, *Adv. Mater.* **2018**, *30*, 1704738.
[134] a) S. Yamazaki, T. Hamada, T. Nagase, S. Tokai, M. Yoshikawa, T. Kobayashi, Y. Michiwaki, S. Watase, M. Watanabe, K. Matsukawa, H. Naito, *Appl. Phys. Express* **2010**, *3*, 091602; b) M. M. Voigt, R. C. I. Mackenzie, S. P. King, C. P. Yau, P. Atienzar, J. Dane, P. E. Keivanidis,

© 2024 The Author(s). Advanced Electronic Materials published by Wiley-VCH GmbH

2199160x, 2024, 10, Downloaded from https://advanced.onlinelibrary.wiley.com/doi/10.1002/aelm.202400212 by Universidade Do Minho, Wiley Online Library on [20/04/2026]. See the Terms and Conditions (https://onlinelibrary.wiley.com/terms-and-conditions) on Wiley Online Library for rules of use; OA articles are governed by the applicable Creative Commons License

I. Zadrazil, D. D. C. Bradley, J. Nelson, *Sol. Energy Mater. Sol. Cells* **2012**, *105*, 77.

[135] E. Carlos, J. Deuermeier, R. Branquinho, C. Gaspar, R. Martins, A. Kiazadeh, E. Fortunato, *J. Mater. Chem. C* **2021**, *9*, 3911.

[136] M. Lanza, H.-S. P. Wong, E. Pop, D. Ielmini, D. Strukov, B. C. Regan, L. Larcher, M. A. Villena, J. J. Yang, L. Goux, A. Belmonte, Y. Yang, F. M. Puglisi, J. Kang, B. Magyari-Köpe, E. Yalon, A. Kenyon, M. Buckwell, A. Mehonic, A. Shluger, H. Li, T.-H. Hou, B. Hudec, D. Akinwande, R. Ge, S. Ambrogio, J. B. Roldan, E. Miranda, J. Suñe, K. L. Pey, et al., *Adv. Electron. Mater.* **2019**, *5*, 1800143.

[137] a) E. J. Merced-Grafals, N. Dávila, N. Ge, R. S. Williams, J. P. Strachan, *Nanotechnology* **2016**, *27*, 365202; b) L. Wu, H. Liu, J. Li, S. Wang, X. Wang, *Nanoscale Res. Lett.* **2019**, *14*, 177; c) X. Sheng, C. E. Graves, S. Kumar, X. Li, B. Buchanan, L. Zheng, S. Lam, C. Li, J. P. Strachan, *Adv. Electron. Mater.* **2019**, *5*, 1800876; d) W. He, H. Sun, Y. Zhou, K. Lu, K. Xue, X. Miao, *Sci. Rep.* **2017**, *7*, 10070.

[138] a) C. Du, W. Ma, T. Chang, P. Sheridan, W. D. Lu, *Adv. Funct. Mater.* **2015**, *25*, 4290; b) S. Kumar, Z. Wang, X. Huang, N. Kumari, N. Davila, J. P. Strachan, D. Vine, A. L. D. Kilcoyne, Y. Nishi, R. S. Williams, *ACS Nano* **2016**, *10*, 11205; c) M. E. Pereira, J. Deuermeier, C. Figueiredo, Â. Santos, G. Carvalho, V. G. Tavares, R. Martins, E. Fortunato, P. Barquinha, A. Kiazadeh, *Adv. Electron. Mater.* **2022**, *8*, 2200642.

[139] a) Z. Hu, F. Cao, T. Yan, L. Su, X. Fang, *J. Mater. Chem. C* **2023**, *11*, 244; b) Y. Gu, M. I. Serna, S. Mohan, A. Londoño-Calderon, T. Ahmed, Y. Huang, J. Lee, S. Walia, M. T. Pettes, K. M. Liechti, D. Akinwande, *Adv. Electron. Mater.* **2022**, *8*, 2100515; c) L. Yin, R. Cheng, Y. Wen, B. Zhai, J. Jiang, H. Wang, C. Liu, J. He, *Adv. Mater.* **2022**, *34*, 2108313.

[140] A. Mehonic, A. L. Shluger, D. Gao, I. Valov, E. Miranda, D. Ielmini, A. Bricalli, E. Ambrosi, C. Li, J. J. Yang, Q. Xia, A. J. Kenyon, *Adv. Mater.* **2018**, *30*, 1801187.

[141] a) Y. Fang, S. Zhai, L. Chu, J. Zhong, *ACS Appl. Mater. Interfaces* **2021**, *13*, 17141; b) K. Yan, M. Peng, X. Yu, X. Cai, S. Chen, H. Hu, B. Chen, X. Gao, B. Dong, D. Zou, *J. Mater. Chem. C* **2016**, *4*, 1375; c) Z. Xiao, J. Huang, *Adv. Electron. Mater.* **2016**, *2*, 1600100; d) X. Xiao, J. Hu, S. Tang, K. Yan, B. Gao, H. Chen, D. Zou, *Adv. Mater. Technol.* **2020**, *5*, 1900914.

[142] a) H.-L. Park, M.-H. Kim, H. Kim, S.-H. Lee, *Adv. Electron. Mater.* **2021**, *7*, 2100299; b) G. Liu, C. Wang, W. Zhang, L. Pan, C. Zhang, X. Yang, F. Fan, Y. Chen, R.-W. Li, *Adv. Electron. Mater.* **2016**, *2*, 1500298; c) M.-H. Kim, H.-L. Park, M.-H. Kim, J. Jang, J.-H. Bae, I. M. Kang, S.-H. Lee, *npj Flexible Electron.* **2021**, *5*, 34.

[143] a) S. Goswami, A. J. Matula, S. P. Rath, S. Hedström, S. Saha, M. Annamalai, D. Sengupta, A. Patra, S. Ghosh, H. Jani, S. Sarkar, M. R. Motapothula, C. A. Nijhuis, J. Martin, S. Goswami, V. S. Batista, T. Venkatesan, *Nat. Mater.* **2017**, *16*, 1216; b) S.-i. Yi, S. P. Rath, Deepak, T. V, N. Bhat, S. Goswami, R. S. Williams, S. Goswami, *Adv. Mater.* **2023**, *35*, 2206128; c) S. Goswami, S. P. Rath, D. Thompson, S. Hedström, M. Annamalai, R. Pramanick, B. R. Ilic, S. Sarkar, S. Hooda, C. A. Nijhuis, J. Martin, R. S. Williams, S. Goswami, T. Venkatesan, *Nat. Nanotechnol.* **2020**, *15*, 380.

[144] a) A. Sokolov, M. Ali, H. Li, Y.-R. Jeon, M. J. Ko, C. Choi, *Adv. Electron. Mater.* **2021**, *7*, 2000866; b) N. B. Mullani, D. D. Kumbhar, D.-H. Lee, M. J. Kwon, S.-y. Cho, N. Oh, E.-T. Kim, T. D. Dongale, S. Y. Nam, J. H. Park, *Adv. Funct. Mater.* **2023**, *33*, 2300343; c) N. He, X. Liu, F. Gao, Q. Zhang, M. Zhang, Y. Wang, X. Shen, X. Wan, X. Lian, E. Hu, L. He, J. Xu, Y. Tong, *Mater. Lett.* **2020**, *266*, 127413; d) K. Liao, P. Lei, M. Tu, S. Luo, T. Jiang, W. Jie, J. Hao, *ACS Appl. Mater. Interfaces* **2021**, *13*, 32606; e) W. Huh, D. Lee, C.-H. Lee, *Adv. Mater.* **2020**, *32*, 2002092; f) H. Duan, S. Cheng, L. Qin, X. Zhang, B. Xie, Y. Zhang, W. Jie, *J. Phys. Chem. Lett.* **2022**, *13*, 7130.

[145] a) Y. Pei, Z. Zhou, A. P. Chen, J. Chen, X. Yan, *Nanoscale* **2020**, *12*, 13531; b) J. Wang, Z. Lv, X. Xing, X. Li, Y. Wang, M. Chen, G. Pang, F. Qian, Y. Zhou, S.-T. Han, *Adv. Funct. Mater.* **2020**, *30*, 1909114; c) X. Yan, Y. Pei, H. Chen, J. Zhao, Z. Zhou, H. Wang, L. Zhang, J. Wang, X. Li, C. Qin, G. Wang, Z. Xiao, Q. Zhao, K. Wang, H. Li, D. Ren, Q. Liu, H. Zhou, J. Chen, P. Zhou, *Adv. Mater.* **2019**, *31*, 1805284; d) Y. Gong, Y. Wang, R. Li, J.-Q. Yang, Z. Lv, X. Xing, Q. Liao, J. Wang, J. Chen, Y. Zhou, S.-T. Han, *J. Mater. Chem. C* **2020**, *8*, 2985; e) Z. Lv, Y. Wang, J. Chen, J. Wang, Y. Zhou, S.-T. Han, *Chem. Rev.* **2020**, *120*, 3941.

[146] S. A. Chekol, S. Menzel, R. W. Ahmad, R. Waser, S. Hoffmann-Eifert, *Adv. Funct. Mater.* **2022**, *32*, 2111242.

[147] a) H. Sun, Q. Liu, C. Li, S. Long, H. Lv, C. Bi, Z. Huo, L. Li, M. Liu, *Adv. Funct. Mater.* **2014**, *24*, 5679; b) B.-G. Chae, J.-B. Seol, J.-H. Song, K. Baek, S.-H. Oh, H. Hwang, C.-G. Park, *Adv. Mater.* **2017**, *29*, 1701752.

[148] a) M. D. Pickett, G. Medeiros-Ribeiro, R. S. Williams, *Nat. Mater.* **2013**, *12*, 114; b) J. M. Goodwill, D. K. Gala, J. A. Bain, M. Skowronski, *J. Appl. Phys.* **2018**, 123.

[149] K. S. Woo, Y. Wang, J. Kim, Y. Kim, Y. J. Kwon, J. H. Yoon, W. Kim, C. S. Hwang, *Adv. Electron. Mater.* **2019**, *5*, 1800543.

[150] L. Goux, X. P. Wang, Y. Y. Chen, L. Pantisano, N. Jossart, B. Govoreanu, J. A. Kittl, M. Jurczak, L. Altimime, D. J. Wouters, *Electrochem. Solid-State Lett.* **2011**, *14*, H244.

[151] R. Dittmann, S. Menzel, R. Waser, *Adv. Phys.* **2021**, *70*, 155.

[152] a) J. S. Moodera, L. R. Kinder, T. M. Wong, R. Meservey, *Phys. Rev. Lett.* **1995**, *74*, 3273; b) T. Miyazaki, N. Tezuka, *J. Magn. Magn. Mater.* **1995**, *139*, L231.

[153] a) J. C. Slonczewski, *J. Magn. Magn. Mater.* **1996**, *159*, L1; b) L. Berger, *Phys. Rev. B* **1996**, *54*, 9353; c) M. Tsoi, A. G. M. Jansen, J. Bass, W. C. Chiang, M. Seck, V. Tsoi, P. Wyder, *Phys. Rev. Lett.* **1998**, *80*, 4281; d) B. Dieny, R. Sousa, J.-P. Nozieres.

[154] a) V. Garcia, M. Bibes, *Nat. Commun.* **2014**, *5*, 4289; b) E. T. Breyer, H. Mulaosmanovic, T. Mikolajick, S. Slesazeck, *Appl. Phys. Lett.* **2021**, 118.

[155] a) D. Pantel, S. Goetze, D. Hesse, M. Alexe, *Nat. Mater.* **2012**, *11*, 289; b) E. Y. Tsymbal, A. Gruverman, V. Garcia, M. Bibes, A. Barthélémy, *MRS Bull.* **2012**, *37*, 138; c) R. Guo, W. Lin, X. Yan, T. Venkatesan, J. Chen, *Appl. Phys. Rev.* **2020**, *7*.

[156] S. Rana, J. Mouro, S. J. Bleiker, J. D. Reynolds, H. M. H. Chong, F. Niklaus, D. Pamunuwa, *Nat. Commun.* **2020**, *11*, 1181.

[157] S. Raoux, M. Wuttig, *Nanoelectronics and Information Technology*, 3rd ed. (Ed: R. Waser), Wiley-VCH, Weinheim **2012**, p. 669.

[158] E. Janod, J. Tranchant, B. Corraze, M. Querré, P. Stoliar, M. Rozenberg, T. Cren, D. Roditchev, V. T. Phuoc, M.-P. Besland, L. Cario, *Adv. Funct. Mater.* **2015**, *25*, 6287.

[159] a) T. Shi, R. Wang, Z. Wu, Y. Sun, J. An, Q. Liu, *Small Struct.* **2021**, *2*, 2000109; b) S. Chen, I. Valov, *Adv. Mater.* **2022**, *34*, 2105022.

[160] a) I. Valov, R. Waser, J. R. Jameson, M. N. Kozicki, *Nanotechnology* **2011**, *22*, 254003; b) R. Waser, presented at *2008 IEEE Int. Electron Devices Meeting*, 15–17 Dec. 2008, IEEE, Piscataway, NJ **2008**.

[161] a) A. Hardtdegen, C. L. Torre, F. Cüppers, S. Menzel, R. Waser, S. Hoffmann-Eifert, *IEEE Trans. Electron Devices* **2018**, *65*, 3229; b) A. Marchewka, B. Roesgen, K. Skaja, H. Du, C.-L. Jia, J. Mayer, V. Rana, R. Waser, S. Menzel, *Adv. Electron. Mater.* **2016**, *2*, 1500233.

[162] E. W. Lim, R. Ismail, *Electronics* **2015**, *4*, 586.

[163] X. Yu, T. Shen, C. Zhu, Q. Zeng, A. Yu, S. Liu, R. Yi, Z. Weng, Y. Zhan, X. Hou, J. Qin, *ACS Appl. Nano Mater.* **2020**, *3*, 11889.

[164] A. Marchewka, R. Waser, S. Menzel, presented at *2015 Int. Conf. on Simulation of Semiconductor Processes and Devices (SISPAD)*, Washington, DC, September **2015**.

[165] C. Nauenheim, C. Kuegeler, A. Ruediger, R. Waser, *Appl. Phys. Lett.* **2010**, 96.

[166] A. Kamyshny, S. Magdassi, *Small* **2014**, *10*, 3515.

[167] C. Costa, C. Pinheiro, I. Henriques, C. A. T. Laia, *ACS Appl. Mater. Interfaces* **2012**, *4*, 1330.

© 2024 The Author(s). Advanced Electronic Materials published by Wiley-VCH GmbH

2199160x, 2024, 10, Downloaded from https://advanced.onlinelibrary.wiley.com/doi/10.1002/aelm.202400212 by Universidade Do Minho, Wiley Online Library on [20/04/2026]. See the Terms and Conditions (https://onlinelibrary.wiley.com/terms-and-conditions) on Wiley Online Library for rules of use; OA articles are governed by the applicable Creative Commons License

[168] T. D. Grant, A. C. Hourd, S. Zolotovskaya, J. B. Lowe, R. J. Rothwell, T. D. A. Jones, A. Abdolvand, *Mater. Des.* **2022**, *214*, 110377.
[169] I. J. Fernandes, A. F. Aroche, A. Schuck, P. Lamberty, C. R. Peter, W. Hasenkamp, T. L. A. C. Rocha, *Sci. Rep.* **2020**, *10*, 8878.
[170] A. Sarantopoulos, R. Waser, R. Dittmann, *Phys. Status Solidi* **2023**, 2300483.
[171] D. M. Goldie, A. C. Hourd, M. R. Harvie, J. Thomson, A. Abdolvand, *J. Mater. Sci.* **2015**, *50*, 1169.
[172] B. Reiser, L. González-García, I. Kanelidis, J. H. M. Maurer, T. Kraus, *Chem. Sci.* **2016**, *7*, 4190.
[173] A. Pourjavadi, H. Abdolmaleki, M. Doroudian, S. H. Hosseini, *J. Alloys Compd.* **2020**, *827*, 154116.
[174] S. Jiang, P.-X. Hou, C. Liu, H.-M. Cheng, *J. Mater. Sci. Technol.* **2019**, *35*, 2447.
[175] H.-j. Kwon, J. Hong, S. Y. Nam, H. H. Choi, X. Li, Y. J. Jeong, S. H. Kim, *Mater. Adv.* **2021**, *2*, 5593.
[176] A. Russo, B. Y. Ahn, J. J. Adams, E. B. Duoss, J. T. Bernhard, J. A. Lewis, *Adv. Mater.* **2011**, *23*, 3426.
[177] a) T. S. Tran, N. K. Dutta, N. R. Choudhury, *Adv. Colloid Interface Sci.* **2018**, *261*, 41; b) L. Liu, Z. Shen, X. Zhang, H. Ma, *J. Colloid Interface Sci.* **2021**, *582*, 12; c) D. Kong, L. T. Le, Y. Li, J. L. Zunino, W. Lee, *Langmuir* **2012**, *28*, 13467.
[178] K. Pan, Y. Fan, T. Leng, J. Li, Z. Xin, J. Zhang, L. Hao, J. Gallop, K. S. Novoselov, Z. Hu, *Nat. Commun.* **2018**, *9*, 5197.
[179] B. J. Worfolk, S. C. Andrews, S. Park, J. Reinspach, N. Liu, M. F. Toney, S. C. B. Mannsfeld, Z. Bao, *Proc. Natl. Acad. Sci. USA* **2015**, *112*, 14138.
[180] X. Tang, H.-j. Kwon, J. Hong, H. Ye, R. Wang, D.-J. Yun, C. E. Park, Y. J. Jeong, H. S. Lee, S. H. Kim, *ACS Appl. Mater. Interfaces* **2020**, *12*, 33999.
[181] M. Delfag, G. Rachovitis, Y. González, J. Jehn, A. H. Youssef, C. Schindler, A. Ruediger, *Flexible Printed Electron.* **2022**, *7*, 045001.
[182] J. Lim, B. Y. Jeong, H. G. Yoon, S.-N. Lee, J. Kim, *J. Nanosci. Nanotechnol.* **2012**, *12*, 1675.
[183] K. Vernieuwe, D. Cuypers, C. E. A. Kirschhock, K. Houthoofd, H. Vrielinck, J. Lauwaert, J. De Roo, J. C. Martins, I. Van Driessche, K. De Buysser, *J. Alloys Compd.* **2017**, *690*, 360.
[184] M. Asadzadeh, F. Tajabadi, D. Dastan, P. Sangpour, Z. Shi, N. Taghavinia, *Ceram. Int.* **2021**, *47*, 5487.
[185] Y. Nishi, Y. Kasai, R. Suzuki, M. Matsubara, A. Muramatsu, K. Kanie, *ACS Appl. Nano Mater.* **2020**, *3*, 9622.
[186] E. Gilshtein, S. Bolat, G. T. Sevilla, A. Cabas-Vidani, F. Clemens, T. Graule, A. N. Tiwari, Y. E. Romanyuk, *Adv. Mater. Technol.* **2020**, *5*, 2000369.
[187] Z. Cui, *Printed Electronics: Materials, Technologies and Applications*, John Wiley & Sons, Hoboken, NJ **2016**.
[188] E. Carlos, R. Martins, E. Fortunato, R. Branquinho, *Chemistry* **2020**, *26*, 9099.
[189] K. Sun, J. Chen, X. Yan, *Adv. Funct. Mater.* **2021**, *31*, 2006773.
[190] F. P. García de Arquer, D. V. Talapin, V. I. Klimov, Y. Arakawa, M. Bayer, E. H. Sargent, *Science* **2021**, *373*, eaaz8541.
[191] a) Y. Wang, Z. Lv, J. Chen, Z. Wang, Y. Zhou, L. Zhou, X. Chen, S.-T. Han, *Adv. Mater.* **2018**, *30*, 1802883; b) H. Hao, M. Wang, Y. Cao, J. He, Y. Yang, C. Zhao, L. Yan, *Small Methods* **2023**, 2301454.
[192] V. K. Sangwan, M. C. Hersam, *Nat. Nanotechnol.* **2020**, *15*, 517.
[193] L. Tang, R. Ji, X. Cao, J. Lin, H. Jiang, X. Li, K. S. Teng, C. M. Luk, S. Zeng, J. Hao, S. P. Lau, *ACS Nano* **2012**, *6*, 5102.
[194] A. Ghaffarkhah, E. Hosseini, M. Kamkar, A. A. Sehat, S. Dordanihaghighi, A. Allahbakhsh, C. van der Kuur, M. Arjmand, *Small* **2022**, *18*, 2102683.
[195] K. A. Ritter, J. W. Lyding, *Nat. Mater.* **2009**, *8*, 235.
[196] S. Mahalingam, A. Manap, A. Omar, F. W. Low, N. F. Afandi, C. H. Chia, N. A. Rahim, *Renewable Sustainable Energy Rev.* **2021**, *144*, 110999.
[197] S. Chung, R. A. Revia, M. Zhang, *Adv. Mater.* **2021**, *33*, 1904362.
[198] L. Wang, J. Yang, Y. Zhang, D. Wen, *Nanomaterials* **2021**, *11*, 2043.
[199] T. Yang, H. Wang, B. Zhang, X. Yan, *Appl. Phys. Lett.* **2020**, 116.
[200] S. Ali, J. Bae, C. H. Lee, K. H. Choi, Y. H. Doh, *Org. Electron.* **2015**, *25*, 225.
[201] J. Ali, G.-u.-d. Siddiqui, Y. J. Yang, K. T. Lee, K. Um, K. H. Choi, *RSC Adv.* **2016**, *6*, 5068.
[202] S. Ali, A. Hassan, G. Hassan, J. Bae, C. H. Lee, *Org. Electron.* **2017**, *51*, 119.
[203] K. S. Novoselov, A. K. Geim, S. V. Morozov, D. Jiang, Y. Zhang, S. V. Dubonos, I. V. Grigorieva, A. A. Firsov, *Science* **2004**, *306*, 666.
[204] R. Mas-Ballesté, C. Gómez-Navarro, J. Gómez-Herrero, F. Zamora, *Nanoscale* **2011**, *3*, 20.
[205] a) J. R. Schaibley, H. Yu, G. Clark, P. Rivera, J. S. Ross, K. L. Seyler, W. Yao, X. Xu, *Nat. Rev. Mater.* **2016**, *1*, 16055; b) X. Liu, M. C. Hersam, *Nat. Rev. Mater.* **2019**, *4*, 669.
[206] a) H. Zhang, M. Chhowalla, Z. Liu, *Chem. Soc. Rev.* **2018**, *47*, 3015; b) Y. Wu, Y. Yu, *Energy Storage Mater.* **2019**, *16*, 323.
[207] J. Zhu, E. Ha, G. Zhao, Y. Zhou, D. Huang, G. Yue, L. Hu, N. Sun, Y. Wang, L. Y. S. Lee, C. Xu, K.-Y. Wong, D. Astruc, P. Zhao, *Coord. Chem. Rev.* **2017**, *352*, 306.
[208] C.-H. Huang, C.-Y. Weng, K.-H. Chen, Y. Chou, T.-L. Wu, Y.-C. Chou, *ACS Appl. Mater. Interfaces* **2023**, *15*, 25838.
[209] a) K. Zhu, S. Pazos, F. Aguirre, Y. Shen, Y. Yuan, W. Zheng, O. Alharbi, M. A. Villena, B. Fang, X. Li, A. Milozzi, M. Farronato, M. Muñoz-Rojo, T. Wang, R. Li, H. Fariborzi, J. B. Roldan, G. Benstetter, X. Zhang, H. N. Alshareef, T. Grasser, H. Wu, D. Ielmini, M. Lanza, *Nature* **2023**, *618*, 57; b) K. Zhu, C. Wen, A. A. Aljarb, F. Xue, X. Xu, V. Tung, X. Zhang, H. N. Alshareef, M. Lanza, *Nat. Electron.* **2021**, *4*, 775.
[210] T.-A. Chen, C.-P. Chuu, C.-C. Tseng, C.-K. Wen, H. S. P. Wong, S. Pan, R. Li, T.-A. Chao, W.-C. Chueh, Y. Zhang, Q. Fu, B. I. Yakobson, W.-H. Chang, L.-J. Li, *Nature* **2020**, *579*, 219.
[211] J. D. Wood, G. P. Doidge, E. A. Carrion, J. C. Koepke, J. A. Kaitz, I. Datye, A. Behnam, J. Hewaparakrama, B. Aruin, Y. Chen, H. Dong, R. T. Haasch, J. W. Lyding, E. Pop, *Nanotechnology* **2015**, *26*, 055302.
[212] a) Y. Shen, W. Zheng, K. Zhu, Y. Xiao, C. Wen, Y. Liu, X. Jing, M. Lanza, *Adv. Mater.* **2021**, *33*, 2103656; b) G. Lupina, J. Kitzmann, I. Costina, M. Lukosius, C. Wenger, A. Wolff, S. Vaziri, M. Östling, I. Pasternak, A. Krajewska, W. Strupinski, S. Kataria, A. Gahoi, M. C. Lemme, G. Ruhl, G. Zoth, O. Luxenhofer, W. Mehr, *ACS Nano* **2015**, *9*, 4776.
[213] A. C. Ferrari, F. Bonaccorso, V. Fal'ko, K. S. Novoselov, S. Roche, P. Bøggild, S. Borini, F. H. L. Koppens, V. Palermo, N. Pugno, J. A. Garrido, R. Sordan, A. Bianco, L. Ballerini, M. Prato, E. Lidorikis, J. Kivioja, C. Marinelli, T. Ryhänen, A. Morpurgo, J. N. Coleman, V. Nicolosi, L. Colombo, A. Fert, M. Garcia-Hernandez, A. Bachtold, G. F. Schneider, F. Guinea, C. Dekker, M. Barbone, et al., *Nanoscale* **2015**, *7*, 4598.
[214] J. Li, M. C. Lemme, M. Östling, *ChemPhysChem* **2014**, *15*, 3427.
[215] T. Carey, S. Cacovich, G. Divitini, J. Ren, A. Mansouri, J. M. Kim, C. Wang, C. Ducati, R. Sordan, F. Torrisi, *Nat. Commun.* **2017**, *8*, 1202.
[216] R. F. Hossain, I. G. Deaguero, T. Boland, A. B. Kaul, *NPJ 2D Mater Appl* **2017**, *1*, 28.
[217] R. Worsley, L. Pimpolari, D. McManus, N. Ge, R. Ionescu, J. A. Wittkopf, A. Alieva, G. Basso, M. Macucci, G. Iannaccone, K. S. Novoselov, H. Holder, G. Fiori, C. Casiraghi, *ACS Nano* **2019**, *13*, 54.
[218] B. Wilk, S. Sahayaraj, M. Ziółek, V. Babu, R. Kudrawiec, K. Wojciechowski, *Adv. Mater. Technol.* **2022**, *7*, 2200606.
[219] G. Vescio, J. Sanchez-Diaz, J. L. Frieiro, R. S. Sánchez, S. Hernández, A. Cirera, I. Mora-Seró, B. Garrido, *ACS Energy Lett.* **2022**, *7*, 3653.

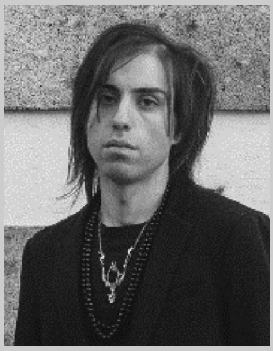
© 2024 The Author(s). Advanced Electronic Materials published by Wiley-VCH GmbH

2199160x, 2024, 10, Downloaded from https://advanced.onlinelibrary.wiley.com/doi/10.1002/aelm.202400212 by Universidade Do Minho, Wiley Online Library on [20/04/2026]. See the Terms and Conditions (https://onlinelibrary.wiley.com/terms-and-conditions) on Wiley Online Library for rules of use; OA articles are governed by the applicable Creative Commons License

[220] K. Tang, Y. Wang, C. Gong, C. Yin, M. Zhang, X. Wang, J. Xiong, *Adv. Electron. Mater.* **2022**, *8*, 2101099.
[221] M. M. Rehman, G. U. Siddiqui, M. M. ur Rehman, H. B. Kim, Y. H. Doh, K. H. Choi, *Mater. Res. Bull.* **2018**, *105*, 28.
[222] C. W. Tang, S. A. VanSlyke, *Appl. Phys. Lett.* **1987**, *51*, 913.
[223] Y. Huang, E.-L. Hsiang, M.-Y. Deng, S.-T. Wu, *Light: Sci. Appl.* **2020**, *9*, 105.
[224] N. Kajal, V. Singh, R. Gupta, S. Gautam, *Environ. Res.* **2022**, *204*, 112320.
[225] K. Fukuda, K. Yu, T. Someya, *Adv. Energy Mater.* **2020**, *10*, 2000765.
[226] H. Chen, W. Zhang, M. Li, G. He, X. Guo, *Chem. Rev.* **2020**, *120*, 2879.
[227] J. Pfleger, in *Solution-Processable Components for Organic Electronic Devices* (Eds: B. Luszczynska, K. Matyjaszewski, J. Ulanski), John Wiley & Sons, Hoboken, NJ **2019**.
[228] F. Chen, Y. Zhou, Y. Zhu, R. Zhu, P. Guan, J. Fan, L. Zhou, N. Valanoor, F. von Wegner, E. Saribatir, I. Birznieks, T. Wan, D. Chu, *J. Mater. Chem. C* **2021**, *9*, 8372.
[229] L. Yuan, S. Liu, W. Chen, F. Fan, G. Liu, *Adv. Electron. Mater.* **2021**, *7*, 2100432.
[230] Y. van de Burgt, A. Melianas, S. T. Keene, G. Malliaras, A. Salleo, *Nat. Electron.* **2018**, *1*, 386.
[231] P. Friederich, A. Fediai, S. Kaiser, M. Konrad, N. Jung, W. Wenzel, *Adv. Mater.* **2019**, *31*, 1808256.
[232] a) H.-L. Park, M.-H. Kim, M.-H. Kim, S.-H. Lee, *Nanoscale* **2020**, *12*, 22502; b) S.-H. Lee, H.-L. Park, M.-H. Kim, M.-H. Kim, B.-G. Park, S.-D. Lee, *ACS Appl. Mater. Interfaces* **2020**, *12*, 51719; c) H.-L. Park, M.-H. Kim, S.-H. Lee, *Org. Electron.* **2020**, *87*, 105927.
[233] a) F. Zeng, S. Li, J. Yang, F. Pan, D. Guo, *RSC Adv.* **2014**, *4*, 14822; b) B. C. Jang, S. Kim, S. Y. Yang, J. Park, J.-H. Cha, J. Oh, J. Choi, S. G. Im, V. P. Dravid, S.-Y. Choi, *Nano Lett.* **2019**, *19*, 839.
[234] S. R. Mohapatra, T. Tsuruoka, T. Hasegawa, K. Terabe, M. Aono, *AIP Advances* **2012**, 2.
[235] a) B. Huber, P. B. Popp, M. Kaiser, A. Ruediger, C. Schindler, *Appl. Phys. Lett.* **2017**, 110; b) J. Jehn, M. Kaiser, U. Moosheimer, A. Ruediger, C. Schindler, *Microelectron. Eng.* **2021**, *239–240*, 111524.
[236] J. Ali, M. M. Rehman, G. U. Siddiqui, S. Aziz, K. H. Choi, *Phys. B* **2018**, *531*, 223.
[237] E. Ramon, E. Sowade, C. Martínez-Domingo, K. Y. Mitra, A. Alcalde, R. R. Baumann, J. Carrabina, *Flexible Printed Electron.* **2021**, *6*, 015003.
[238] R. Sajapin, D. Vurro, P. D'Angelo, G. Tarabella, S. L. Marasso, M. Cocuzza, M. Botti, M. Buttrini, A. Calderaro, T. Berzina, S. Iannotta, *ACS Appl. Electron. Mater.* **2022**, *4*, 5875.
[239] Y. van de Burgt, E. Lubberman, E. J. Fuller, S. T. Keene, G. C. Faria, S. Agarwal, M. J. Marinella, A. Alec Talin, A. Salleo, *Nat. Mater.* **2017**, *16*, 414.
[240] a) J. S. Lee, S. Chang, S. M. Koo, S. Y. Lee, *IEEE Electron Device Lett.* **2010**, *31*, 225; b) M. Moreira, E. Carlos, C. Dias, J. Deuermeier, M. Pereira, P. Barquinha, R. Branquinho, R. Martins, E. Fortunato, *Nanomaterials* **2019**, *9*, 1273; c) J. Sheng, T. Hong, H.-M. Lee, K. Kim, M. Sasase, J. Kim, H. Hosono, J.-S. Park, *ACS Appl. Mater. Interfaces* **2019**, *11*, 40300.
[241] R. A. Martins, E. Carlos, J. Deuermeier, M. E. Pereira, R. Martins, E. Fortunato, A. Kiazadeh, *J. Mater. Chem. C* **2022**, *10*, 1991.
[242] H. Wang, X. Yan, *Phys. Status Solidi Rapid Res. Lett.* **2019**, *13*, 1900073.
[243] J. W. Park, B. H. Kang, H. J. Kim, *Adv. Funct. Mater.* **2020**, *30*, 1904632.
[244] M. N. Awais, N. M. Muhammad, D. Navaneethan, H. C. Kim, J. Jo, K. H. Choi, *Microelectron. Eng.* **2013**, *103*, 167.
[245] S. Zou, P. Xu, M. Hamilton, *Electron. Lett.* **2013**, *49*, 829.
[246] M. N. Awais, H. C. Kim, Y. H. Doh, K. H. Choi, *Thin Solid Films* **2013**, *536*, 308.
[247] G.-u.-d. Siddiqui, J. Ali, Y.-H. Doh, K. H. Choi, *Mater. Lett.* **2016**, *166*, 311.
[248] P. Vilmi, M. Nelo, J.-V. Voutilainen, J. Palosaari, J. Pörhönen, S. Tuukkanen, H. Jantunen, J. Juuti, T. Fabritius, *Flexible Printed Electron.* **2016**, *1*, 025002.
[249] S. Ali, J. Bae, C. H. Lee, *Curr. Appl. Phys.* **2016**, *16*, 757.
[250] G. Vescio, A. Crespo-Yepes, D. Alonso, S. Claramunt, M. Porti, R. Rodriguez, A. Cornet, A. Cirera, M. Nafria, X. Aymerich, *IEEE Electron Device Lett.* **2017**, *38*, 457.
[251] A. I. Ivanov, A. K. Gutakovskii, I. A. Kotin, R. A. Soots, I. V. Antonova, *Adv. Electron. Mater.* **2019**, *5*, 1900310.
[252] K. J. Yoon, J.-W. Han, D.-I. Moon, M. L. Seol, M. Meyyappan, H. J. Kim, C. S. Hwang, *Nanoscale Adv.* **2019**, *1*, 2990.
[253] G. Vescio, G. Martin, A. Crespo-Yepes, S. Claramunt, D. Alonso, J. Lopez-Vidrier, S. Estrade, M. Porti, R. Rodriguez, F. Peiro, *ACS Appl. Mater. Interfaces* **2019**, *11*, 23659.
[254] B. Salonikidou, T. Yasunori, B. Le Borgne, J. England, T. Shizuo, R. A. Sporea, *ACS Appl. Electron. Mater.* **2019**, *1*, 2692.
[255] A. F. Rafique, J. Haji Zaini, M. Z. Bin Esa, M. M. Nauman, *Appl. Phys. A* **2020**, *126*, 134.
[256] H. Hu, A. Scholz, S. A. Singaraju, Y. Tang, G. C. Marques, J. Aghassi-Hagmann, *Appl. Phys. Lett.* **2021**, 119.
[257] B. Salonikidou, A. Mehonic, Y. Takeda, S. Tokito, J. England, R. A. Sporea, *Adv. Eng. Mater.* **2022**, *24*, 2200439.
[258] H. Hu, A. Scholz, Y. Liu, Y. Tang, G. C. Marques, J. Aghassi-Hagmann, *IEEE Trans. Electron. Devices* **2023**.
[259] A. Varanasi, N. Devabharathi, M. Divya, S. K. Mondal, S. Dasgupta, *IEEE J. Flexible Electronics* **2023**, 1.
[260] M. Franco, A. Kiazadeh, J. Deuermeier, S. Lanceros-Méndez, R. Martins, E. Carlos, *Sci. Rep.* **2024**, *14*, 7469.
[261] J. Chen, Q. Xu, Y. Li, J. Cao, X. Liu, J. Qiu, Y. Chen, M. Liu, J. Yu, X. Zhang, Z. Zheng, M. Wang, *IEEE Electron. Device Lett.* **2024**, 1.
[262] a) E. Gale, *Semiconductor Sci. Technol.* **2014**, *29*, 104004; b) I. Salaoru, Q. Li, A. Khiat, T. Prodromakis, *Nanoscale Res. Lett.* **2014**, *9*, 552.
[263] H. Zhang, B. Chen, J. F. Banfield, G. A. Waychunas, *Phys. Rev. B* **2008**, *78*, 214106.
[264] K. Rahman, M. Mustafa, N. M. Muhammad, K. H. Choi, *Electron. Lett.*
[265] A. E. Danks, S. R. Hall, Z. Schnepp, *Mater. Horiz.* **2016**, *3*, 91.
[266] J. S. Chang, A. F. Facchetti, R. Reuss, *IEEE J Emerg Sel Top Circuits Syst* **2017**, *7*, 7.
[267] X. Li, J. Tang, Q. Zhang, B. Gao, J. J. Yang, S. Song, W. Wu, W. Zhang, P. Yao, N. Deng, L. Deng, Y. Xie, H. Qian, H. Wu, *Nat. Nanotechnol.* **2020**, *15*, 776.
[268] D. Marković, A. Mizrahi, D. Querlioz, J. Grollier, *Nat Rev Phys* **2020**, *2*, 499.
[269] K. Roy, A. Jaiswal, P. Panda, *Nature* **2019**, *575*, 607.
[270] E. Linn, R. Rosezin, C. Kügeler, R. Waser, *Nat. Mater.* **2010**, *9*, 403.
[271] F. C. Krebs, *Sol. Energy Mater. Sol. Cells* **2009**, *93*, 394.

© 2024 The Author(s). Advanced Electronic Materials published by Wiley-VCH GmbH

2199160x, 2024, 10, Downloaded from https://advanced.onlinelibrary.wiley.com/doi/10.1002/aelm.202400212 by Universidade Do Minho, Wiley Online Library on [20/04/2026]. See the Terms and Conditions (https://onlinelibrary.wiley.com/terms-and-conditions) on Wiley Online Library for rules of use; OA articles are governed by the applicable Creative Commons License



Miguel Franco graduated in Micro and Nanotechnologies engineering from NOVA School of Sciences and Technologies in 2016. Currently, he is taking a Ph.D. in materials engineering in Minho University under the supervision of Prof. Senentxu and Dr. Asal Kiazadeh in the field of printed electronics. Additionally, during his Ph.D., he collaborated with BCMaterials namely on the European project ICT-02-2018: Flexible and Wearable Electronics. Since 2017, he has been working in environmentally friendly ink formulations, focusing on sustainable materials to be applied on electronic devices.



Asal Kiazadeh received her Ph.D. degree in electronics and optoelectronics at the University of Algarve in a collaborative project with Philips Research Laboratories, in 2014. She is a principal researcher and research group leader of memristors at i3N/CENIMAT of FCT NOVA. Her current research team aims to model and design semiconductor amorphous oxide-based memristors and thin film transistors from physical and device level toward system level. The fundamental objective is to achieve a full integration of memristive devices and thin film transistors to develop hardware capable of performing neuromorphic computing and RRAM networks.



Senentxu Lanceros-Méndez graduated in physics at the University of the Basque Country, Leioa, Spain. He obtained his Ph.D. degree at the Institute of Physics of the Julius-Maximilians-Universität Würzburg, Germany. He was a Research Scholar at Montana State University, Bozeman, MT, USA and visiting scientist at the Pennsylvania State University, USA, and the University of Potsdam, among others. He is an associate professor at the Physics Department of the University of Minho, Portugal (on leave), and from 2012 to 2014, he was also an associate researcher at the INL – International Iberian Nanotechnology Laboratory. Since 2016, he has been Ikerbasque Professor at the BCMaterials, Basque Center for Materials, Applications and Nanostructures, Derio, Spain. His work is focused on the area of smart materials for sensors and actuators, energy, and biomedical applications.



Emanuel Carlos finished his Ph.D. in Nanotechnologies and Nanosciences with a focus on printed electronic devices at NOVA University Lisbon in 2021. Currently, he is an Assistant Researcher and Research area group leader of Sustainable and Flexible Electronics at the CENIMAT|i3N of NOVA Science and Technology School (FCT-NOVA). He has been working in solution-based metal oxide electronics since 2015, focusing on sustainable materials and technologies. His work involves the design, deposition, and characterization of solution-based metal oxide thin films, fabrication, and characterization of electronic devices (transistors, memristors, diodes, among others).

© 2024 The Author(s). Advanced Electronic Materials published by Wiley-VCH GmbH

2199160x, 2024, 10, Downloaded from https://advanced.onlinelibrary.wiley.com/doi/10.1002/aelm.202400212 by Universidade Do Minho, Wiley Online Library on [20/04/2026]. See the Terms and Conditions (https://onlinelibrary.wiley.com/terms-and-conditions) on Wiley Online Library for rules of use; OA articles are governed by the applicable Creative Commons License